UNIVERSITY OF CALIFORNIA

Santa Barbara

New aspect in MOCVD of metal- and N-polar (Al,Ga)N and its device applications

A dissertation submitted in partial satisfaction of the

requirements for the degree Doctor of Philosophy

in Electrical and Computer Engineering

by

Haoran Li

Committee in charge:

Professor Umesh K. Mishra, Chair

Professor Steven P. Denbaars

Professor Shuji Nakamura

Dr. Stacia Keller

March 2018

The dissertation of Haoran Li is approved.

_____
Stacia Keller

_____
Shuji Nakamura

_____
Steven P. Denbaars

_____
Umesh K. Mishra, Committee Chair

March 2018

[This page is optional]

New aspect in MOCVD of metal- and N-polar (Al,Ga)N and its device applications

by

Haoran Li

ACKNOWLEDGEMENTS

It was one of the best thing in my life to pursue my Ph.D. in Professor Mishra's group which is encouraging, enlightening and cordial. I'd like to let all those who encouraged me, helped me and supported me how grateful I am and how fortunate I felt to have you around during these years. It could be a much more difficult journey without you.

First of all, I would like to thank my advisor, Professor Umesh Mishra, who admitted me into the group, providing me the chance to study, work and research in the best labs with the best colleagues. He is an admirable leader who exhibits great visions in the fields of study and unites the group by his integrity, assertiveness, dedication and solicitude. His insights in the technologies are always enlightening and his humor brings laughs in the group every time we meet. I am very grateful to have him as my advisor in research as well as instructor in life. When I was stressful and frustrated, his unreserved support, understanding and encouragement helped me get over those difficult times. His attitude towards research and life are one of those most important treasures I acquired in these years.

Dr. Stacia Keller, practically my second advisor, taught me every aspect of MOCVD and answered every question I have. I was always amazed by her expertise in MOCVD growth. Most of the skills and knowledge I acquired during my Ph.D. studies were from her. I am very grateful for her exceptional patience in answering questions, revising manuscripts and discussing disputable experimental results. Not only her influence can be find in each page of my dissertation, her help and support were also the necessity for me to overcome the frustration and anxiety in the difficult times. All those chats we had comforted me. I can not say enough thanks to her. I learned my technical skills as well as the way to be a nice and supportive person from her.

I would also like to thank Professors Steven Denbaars and Shuji Nakamura for serving on my committee and sharing their insights and advices on this work. Their intuition in MOCVD growth enlightened me every time we discussed. Also thank them for leading the world-class MOCVD lab which makes this work possible.

Next I would like to thank Professor Jim Speck, Doctors Baishakhi Mazumder, Bastien Bonef and Feng Wu for doing the atom probe measurements and the scanning transmission electron microscopy as well as sharing their knowledge on material analysis. Special thanks to Bastien for finishing so many measurements in incredibly short times, giving instant feedbacks in discussions, and more importantly, being a friend full of empathy and joy.

Now on to all the MOCVD growers I worked with. Jing Lu trained me on Thomas Swan and Veeco when I was first beginning, getting me familiar with the machine operations and giving me many valuable suggestions on research. Matt Laurent, the expert of Veeco, trained me on the machine and provided a lot of help in maintenance and troubleshooting. Cory Lund, who also trained me on Thomas Swan, showed me the persistence essential to overcome obstacles in research. I met Nirupam Hatui in my last year and I am grateful to gain his help with growth as well as his friendship outside of work. It was magnificent to work with all these growers including Xiang Liu, Silvia Chan, Anchal Agarwal and Athith Krishna.

Many other group mates offered me crucial help in these years. Steven Wienecke provided elaborate answers whenever I asked him questions. Elahe offered a lot of help when I need to use the electron mobility model she built. Trey Suntrup, Brian Romanczyk, Xun Zheng, Onur Koksaldi, Jeonghee Kim and Matt Guidry were always open to discussions and very pleasant to work with. Carl Neufeld, Shalini Lal, Ramya Yeluri,

Geetak Gupta, Karine Hestroffer, Maher Tahhan, Chirag Gupta, Shubhra Shweta, Pawana Shrestha, Christian Bayless, Christian Wurm and Weiyi Li, I'd like to thank everyone of you who have been in our group for providing an enjoyable research environment and making the group a cheerful place. I am lucky to have your accompany in these years.

Many thanks to all the staff members in the MOCVD lab for their great work on the maintenance of MOCVD machines, especially David Whitlatch and Brian Carralejo who solved every problem on the machines I used. David came to the lab at night when I called and asked for help and Brian fixed the malfunctioning facilities in the weekends when it was urgent. Thanks to them, my research was never delayed because of machine breakdown. In addition, I learned a lot from them about the maintenance and operation of MOCVD machines.

I appreciate the works of the staffs in the MBE labs who maintain the Hall system and those in the Materials Research Laboratory who run the material characterization facilities. Also thanks the administrative staffs for taking care of the paperwork and helping with every question I had.

Finally, I'd like to say thank you to all my friends and families. Mom and Dad, thank you for supporting my choice to study on the other side of the earth. Thank you for taking care of yourself and enjoy life without me so that I don't need to worry too much. Thank you for listening to my complaints and forgiving my occasional bad tempers. There are so many thanks I want to say to you that I can have another chapter for them. My husband, my love, without your support in my most difficult days I won't be able to achieve what I did. Thanks to your forbearance we never had an argument even though I extended the already seven years of long-distance relationship for another one and half year. I want to let you

know that I am very grateful for everything you did for me and I believe I am the luckiest and happiest person with you by my side.

VITA OF HAORAN LI

Mar 2018

EDUCATION

March 2018	**Doctor of Philosophy in Electrical and Computer Engineering** University of California, Santa Barbara, USA
March 2014	**Master of Science in Electrical and Computer Engineering** University of California, Santa Barbara, USA
June 2011	**Bachelor of Engineering in Optical Engineering** Zhejiang University, China

PROFESSIONAL EMPLOYMENT

Department of Electrical and Computer Engineering, University of California, Santa Barbara
Graduate Student Researcher

October 2012 – present

MOCVD growth of (Al,In,Ga)N-based epitaxial structures of electronic devices.

- Developed epitaxial growth techniques for thick AlGaN films with high Al-compositions fully strained to GaN in GaN/AlGaN/GaN heterostructures.
- Explored the impact of various growth conditions on metal-polar and N-polar AlN films deposited by MOCVD, minimizing unintentional Ga incorporation into the films.
- Developed growth processes for N-polar III-N Hot Electron Transistors (HETs).
- Design and epitaxial growth of N-polar AlGaN/GaN HEMT structures with thin channel layers for high-frequency power electronic devices based on which the state-of-the-art performance of P_{out} = 8 W/mm with associated PAE = 27% at 94 GHz was obtained.
- Developed and optimized HEMT structures with GaN/InGaN composite channels leading to successful scaling down of channel thickness to 4 nm, largely increasing the lateral scalability of the devices.
- Developed growth techniques for N-polar n+ GaN contact with a Si doping level up to 2.2×10^{20} cm^{-3}.

Department of Optical Engineering, Zhejiang University, Hangzhou, China
Undergraduate Student Researcher

Oct. 2009 – Jun. 2011

- Developed a software program to reconstruct the surface morphology from interference images using Algebraic Reconstruction Techniques (ART).
- Developed a software program to corrected the mounting error of the object in interference measurements, simplifying the elaborate calibration process.

PATENT

A STRUCTURE FOR INCREASING MOBILITY IN A HIGH ELECTRON MOBILITY TRANSISTOR filed by Brian Romanczyk, Haoran Li, Elahe Ahmadi, Steven Wienecke, Matthew Guidry, Xun Zheng, Stacia Keller, and Umesh K. Mishra, Application number: 62423101.

JOURNAL PUBLICATIONS

Haoran Li, Steven Wienecke, Brian Romanczyk, Elaheh Ahmadi, Matthew Guidry, Xun Zheng, Stacia Keller, and Umesh K. Mishra, "Enhanced mobility in vertically scaled N-polar high-electron-mobility transistors using GaN/InGaN composite channels." *Appl. Phys. Lett*. 112, 073501 (2018).

Haoran Li, Baishakhi Mazumder, Bastien Bonef, Stacia Keller, Steven Wienecke, James S Speck, Steven P Denbaars and Umesh K Mishra, "Characterization of N-polar AlN in GaN/AlN/(Al,Ga)N heterostructures grown by metalorganic chemical vapor deposition." *Semicond. Sci. Technol.* 32, 115004 (2017).

Haoran Li, Stacia Keller, Silvia H Chen, Jing Lu, Steve P. DenBaars, and Umesh K. Mishra, "Unintentional gallium incorporation in AlN and its impact on the electrical properties of GaN/AlN and GaN/AlN/AlGaN heterostructures." *Semicond. Sci. Technol.* 30, 055015 (2015).

Haoran Li, Stacia Keller, Steve P. DenBaars, and Umesh K. Mishra, "Improved properties of high-Al-composition AlGaN/GaN high electron mobility transistor structures with thin GaN cap layers." *Jpn. J. Appl. Phys.* 53, 095504 (2014).

Xun Zheng, **Haoran Li**, Matthew Guidry, Brian Romanczyk, Elaheh Ahmadi, Karine Hestroffer, Steven Wienecke, Stacia Keller, and Umesh K. Mishra, "Analysis of MOCVD SiN_x Passivated N-Polar GaN MIS-HEMTs on Sapphire With High $f_{max} \cdot V_{DS,Q}$." *IEEE Electron Device Lett.* 39, 409 (2018).

Brian Romanczyk, Steven Wienecke, Matthew Guidry, **Haoran Li**, Elaheh Ahmadi, Xun Zheng, Stacia Keller, and Umesh K. Mishra, "Demonstration of Constant 8 W/mm Power Density at 10, 30, and 94 GHz in State-of-the-Art Millimeter-Wave N-Polar GaN MISHEMTs." *IEEE Trans. Electron Devices* 65, 45 (2018).

M.N. Fireman, **Haoran Li**, Stacia Keller, Umesh K. Mishra, James S. Speck, "Growth of N-polar GaN by ammonia molecular beam epitaxy." *J. Cryst. Growth* 481, 65 (2018).

M. N. Fireman, **Haoran Li**, Stacia Keller, Umesh K. Mishra, and James S. Speck, "Vertical transport in isotype InAlN/GaN dipole induced diodes grown by molecular beam epitaxy." *J. Appl. Phys.* 121, 205702 (2017).

Karine Hestroffer, Cory Lund, Onur Koksaldi, **Haoran Li**, Gordon Schmidt, Max Trippel, Peter Veit, Frank Bertram, Ning Lu, Qingxiao Wang, Jürgen Christen, Moon J. Kim, Umesh K. Mishra, Stacia Keller, "Compositionally graded InGaN layers grown on vicinal N-face GaN substrates by plasma-assisted molecular beam epitaxy." *J. Cryst. Growth* 465, 55 (2017).

Steven Wienecke, Brian Romanczyk, Matthew Guidry, **Haoran Li**, Elaheh Ahmadi, Karine Hestroffer, Xun Zheng, Stacia Keller, and Umesh K. Mishra, "N-Polar GaN Cap MISHEMT With Record Power Density Exceeding 6.5 W/mm at 94 GHz." *IEEE Electron Device Lett.* 38, 359 (2017).

Karine Hestroffer, Cory Lund, **Haoran Li**, Stacia Keller, James S. Speck, and Umesh K. Mishra, "Plasma-assisted molecular beam epitaxy growth diagram of InGaN on (0001) GaN for the optimized synthesis of InGaN compositional grades." *Phys. Status Solidi (B)* 253, 626–629 (2016).

Maher Tahhan, Joseph Nedy, Silvia H. Chan, Cory Lund, **Haoran Li**, Geetak Gupta, Stacia Keller, and Umesh K. Mishra, "Optimization of a chlorine-based deep vertical etch of GaN demonstrating low damage and low roughness." *J. Vac. Sci. Technol. A* 34, 031303 (2016).

Silvia H. Chan, Maher Tahhan, Xiang Liu, Davide Bisi, Chirag Gupta, Onur Koksaldi, **Haoran Li**, Tom Mates, Steve P. DenBaars, Stacia Keller, and Umesh K. Mishra,

"Metalorganic chemical vapor deposition and characterization of (Al,Si)O dielectrics for GaN- based devices." *Jpn. J. Appl. Phys.* 55, 021501 (2016).

Silvia H. Chan, Stacia Keller, Maher Tahhan, **Haoran Li**, Brian Romanczyk, Steven P. DenBaars, and Umesh K. Mishra, "High electron mobility recovery in AlGaN/GaN 2DEG channels regrown on etched surfaces." *Semicond. Sci. Technol.* 31, 065008 (2016).

Steven Wienecke, Brian Romanczyk, Matthew Guidry, **Haoran Li**, Xun Zheng, Elaheh Ahmadi, Karine Hestroffer, Ludovico Megalini, Stacia Keller, and Umesh K. Mishra, "N-Polar Deep Recess MISHEMTs with Record 2.9 W/mm at 94 GHz." *IEEE Electron Device Lett.* 37, 713–716 (2016).

Xun Zheng, Matthew Guidry, **Haoran Li**, Elaheh Ahmadi, Karine Hestroffer, Brian Romanczyk, Steven Wienecke, Stacia Keller, and Umesh K. Mishra, "N-Polar GaN MIS-HEMTs on Sapphire with High Combination of Power Gain Cutoff Frequency and Three-Terminal Breakdown Voltage." *IEEE Electron Device Lett.* 37, 77–80 (2016).

Brian Romanczyk, Matthew Guidry, Steven Wienecke, **Haoran Li**, Elaheh Ahmadi, Xun Zheng, Stacia Keller, Umesh K. Mishra, "Record 34.2% efficient mm-wave N-polar AlGaN/GaN MISHEMT at 87 GHz." *Electronics Lett.* 52, 1813 (2016).

Donald J. Suntrup III, Geetak Gupta, **Haoran Li**, Stacia Keller, and Umesh K. Mishra, "Barrier height fluctuations in InGaN polarization dipole diodes." *Appl. Phys. Lett.* 107, 173503 (2015).

Donald J. Suntrup III, Geetak Gupta, **Haoran Li**, Stacia Keller, and Umesh K. Mishra, "Measuring the signature of bias and temperature-dependent barrier heights in III-N materials using a hot electron transistor." *Semicond. Sci. Technol.* 30, 105003 (2015).

Elaheh Ahmadi, Feng Wu, **Haoran Li**, Stephen W. Kaun, Maher Tahhan, Karine Hestroffer, Stacia Keller, James S. Speck, and Umesh K. Mishra, "N-face GaN/AlN/GaN/InAlN and GaN/AlN/AlGaN/GaN/InAlN high-electron-mobility transistor structures grown by plasma-assisted molecular beam epitaxy on vicinal substrates." *Semicond. Sci. Technol.* 30, 55012 (2015).

Geetak Gupta, Matthew Laurent, **Haoran Li**, Donald J. Suntrup III, Edwin Acuna, Stacia Keller, and Umesh K. Mishra, "Design space of III-N hot electron transistors using AlGaN and InGaN polarization-dipole barriers." *IEEE Electron Device Lett.* 36, 23–25 (2015).

Jeonghee Kim, Matthew A. Laurent, **Haoran Li**, Shalini Lal, and Umesh K. Mishra, "Barrier reduction via implementation of InGaN interlayer in wafer-bonded current aperture vertical electron transistors consisting of InGaAs channel and N-polar GaN drain." *Appl. Phys. Lett.* 106, 1–5 (2015).

Karine Hestroffer, Feng Wu, **Haoran Li**, Cory Lund, Stacia Keller, James S. Speck, and Umesh K. Mishra, "Relaxed c -plane InGaN layers for the growth of strain-reduced InGaN quantum wells." *Semicond. Sci. Technol.* 30, 105015 (2015).

Donald J. Suntrup III, Geetak Gupta, **Haoran Li**, Stacia Keller, and Umesh K. Mishra, "Measurement of the hot electron mean free path and the momentum relaxation rate in GaN." *Appl. Phys. Lett.* 105, 1–4 (2014).

Keller, Stacia, **Haoran Li**, Matthew Laurent, Yanling Hu, Nathan Pfaff, Jing Lu, David F. Brown, *et al.* "Recent progress in metal-organic chemical vapor deposition of (000-1) N-polar group-III nitrides." *Semicond. Sci. Technol.* 29, 113001 (2014).

Xiang Liu, Jeonghee Kim, Donald J. Suntrup III, Steven Wienecke, Maher Tahhan, Ramya Yeluri, Silvia H. Chan, Jing Lu, **Haoran Li**, Stacia Keller, and Umesh K. Mishra, "In situ metalorganic chemical vapor deposition of Al_2O_3 on N-face GaN and evidence of polarity induced fixed charge." *Appl. Phys. Lett.* 104, 263511 (2014).

CONFERENCE PAPERS

Andrea Arias, Petra Rowell, Joshua Bergman, Miguel Urteaga, Keisuke Shinohara, Xun Zheng, **Haoran Li**, Brian Romanczyk, Matthew Guidry, Steven Wienecke, Elaheh Ahmadi, Stacia Keller and Umesh K. Mishra, "High Performance N-Polar GaN HEMTs with *OIP3/*P_{DC} ~ 12dB at 10GHz." *Compound Semiconductor Integrated Circuit Symposium (CSICS)*, October 2017, Miami, FL, USA.

Xun Zheng, Matthew Guidry, **Haoran Li**, Brian Romanczyk, Elaheh Ahmadi, Karine Hestroffer, Steven Wienecke, Stacia Keller, and Umesh K. Mishra, "N-Polar GaN MIS-HEMTs on Sapphire with a Proposed Figure of Merit $f_{max} \cdot V_{DS,Q}$ of 9.5 THz·V." *Device Research Conference*, June 2017, South Bend, IN, USA.

Brian Romanczyk, Steven Wienecke, Matthew Guidry, **Haoran Li**, Karine Hestroffer, Elaheh Ahmadi, Xun Zheng, Stacia Keller, and Umesh K. Mishra, "mm-Wave N-polar GaN MISHEMT with a Self-Aligned Recessd Gate Exhibiting Record 4.2 W/mm at 94 GHz on Sapphire." *Device Research Conference*, June 2016, Newark, DE, USA.

Brian Romanczyk, Matthew Guidry, Steven Wienecke, **Haoran Li**, Elaheh Ahmadi, Xun Zheng, Stacia Keller, and Umesh K. Mishra, "W-band N-polar GaN MISHEMTs with high power and record 27.8% efficiency at 94 GHz*." IEEE International Electron Devices Meeting (IEDM)*, December 2016, San Francisco, CA, USA.

Matthew Guidry, Steven Wienecke, Brian Romanczyk, Xun Zheng, **Haoran Li**, Elaheh Ahmadi, Karine Hestroffer, Stacia Keller, and Umesh K. Mishra, "W-band passive load pull system for on-wafer characterization of high power density N-polar GaN devices based on output match and drive power requirements vs. gate width." *87th ARFTG Microwave Measurement Conference*, May 2016, San Francisco, CA, USA.

Matthew Guidry, Steven Wienecke, Brian Romanczyk, **Haoran Li**, Xun Zheng, Elahe Ahmadi, Karine Hestroffer, Stacia Keller, and Umesh K. Mishra, "Small-signal model extraction of mm-wave N-polar GaN MISHEMT exhibiting record performance: Analysis of gain and validation by 94 GHz loadpull." *IEEE MTT-S International Microwave Symposium Digest*, May 2016, San Francisco, CA, USA.

Steven Wienecke, Brian Romanczyk, Matthew Guidry, **Haoran Li**, Elaheh Ahmadi, Xun Zheng, Karine Hestroffer, Stacia Keller, and Umesh K. Mishra, "N-polar GaN Cap MISHEMT with record 6.7 W/mm at 94 GHz." *Device Research Conference*, June 2016, Newark, DE, USA.

Xun Zheng, **Haoran Li**, Elaheh Ahmadi, Karine Hestroffer, Matthew Guidry, Brian Romanczyk, Steven Wienecke, Stacia Keller, and Umesh K. Mishra, "High frequency N-polar GaN planar MIS-HEMTs on sapphire with high breakdown and low dispersion." *Lester Eastman Conference*, August 2016, Bethlehem, PA, USA.

Cheng-Ying Huang, Xinyu Bao, Zhiyuan Ye, Sanghoon Lee, Hanwei Chiang, **Haoran Li**, Varistha Chobpattana, Brian Thibeault, William Mitchell, Susanne Stemmer, Arthur Gossard, Errol Sanchez, and Mark Rodwell, "Ultrathin InAs-Channel MOSFETs on Si substrates." *International Symposium on VLSI Technology, Systems and Application (VLSI-TSA)*, April 2015, Hsinchu, Taiwan.

Gupta, Geetak, Matthew Laurent, **Haoran Li**, Donald J. Suntrup, Edwin Acuna, Stacia Keller, and Umesh Mishra, "Common emitter operation of III-N HETs using AlGaN and InGaN polarization-dipole induced barriers." *Device Research Conference*, June 2014, Santa Barbara, CA, USA.

ABSTRACT

New aspect in MOCVD of metal- and N-polar (Al,Ga)N and its device applications

by

Haoran Li

(Al,Ga,In)N semiconductor materials are widely used in high-frequency, high-power electronics due to their wide bandgaps. Both metal- and N-polar AlGaN/GaN high-electron-mobility transistors (HEMTs) demonstrated excellent performances as high-frequency signal amplifiers. While the majority of today's III-N transistors are based on metal-polar heterostructures, N-polar materials have gained attention following the breakthrough in the deposition of high quality films. Compared to their metal-polar counterparts, N-polar HEMT structures improve the scalability of devices, increase the electron confinement and reduce contact resistance, exhibiting great potentials in high-frequency device fabrications.

In order to suppress alloy scattering in the HEMT structures, a thin AlN interlayer is usually introduced between the AlGaN barrier and the GaN channel. However, a significant amount of unintentional Ga incorporation was observed in AlN films grown by metal-organic chemical vapor deposition (MOCVD), one of the major techniques to produce the HEMT epi structures. In the first part of my thesis, the impact of impure AlN interlayers on HEMTs was examined, explaining the significant improvement in electron mobility despite of the high Ga concentration of ~ 50%. Moreover, both metal-polar and N-polar AlN films

grown by MOCVD under various conditions were investigated, the results of which indicated that the major source of unintentional Ga was the former Ga deposition on the susceptor in the same run. It was also observed that N-polar AlN films contained less Ga compared to metal-polar ones when they were grown under same conditions. Methods to suppress the Ga were also discussed. In addition, the morphological and electrical properties of the GaN/AlN/GaN heterostructures with AlN films grown under different conditions were analyzed by atomic force microscopy (AFM) and room temperature Van der Pauw hall measurement.

Following the study of AlN interlayers in the HEMT structures, the development of N-polar HEMT epitaxial structures with highly-scaled channel thicknesses was discussed in detail. Small channel thickness is critical to prevent short channel effects when scaling down the lateral size of N-polar HEMT devices. By modifying the Si doping level in the back-barrier and the Al composition of the AlGaN cap, the channel thickness of the conventional N-polar HEMT structure with pure GaN channel was successfully scaled down to 8 nm. To further reduce the channel thickness, a thin InGaN layer was introduced between the channel and the AlGaN cap, leading to a decrease of the electric field in the channel and an increase of the distance between the centroid of the 2DEG and the AlN/GaN interface, which suppressed the scattering at the interface and significantly improved the electron mobility. The sheet charge density also increased due to the net positive polarization charge at the GaN/InGaN interface. The design was demonstrated by MOCVD. An increase of 73% in electron mobility from 606 to 1141 $cm^2/(V \cdot s)$ was observed when the 6 nm thick pure GaN channel was replaced by a 4 nm GaN / 2 nm $In_{0.1}Ga_{0.9}N$ composite channel. The smallest applicable channel thickness was decreased to 4 nm with the composite channel design.

TABLE OF CONTENTS

Chapter 1

Introduction

The III-nitride system (Al,Ga,In)N has a direct band-gap ranging from 0.6 eV (InN) to 6.2 eV (AlN). Since the ternary and quaternary III-nitride alloys provide a tunable band-gap which covers the infrared spectrum to deep UV region, they are widely used in solid state lightening such as light-emitting diodes (LED) and laser diodes (LD).

Besides optical applications, (Al,Ga,In)N alloys are also excellent materials for electronic applications thanks to their high mechanical and thermal stability, high thermal conductivity, large piezoelectric constants, high breakdown voltage and reasonably high electron saturation velocity. The wide band-gaps largely suppress the impact ionization which would not happen before the hot electrons gain the energy equivalent to the band-gaps to create electron-hole pairs, preventing avalanche breakdown of the devices under high electric fields. Moreover, thanks to the large energy separation of electrons between the conduction band Γ and L valleys, the intervalley transition under high electric fields is suppressed, leading to high electron saturation velocities.[1] Thereby, GaN-based electronic devices are particularly suitable for high-power, high-frequency applications.

1.1 *Metal-polar GaN-based HEMTs grown by MOCVD*

1.1.1 MOCVD of GaN

One of the most common growth techniques for (Al,Ga,In)N materials is the metal-organic chemical vapor deposition (MOCVD). Ambacher discussed the growth of metal-polar (Al,Ga,In)N materials by MOCVD in detail in his review published in 1998.[2] Trimethylgallium, trimethylaluminum, trimethylindium and NH_3 are the most common precursors used in the deposition. Due to the high thermal stability of NH_3, the growth temperature for (Al,Ga)N is usually high (> 900 °C). Films with In are grown at a lower temperature in order to obtain higher In content. Sapphire and 6H-SiC are two of the common substrates. While sapphire is inexpensive, SiC has a better thermal conductivity which is beneficial for high-power operations.[3] Unless specified, the samples discussed in this work were grown on sapphire. In our typical GaN growth by MOCVD, the surface of the sapphire substrate is first nitridated using NH_3, followed by a nucleation layer grown at a relatively low temperature. Then both of the growth temperature and growth rate are increased for the buffer growth, which starts with island formation and after the islands coalesce, the dislocation density decreases as the layer grows thicker and the typical dislocation density for layers thicker than 1 μm is in the magnitude of 10^8 cm^{-2}.

1.1.2 Metal-polar HEMTs

The spontaneous and piezoelectric polarization in the wurtzite (Al,Ga,In)N alloys and the high electron drift velocities (2.5×10^7 cm/s)[4] of GaN make them excellent materials to fabricate high-electron-mobility transistors (HEMTs). As shown in Figure 1.1, the

polarization fields in the AlGaN and GaN layers form a two-dimensional electron gas (2DEG) at the AlGaN/GaN interface. Note that all the band diagrams presented in this work were simulated using a one-dimensional self-consistent Poisson-Schrödinger solver.[5] In a typical Ga-polar AlGaN/GaN HEMT structure with AlN interlayer, the sheet charge density (n_s) measures ~ 1×10^{13} cm^{-2} with an associated electron mobility (μ) of ~ 2000 cm^2/Vs, resulting in high conductivity in the channel.

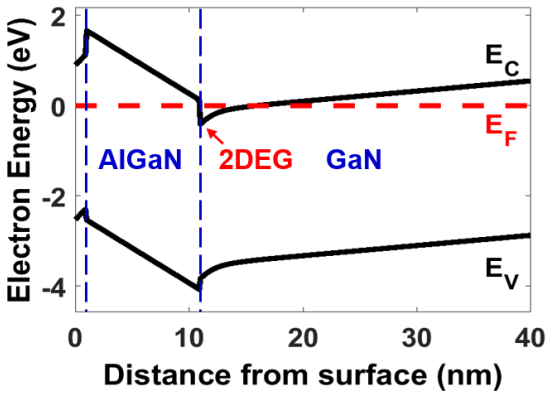

Figure 1.1 Band diagram of Ga-polar GaN/AlGaN/GaN heterostructure.

The high breakdown field in GaN of ~ 3 MV/cm indicates its great potential in high-power applications. The Johnson[6] and Baliga[7] figures of merit (JFoM and BFoM) are indicators of high-frequency power performance, taking into account the critical electric field (or band gap) and electron saturation velocity (or electron mobility) in the materials. The JFoM and BFoM of GaN are one order of magnitude higher than that of Si and GaAs material systems and also superior to SiC. Thereby, GaN-based HEMT structures are very attractive in high-frequency, high-power electronics applications.

The AlGaN/GaN HEMT was first demonstrated by Asif Khan *et al.* in 1993.[8] The first radio-frequency (RF) and power performance of GaN HEMT was demonstrated by Wu *et*

al. in 1996.[9] Since then, the GaN-based high-power-density RF HEMTs has been developed rapidly. In 2012, Shinohara *et al.* reported simultaneously f_T and f_{max} of 342 and 518 GHz.[10] High power densities were also reported: 41.4 W/mm at 4 GHz,[11] 30.6 W/mm at 8 GHz,[12] 13.7 W/mm at 30 GHz[13] and 10.5 W/mm at 40 GHz.[14]

1.1.3 High-frequency device and short-channel effect

It is necessary to shorten the carrier transit time τ between the source and drain spacing l for the high-frequency operation. Given the relationship $\tau = l/v_{sat}$ and the fact that the saturation velocity is material dependent, the source to drain spacing need to be scaled down for high-frequency devices.

However, for highly scaled l, the devices are strongly affected by short-channel effects such as drain-induced barrier lowering and punch-through,[15,16] which can be mitigated by enhancing the electron confinement in the channel and increasing the aspect ratio of a device. The aspect ratio is defined as gate length divided by gate-to-2DEG separation (L_g/a). For highly scaled devices, decrease of gate-to-2DEG separation is necessary. In Ga-polar HEMTs, the electron confinement can be improved by adding InGaN back-barriers.[17,18] However, to decrease the gate-to-2DEG separation, the barrier thicknesses of the Ga-polar HEMTs need to be shrunk down, which in turn leads to 2DEG density drop, resulting in undesirably lower current densities in the devices. This tradeoff is well resolved in N-polar HEMTs as described in the following section.

1.2 *N-polar HEMTs*

1.2.1 Merits of N-polar HEMTs

As polar materials [Figure 1.2], the N-polar (Al,Ga,In)N have opposite polarization fields to the metal-polar ones. The charge inducing layer is positioned below the 2DEG in the N-polar HEMT structure [Figure 1.3(b)], rather than between the 2DEG and gate metal like in Ga-polar structures [Figure 1.3(a)]. As a result, this layer can be modified to increase the sheet charge density independent of gate-to-channel distance, significantly improving the scalability of N-polar devices relative to Ga-polar transistors. Also, the back-barrier in N-polar HEMTs provides a natural quantum confinement of the 2DEG, displacing it towards the gate. What's more, in the N-polar case ohmic contacts can be made directly to the GaN channel, easing the formation of low resistance ohmic contacts.[19] Even with an AlGaN cap on top of the channel in the N-polar HEMT to improve the breakdown voltage, it is easier to make low resistance contacts given the usually thin AlGaN cap with a thickness of 2 – 3 nm, which is much thinner than the typical AlGaN barriers in Ga-polar HEMTs.

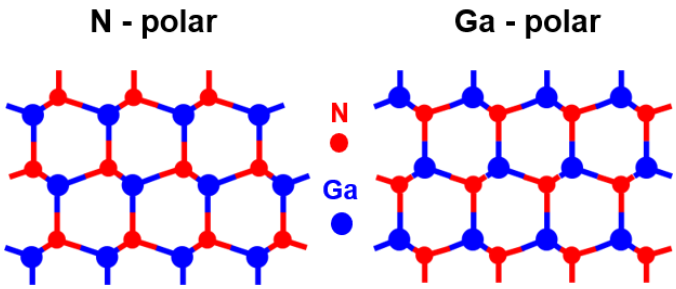

Figure 1.2 Schematic atomic structure of Ga- and N-polar GaN.

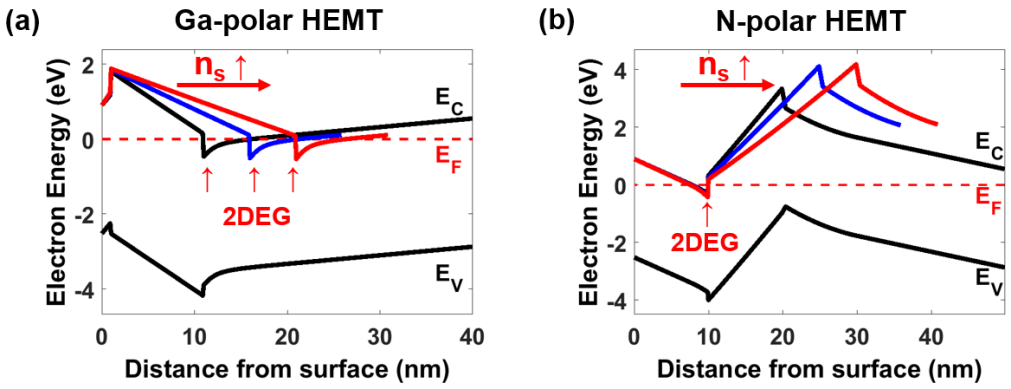

Figure 1.3 Band diagrams of (a) Ga-polar and (b) N-polar GaN/AlGaN/GaN heterostructure with various AlGaN barrier thicknesses.

1.2.2 N-polar material grown by MOCVD

To grow N-polar GaN on c-plane sapphire substrates, a higher nitridation temperature is used compared to the metal-polar GaN deposition.[20] An interfacial AlN layer is formed during the nitridation step which typically leads to growth of N-polar films.[21] On SiC substrates, the N-polar GaN is simply grown on the C-face and the growth is usually initiated with an AlN nucleation layer.[22]

Due to the lower surface mobility of the group-III adatoms on N-polar than metal-polar during film deposition, hexagons are likely to form as the layer grow thicker [Figure 1.4].[23,24,25] In order to maintain a step-flow growth, the adatom surface diffusion length has to be longer than the terrace width. Thereby, vicinal substrates were introduced into N-polar GaN growth.

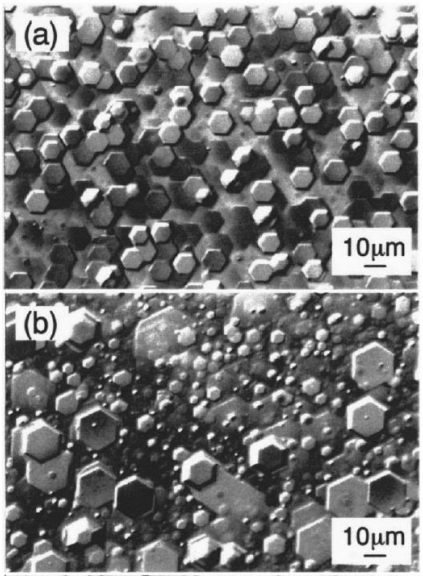

Figure 1.4 Microscopic image of GaN surface deposited on sapphire substrates having a varying thickness of (a) 100 nm (5 min deposition) and (b) 200 nm (10 min).[24]

In 2007, Keller *et al.* reported smooth N-polar GaN films grown on vicinal c-plane sapphire substrates with misorientations of 0.5° – 4° toward a-plane and m-plane.[26] The optical micrographs are presented in Figure 1.5. It is shown that a 2° misorientation towards a- or m-plane effectively suppressed hexagon formation. The smooth surface morphology maintained when the misorientation was increased to 4°.

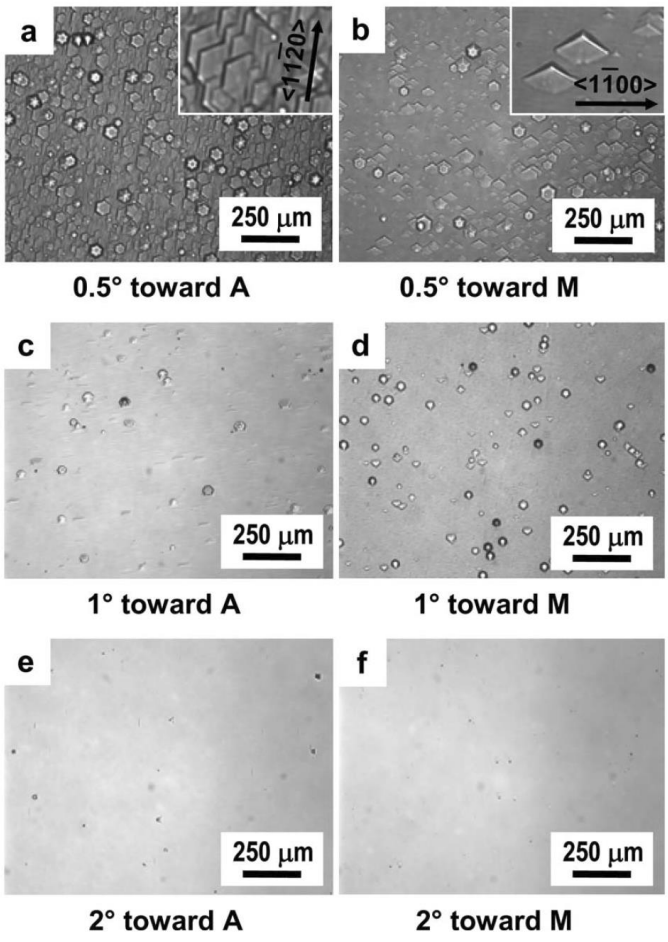

Figure 1.5 Optical micrographs of 0.8 μm thick GaN films grown on (0001) sapphire substrates with misorientation angles of (a) 0.5°, (c) 1°, and (e) 2° toward the a-plane, and (b) 0.5°, (d) 1°, and (f) 2° toward the m-plane. The inserts in (a) and (b) are enlarged threefold.[26]

The samples were measured by high-resolution x-ray diffraction (XRD) and the full width at half maximum (FWHM) of the XRD rocking curves for the (000-2) and (20-2-1) diffraction peaks are shown in Figure 1.6. While the FWHM of the symmetric (000-2) rocking curve correlates with the number of threading dislocations (TDs) with screw component, the off-axis (20-2-1) curve is sensitive to the presence of pure edge threading

dislocations. With increasing misorientation angles from 0.5 to 4° the FWHM of the (20-2-1) diffraction peak decreased from about 1100 to 510 arc sec. The FWHM of the (000-2) diffraction peak was the lowest for the 2A and 2M samples (80 arc sec) and increased to 300 arc sec for the 4A and 4M samples. Considering the more significant reduction of pure edge TDs with increasing misorientation angles, the 4° misorientation of the substrate is preferred for N-polar GaN growth.

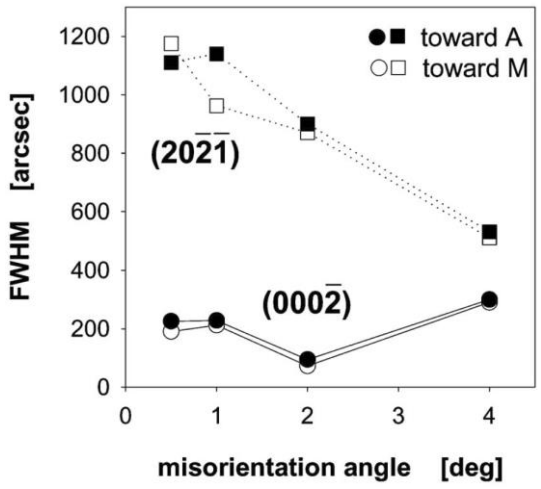

Figure 1.6 Full width at half maximum (FWHM) of the XRD rocking curves measured for the (000-2) and (20-2-1) diffraction peaks of 0.8 μm thick GaN films grown on (0001) Al_2O_3 substrates with different misorientation angles and directions.[26]

While the misorientation direction showed little impact on the structural and optical properties of the N-polar GaN films as reported in reference 26, smoother surfaces were observed for samples misoriented toward the sapphire-a-plane, particularly at the highest misorientation angle of 4°.

Therefore, sapphire substrates with 4° misorientation towards a-plane were chosen for epitaxy of the N-polar samples in this work.

1.2.3 Typical epitaxial structure of N-polar HEMTs

As shown in Figure 1.7, a typical N-polar AlGaN/GaN HEMT structure in our study consisted of a 1.5 µm thick semi-insulating (S.I.) GaN buffer, a 10 nm thick Si-doped GaN layer, a 20 nm thick Si-doped graded $Al_xGa_{1-x}N$ (x_{Al} = 0.05 - 0.38) back-barrier, a 10 nm thick unintentionally doped (UID) $Al_{0.38}Ga_{0.62}N$ back-barrier, a 0.7 nm thick AlN interlayer, a GaN of different thicknesses, a 2.6 nm thick $Al_xGa_{1-x}N$ (x_{Al} = 0.27 or 0.46) cap and a 5 nm thick in-situ SiN_x layer for surface protection. The corresponding band diagram is shown in Figure 1.8.

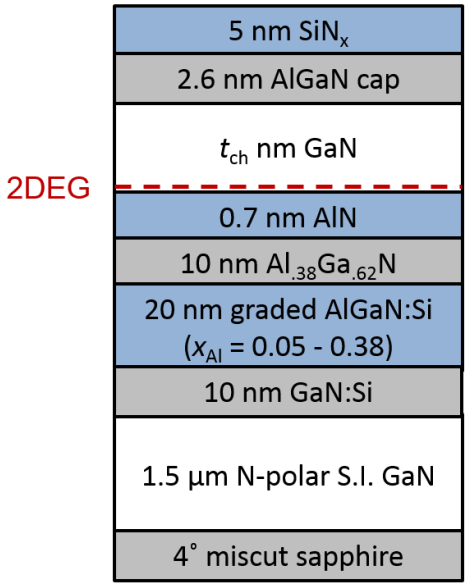

Figure 1.7 Typical N-polar AlGaN/GaN HEMT structure with a channel thickness of t_{ch}.

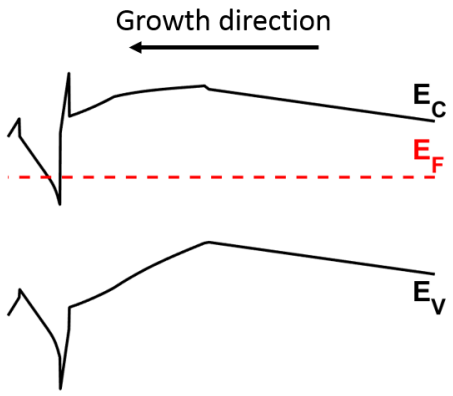

Figure 1.8 Band diagram of a typical N-polar AlGaN/GaN HEMT structure with a channel thickness of 9 nm. The SiN_x cap is not included. Top surface is on the left. The simulation was carried out by BANDENG.[5]

The Si doped graded AlGaN layer was introduced to prevent the donorlike hole trap levels at the negatively polarized bottom GaN/AlGaN interface[27] [Figure 1.3(b)] from getting close to the fermi level and introduce dispersion.[28,29,30] The 10 nm thick UID AlGaN spacer layer suppresses the impact of the ionized donors in the graded AlGaN on the 2DEG mobility. A thin AlN layer was introduced to suppress alloy scattering.[31] On top of the GaN channel, a thin AlGaN cap is deposited to reduce gate leakage of the HEMT device.[32]

1.2.4 Critical aspects in design of N-polar HEMTs

When the channel thickness decreases as required by high-frequency operation, the sheet charge density drops due to surface pinning, which will be discussed in section 1.3.1. According to the simulation using a one-dimensional self-consistent Poisson-Schrödinger solver,[5] the Si doping level affects n_s more significantly than the thickness and composition

of the AlGaN back-barrier. Thereby, increasing the doping level is one of the major method to compensate the n_s drop. However, for extremely high Si doping levels, it is possible that a parasitic 2DEG forms close to the graded AlGaN / GaN interface, resulting in additional dispersion in the device. The tradeoff needs to be carefully evaluated during the design of N-polar HEMT structures.

Another critical layer in the HEMT is the AlN interlayer which is supposed to suppress alloy scattering in the AlGaN back-barrier. However, significant amounts of unintentional Ga incorporation were observed in AlN films grown on GaN by MOCVD.[33] In this work, comprehensive study in metal- and N-polar AlN films grown by MOCVD is presented in Chapter 3 and 4.

The thickness of the channel layer, as mentioned above, is required to be shrunk down for high-frequency devices. In Chapter 5, this crucial aspect is discussed in detail.

The thin AlGaN cap is introduced into the structure to reduce gate leakage. However, adding the AlGaN cap also reduces the aspect ratio, which is undesirable for highly scaled devices with small gate length in high-frequency application. A balance between the gate leakage and short channel effect needs to be considered during structure design.

1.2.5 State-of-art of N-polar HEMT devices

In order to suppress surface states related scattering and dispersion, a thick in-situ GaN cap layer was grown on top of the AlGaN cap to move the trap states associated with the ex-situ surface far from the channel [Figure 1.9]. [34,35,36] This is called a deep recess structure. The design also improves the access region (where the GaN cap is not etched) conductivity and minimizing source-choke effects[37] due to the built-in polarization of the structure.

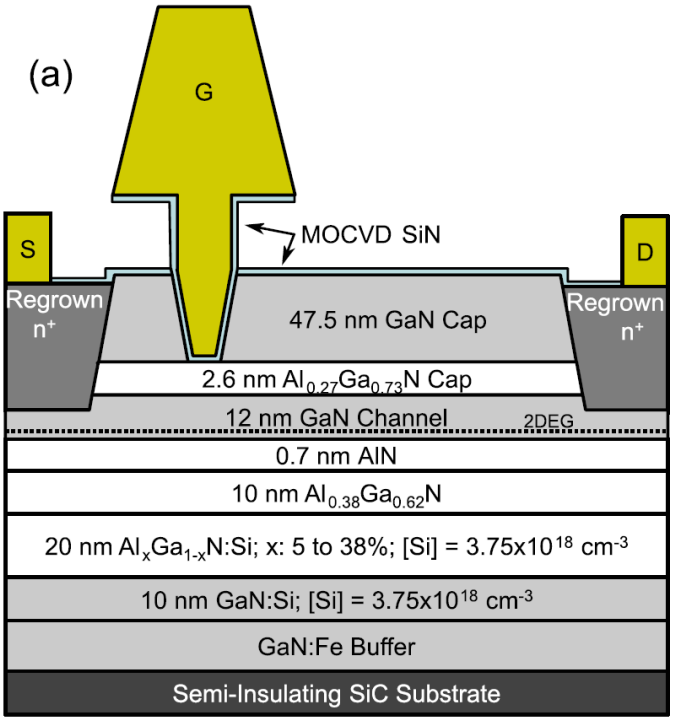

Figure 1.9 Device cross-sectional schematic (not drawn to scale) and epitaxial layer profile of the N-polar deep recess MISHEMT with the foot-gate self-aligned to the GaN cap recess.[36]

The state-of-the-art output power density (P_o) and power-added-efficiency (PAE) at 94 GHz were reported by Romanczyk *et al.* in 2018 with the structure shown in Figure 1.9.[36] High P_o and PAE were obtained simultaneously. The peak PAE of 28.8% was measured at 16 V with 5.3 W/mm associated P_o and the peak P_o of 7.94 W/mm was measured at 20 V, while the PAE remains above 26.9%.

As shown in Figure 1.10, in W-band, the 7.94 W/mm peak output power density of this device represents more than two times improvement in power density over the best previously reported Ga-polar device with a comparable PAE.

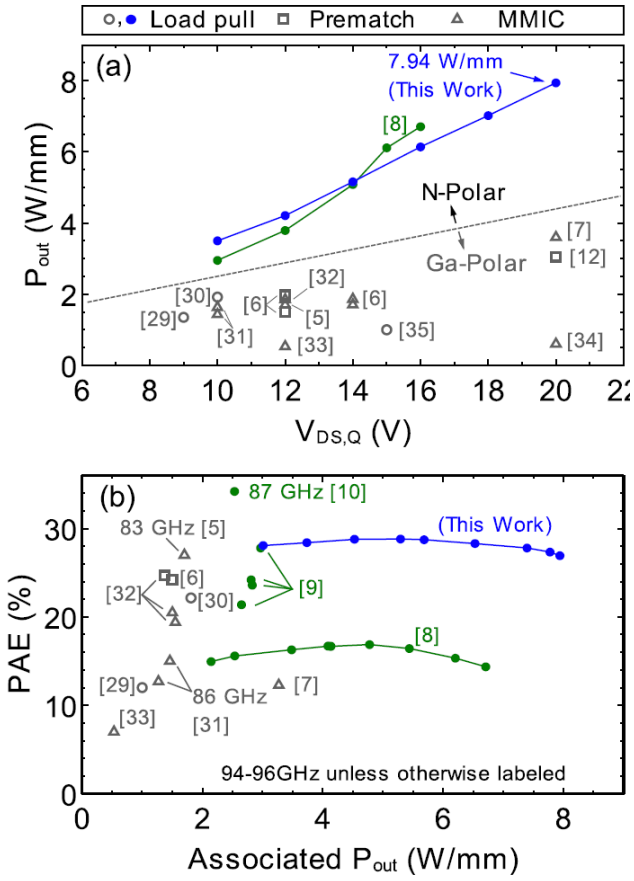

Figure 1.10 Comparison of 94-GHz load-pull results from this paper with prior N-polar devices (green circles) and W-band Ga-polar devices and MMICs reported in the literature (grey). (a) P_o as a function of $V_{DS,Q}$ showing N-polar offering greater power at a given V_{DS}. (b) PAE as a function of associated P_o where this paper demonstrates the highest reported combination of reported device-level efficiency and power density in W-band.[34]

Additionally, Zheng *et al.* presented a high power gain cutoff frequency (f_{max}) of 248 GHz together with a high breakdown voltage of 114 V for a device with an epitaxial structure design without the thick GaN cap.[38] A thick PECVD SiN_x layer was instead used to passivate the surface states and address dispersion. In 2018, the same authors reported a

high $f_{max} \cdot V_{DS,Q}$ of 8.1 THz·V, exhibiting great potential of the device in high-frequency power applications.[39]

1.3 *Channel thickness scaling in N-polar HEMTs*

1.3.1 Challenges in channel thickness scaling for N-polar HEMTs

As the channel thickness (t_{ch}) decreases, the electric field in the channel increases, the sheet charge density in the channel decreases and the centroid of the 2DEG moves closer to the back-barrier/channel interface, resulting in a sharp decrease of the electron mobility (μ) in HEMT structures with ultra-scaled channels.[40,41] Considering that the alloy scattering is suppressed by the AlN interlayer between the AlGaN back-barrier and GaN channel, we speculate that the scattering at the AlN/GaN interface is the major reason for the mobility drop with decreasing t_{ch}.

Singisetti *et al.* reported 2DEG density and mobility drop with decreasing channel thickness [Figure 1.11(b)] in N-polar AlGaN/GaN HEMT structures [Figure 1.11(a)] in 2012.[40] The mobility decrease became sharper for thinner channels. With a channel thickness of 3.5 nm, the electron mobility dropped below 100 cm^2/Vs with a sheet charge density smaller than 5×10^{12} cm^{-2}. The n_s decreased due to the depletion from the surface pinning at the GaN/SiN_x interface, and the authors suggested the GaN/AlN interface roughness scattering being the dominant reason for the mobility drop with decreasing channel thickness.

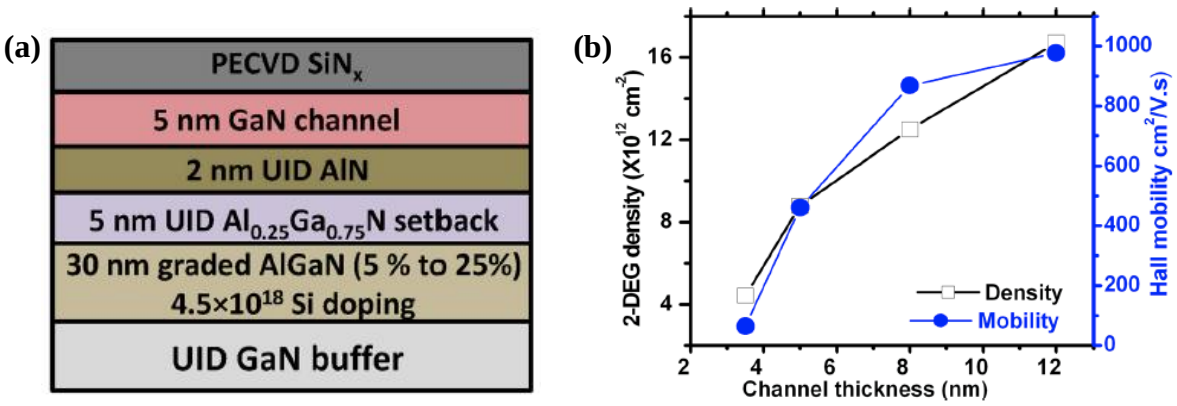

Figure 1.11 (a) Schematic of a N-polar AlGaN/GaN HEMT structure. (b) 2DEG densities and mobilities measured by room temperature Hall for N-polar HEMT structures shown in (a) with various channel thicknesses.[40]

In a recent report, Ahmadi *et al.* attributed this mobility drop to an increase in charged interface states (CIS) scattering, which worsens as the 2DEG wavefunction moves closer to the AlN/GaN interface and as the n_s of the 2DEG reduces due to less screening.[42] According to Ahmadi's mobility model for the N-polar AlGaN/GaN HEMT structures, the CIS scattering limited mobility dropped below 7500 and 2000 cm^2/Vs when the channel thickness decreased to 7 and 5 nm, respectively, assuming a charged interface state density of 8×10^{11} cm^{-2}, [Figure 1.12] while the interface roughness scattering limited mobility was in the range of 3×10^5 to 6×10^5 cm^2/Vs for all the simulated channel thicknesses.[43]

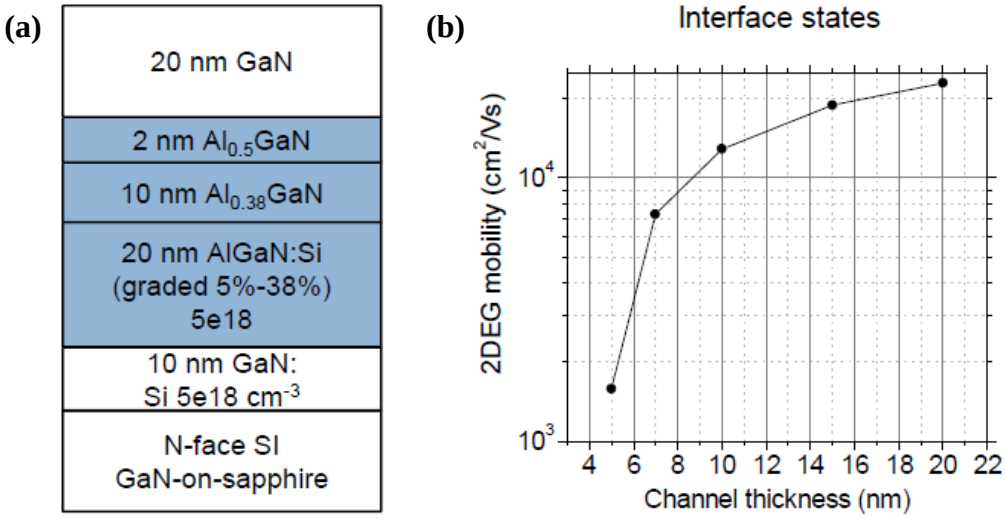

Figure 1.12 (a) Schematic of a N-polar AlGaN/GaN HEMT structure and (b) the charged interface states scattering limited mobility calculated using Ahmadi's mobility model for the structure shown in (a) with various channel thicknesses.[43]

1.3.2 Former effort in channel thickness scaling

One approach previously reported by Lu et al. to achieve high conductivity in N-polar ultra-thin channel HEMTs was to insert an InAlN layer into the conventional AlGaN back-barrier, thereby increasing n_s to achieve a better screening of the scattering centers and hence mitigate the mobility degradation as t_{ch} decreased.[44] All samples were grown in a vertical reactor with the susceptor 10 cm away from the showerhead. Three different structures with various back-barrier designs of AlN/$In_{0.18}Al_{0.82}N$ (series-1, variable: InAlN thickness), AlN/$In_{0.18}Al_{0.82}N$/$Al_{0.35}Ga_{0.65}N$ (series-2, variable: InAlN thickness) and AlN/$Al_{0.35}Ga_{0.65}N$/$In_{0.18}Al_{0.82}N$ (series-3, variable: AlGaN thickness) were investigated [Figure 1.13]. No AlGaN cap was deposited on any of the samples. The structure with the lowest R_{sh} in each series was chosen for the channel scaling experiments.[44]

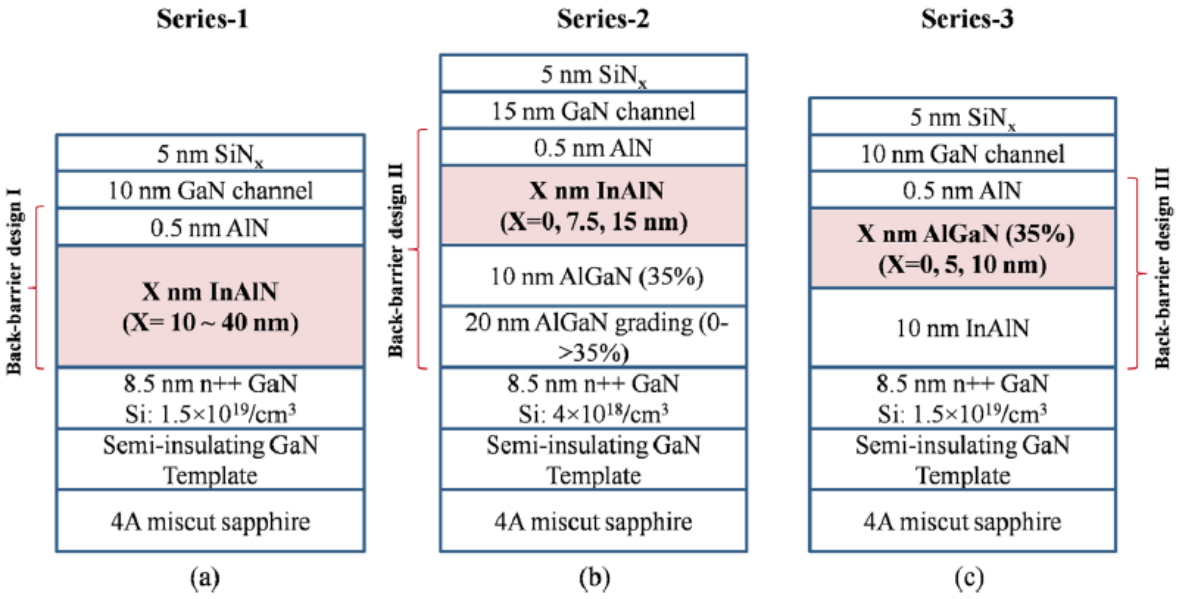

Figure 1.13 Schematic of epitaxial structures for different back barrier designs: (a) series-1 with an AlN/InAlN back barrier; (b) series-2 with an AlN/InAlN/AlGaN back barrier; (c) series-3 with an AlN/AlGaN/InAlN back barrier. Highlighted layers are with various thicknesses.[44]

Note that since 4˚ misoriented substrates were used to ensure the growth of high quality N-polar films, the associated crystal misorientation resulted in the formation of surface steps, which in turn lead to a higher electron mobility parallel to the steps compared to the perpendicular direction. In devices, the higher μ parallel to the steps is taken advantage of by aligning the devices in such a way that the electron transport occurs parallel to the steps.[45] Transmission line measurements (TLM) were done to obtain the sheet resistance (R_{sh}) parallel to the steps, according to which parallel mobility can be calculated using n_s measured by Hall.

Figure 1.14 shows the sheet charge density, electron mobility and sheet resistance measured by room temperature Hall for different channel thicknesses in samples with three

different back-barrier designs: (a) 0.5-nm-AlN/25-nm-$In_{0.18}Al_{0.82}N$, (b) 0.5-nm-AlN/10-nm-$Al_{0.35}Ga_{0.65}N$/10-nm-$In_{0.18}Al_{0.82}N$ and (c) 0.5-nm-AlN/7.5-nm-$In_{0.18}Al_{0.82}N$/30-nm-$Al_{0.35}Ga_{0.65}N$. While both design-a and -c showed pretty flat n_s and μ values, design-c presented the best mobility and sheet resistance as the channel thickness scaled down to 5.3 nm. High channel conductivities with $R_{sh,//}$ = 230 ohm/sq, $n_s = 2\times10^{13}$ cm^{-2} and $\mu_{//}$ = 1400 cm^2/Vs were obtained.[44]

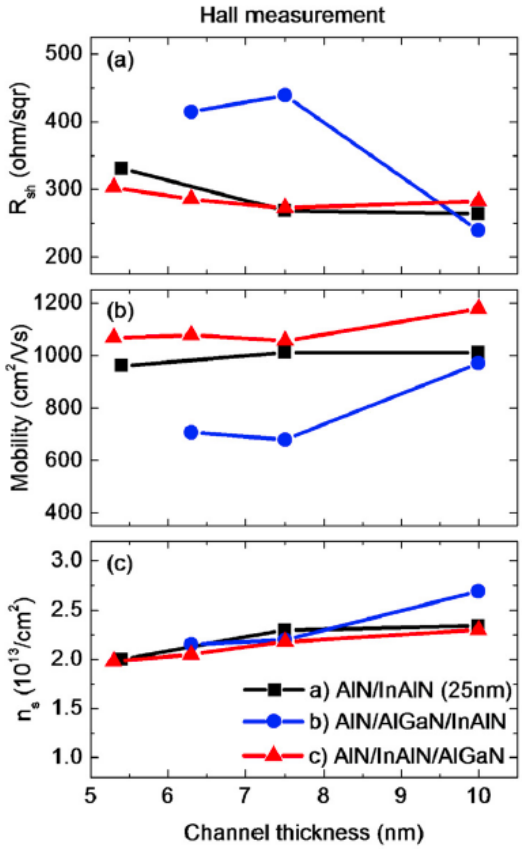

Figure 1.14 The impact of scaling the channel-thickness on (a) hall sheet resistance, (b) hall mobility, and (c) 2DEG charge density, in each of the design methodologies (Design-a: 0.5-nm-AlN/25-nm-$In_{0.18}Al_{0.82}N$, Design-b: 0.5-nm-AlN/10-nm-$Al_{0.35}Ga_{0.65}N$/10-nm-$In_{0.18}Al_{0.82}N$, and Design-c: 0.5-nm-AlN/7.5-nm-$In_{0.18}Al_{0.82}N$/30-nm-$Al_{0.35}Ga_{0.65}N$).[44]

The channel thickness of the HEMT structure with a back-barrier design of 0.5-nm-AlN/7.5-nm-$In_{0.18}Al_{0.82}N$/30-nm- $Al_{0.35}Ga_{0.65}N$ (Design-c) was further shrunk down to 4.3 nm. However, sharp drop of n_s and μ was observed. In order to recover n_s, the InAlN thickness was increased to 15 nm, leading to 30% increase of n_s and 80% increase of μ. [Figure 1.15] The parallel sheet resistance was measured $R_{sh,//}$ = 294 ohm/sq.[41]

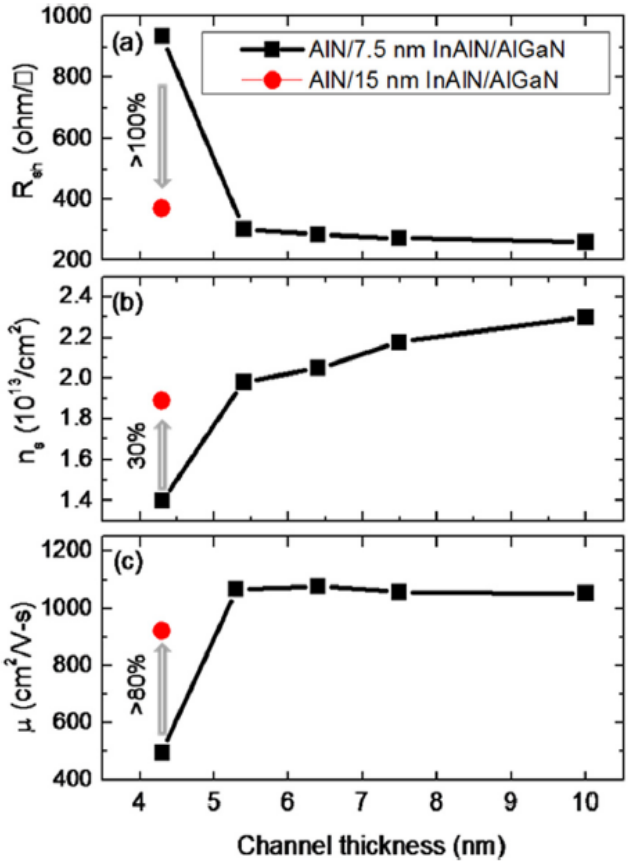

Figure 1.15 Hall measurements showing the dependence of (a) sheet resistance (R_{sh}), (b) 2DEG charge density (n_s), and (c) mobility (μ) on the channel-thickness. Comparative trends for 2DEG-channels with two InAlN thicknesses in the back-barrier designs are shown wherein, black squares denote the 7.5-nm-thick InAlN, red circles 15-nm-thick InAlN.

Block arrows signify the changes observed in R_{sh}, n_s, and l for t_{ch} = 4 nm with increasing InAlN barrier thickness.[41]

As the channel thickness was scaled down to 3.2 nm, negligible improvement of conductivities in the channel was observed even the InAlN thickness was increased to 40 nm. The band diagrams in Figure 1.16 explained the phenomenon. Considering the high unintentional oxygen doping level in the N-polar InAlN films, when the InAlN layer grew thicker than 15 nm, the effective barrier high gradually decreased with increasing layer thickness, leading to more 2DEG wave function penetration into the barrier. Moreover, the thicker InAlN layers introduced higher interface roughness due to the low growth temperature necessary for In incorporation.[41]

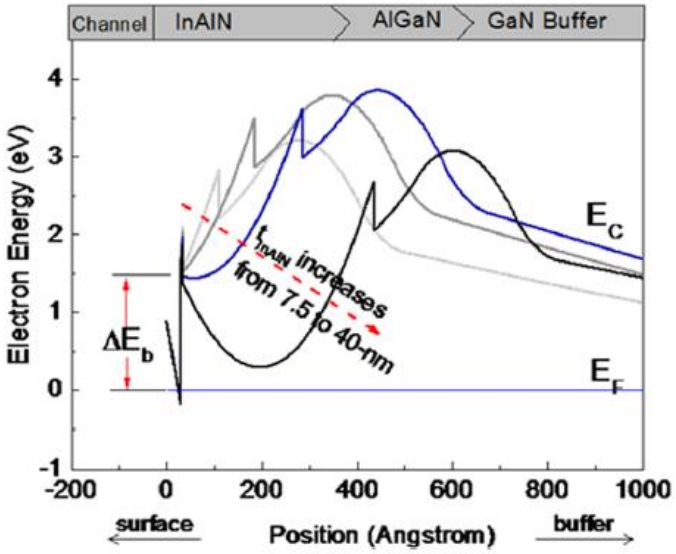

Figure 1.16 Comparison of the simulated band diagrams for the epitaxial structures consisting of 7.5 (light grey), 15 (dark grey), 25 (blue), and 40 nm (black) thick InAlN layers.[41]

An alternative method was introduced to increase n_s and the effective barrier height. As shown in Figure 1.17, by adding a 2 nm thick layer graded from InAlN to AlN, the effective barrier height increased, leading to an increase of n_s by > 30%, μ by > 140% and a decrease of R_{sh} by > 200%. [Figure 1.18] High n_s = 1.8e13 cm-2, $\mu_{//}$ = 896 cm2/Vs and low $R_{sh,//}$ = 329 ohm/sq were achieved for the sample with 3.2 nm thick channel.[41]

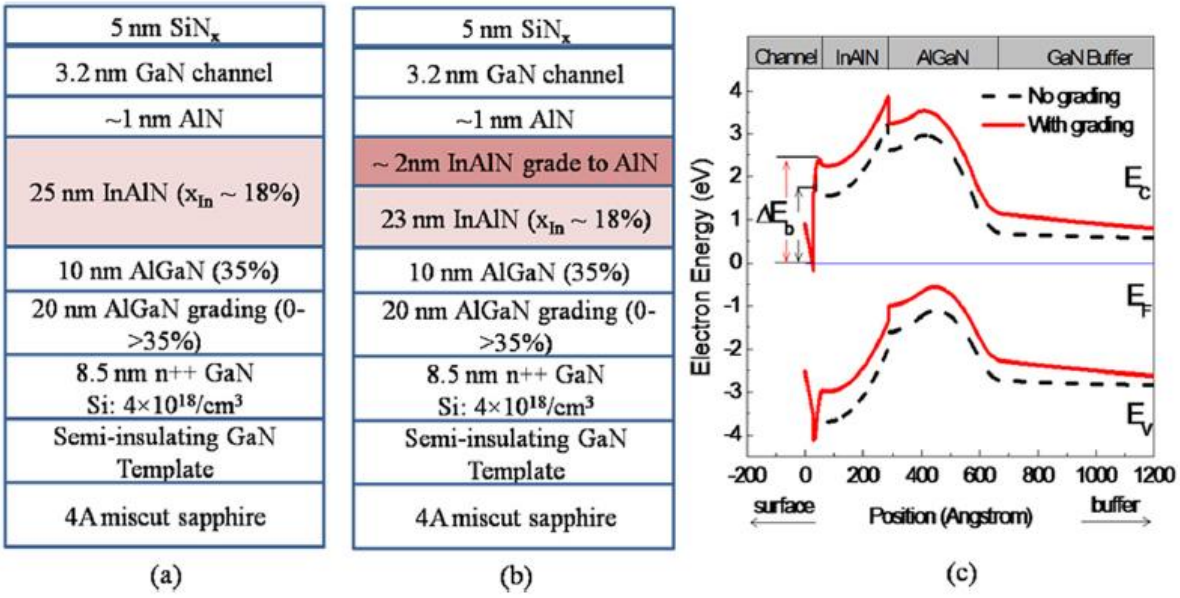

Figure 1.17 Schematic of epitaxial structures for 3-nm-thick channel HEMTs: (a) without and (b) with a grade in InAlN layer. Specifically, the grade was applied in a 2-nm-thick transition region wherein the In composition was varied from 18% to 0%. (c) Comparison of the simulated band diagrams for the epitaxial structures with/without grading in the InAlN layer.[41]

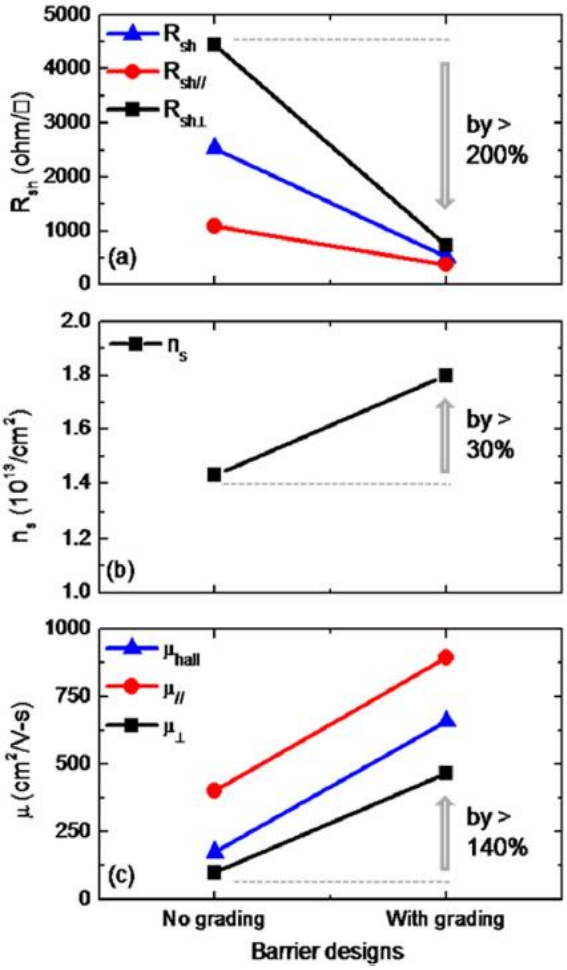

Figure 1.18 For HEMTs with t_{ch} = 3 nm, (a) sheet resistance (R_{sh}, $R_{sh,//}$, $R_{sh,\perp}$), (b) 2DEG charge density (n_s), and (c) mobility (μ, $\mu_{//}$, $\mu_{\perp}$) versus the back barrier design, wherein one is with and the other without grading in the InAlN layer. Arrows show the significant improvements observed in R_{sh}, n_s, and μ when implementing the grade into the barrier design.[41]

However, when adding an AlGaN cap, the 2DEG will be partially depleted by the net negative polarization charge at the AlGaN cap / GaN channel interface and it becomes more difficult to scale the channel thickness down to 3 nm, while an AlGaN cap is beneficial to

suppress gate leakage in a device. Thereby, further investigations into channel thickness scaling in HEMT structures with AlGaN caps is necessary to widen the design window of scaled HEMT devices.

1.4 *This work*

This dissertation focuses on two major aspects of the design and growth of AlGaN/GaN HEMT structures by MOCVD: the AlN interlayer and gate-to-2DEG distance scaling, especially for the N-polar devices.

It is worth mentioning that all samples discussed in this work were grown in a close-coupled showerhead reactor with a distance of 0.7 cm between the susceptor and showerhead, if not specified otherwise, because the non-ideality of the AlN deposition under investigation is very likely to be reactor-dependent, which will be discussed in detail in Chapter 3.

As the beginning of this work, Chapter 2 demonstrates thick AlGaN films with high Al-compositions fully strained to GaN in GaN/AlGaN/GaN heterostructures grown by MOCVD and discusses the relaxation mechanisms of AlGaN on GaN. Thin GaN caps are shown to be highly effective to protect AlGaN layers from relaxation. This result widens the design window of the structures in the following investigations into AlN films and AlGaN/GaN HEMT structures.

In Chapter 3, the impacts of growth temperatures, carrier gases, TMAl and NH_3 flows, reactor pressures and other variations in the growth process on the property of metal-polar AlN films are investigated. Three major aspects, the Al compositions, surface morphologies and electrical properties of the GaN/AlN/GaN heterostructures, are examined. The major

source of the unintentional Ga is identified and the reason for the significant 2DEG mobility improvement introduced by adding the nominal AlN interlayers, which actually contain 40 – 50% Ga, is analyzed. Selected growth conditions are investigated for N-polar AlN growth and Chapter 4 reports the results, including the Al compositional profiles, electrical data and interface morphologies of the N-polar GaN/AlN/GaN heterostructures. The difference between metal- and N-polar AlN films grown by MOCVD is discussed.

Chapter 5 focuses on channel thickness scaling for the N-polar AlGaN/GaN HEMTs. The process of scaling down the pure GaN channel thickness to 8 nm by modifying the Si doping level in the back-barrier and the Al composition of the AlGaN cap is first presented. To further reduce the channel thickness, we propose a N-polar HEMT structure with GaN/InGaN composite channel which maintains high 2DEG density and mobility for ultra-scaled channel thicknesses by introducing a net positive polarization charge at the GaN/InGaN interface. The design was demonstrated by MOCVD and proven to be exceptionally effective, and thus has the potential to improve the lateral scalability of N-polar HEMT devices for high-frequency operations.

Chapter 6 summarizes the work and provides several outlooks about the future works to improve material qualities and to facilitate the design of N-polar AlGaN/GaN HEMT structures.

1.5 *References*

[1] O'Leary K, Foutz B E, Shur M S, Eastman L F, *J Mat Sci: Mater Electron* **17**, 87 (2006).

[2] Ambacher O, *J. Phys. D: Appl. Phys*. **31**, 2653 (1998).

[3] Gaska R, Osinsky A, Yang J W, Shur M S, *IEEE Electron Device Lett*.**19**, 89 (1998).

[4] NSM Archive at http://www.ioffe.ru/SVA/NSM/Semicond/

[5] Grundmann M, BANDENG (http://my.ece.ucsb.edu/mgrundmann/bandeng).

[6] Johnson E, *IRE International Convention Record* **13**, 27 (1966).

[7] Baliga B J, *IEEE Electron Device Lett*.**10**, 455 (1989).

[8] Asif Khan M, Bhattarai A, Kuznia J N, Olson D T, *Appl. Phys. Lett*. **63**, 1214 (1993).

[9] Wu Y F, Keller B P, Keller S, Kapolnek D, DenBaars S P, Mishra U K, *IEEE Electron Device Lett.* **17**, 455 (1996).

[10] Shinohara K, Regan D, Corrion A, Brown D, Tang Y, Wong J, Candia G, Schmitz A, Fung H, Kim S, Micovic M, IEEE International Electron Devices Meeting (IEDM), 27.2.1 - 27.2.4, 2012.

[11] Wu Y F, Moore M, Saxler A, Wisleder T, Parikh P, Device Research Conference, 64th, pp.151-152, 2006.

[12] Wu Y F, Saxler A, Moore M, Smith R P, Sheppard S, Chavarkar P M, Wisleder T, Mishra U K, Parikh P, *IEEE Electron Device Lett.* **25**, 117 (2004).

[13] Wu Y F, Moore M, Abrahamsen A, Jacob-Mitos M, Parikh P, Heikman S, Burk A, IEEE International Electron Devices Meeting (IEDM), pp.405-407, 2007.

[14] Palacios T, Chakraborty A, Rajan S, Poblenz C, Keller S, DenBaars S P, Speck J S, Mishra U K, *IEEE Electron Device Lett*. **26**, 781 (2005).

[15] Jessen G H, Fitch R C, Gillespie J K, Via G, Crespo A, Langley D, Denninghoff D J, Trejo M, Heller E R, *IEEE Trans. Electron Devices* **54**, 2589 (2007).

[16] T. Palacios, *Phys. Status Solidi* A **206**, 1145 (2009).

[17] Palacios T, Chakraborty A, Heikman S, Keller S, DenBaars S P, Mishra U K, IEEE *Electron Device Lett.* **27**, 13 (2006).

[18] Lee D S, Gao X, Guo S, Kopp D, Fay P, Palacios T, *IEEE Electron Device Lett*. **32**, 1525 (2011).

[19] Nidhi, Brown D F, Keller S, and Mishra U K, *Jpn. J. Appl. Phys*. **49**, 021005 (2010).

[20] Grandjean N, Massies J and Leroux M, *Appl. Phys. Lett*. **69**, 2071 (1996).

[21] Sumiya M, and Fuke S, *MRS Internet J. Nitride Semicond. Res*. **9**, 1 (2004).

[22] Sasaki T and Matsuoka T, *J. Appl. Phys*. **64**, 4531 (1988).

[23] Dimitrov R, Murphy M, Smart J, Schaff W, Shealy J R, Eastman L F, Ambacher O, Stutzmann M, *J. Appl. Phys*. **87**, 3375 (2000).

[24] Sumiya M, Yoshimura K, Ito T, Ohtsuka K, Fuke S, Mizuno K, Yoshimoto M, Koinuma H, Ohtomo A, and Kawasaki M, *J. Appl. Phys*. **88**, 1158 (2000).

[25] Keller S, Li H, Laurent M, Hu Y, Pfaff N, Lu J, Brown D F, Fichtenbaum N A, Speck J S, DenBaars S P and Mishra U K, *Semicond. Sci. Technol.* **29**, 113001 (2014).

[26] Keller S, Fichtenbaum N A, Wu F, Brown D, Rosales A, DenBaars S P, Speck J S, and Mishra U K, *J. Appl. Phys*. **102**, 083546 (2007).

[27] Chini A, Fu Y, Rajan S, Speck J, Mishra U K, 32nd international symposium on compound semiconductors (ISCS), vol 1, pp 1–2 (2005).

[28] Rajan S, Chini A, Wong M H, Speck J S, Mishra U K, *J. Appl. Phys.* **102**, 044501 (2007).

[29] Wong M H, Singisetti U, Lu J, Speck JS, Mishra UK, *IEEE Trans. Electron Devices* **59**, 2988 (2012).

[30] Wienecke S, Guidry M, Li H, Ahmadi E, Hestroffer K, Zheng X, Keller S, Mishra U K, (poster) 2014 IEEE lester eastman conference, New York, 5–7 Aug 2014.

[31] Shen L, Heikman S, Moran B, Coffie R, N -Q Zhang, Buttari D, Smorchkova I P, Keller S, DenBaars S P, and Mishra U K, *IEEE Electron Device Lett.* **22**, 457 (2001).

[32] Kolluri S, Member S, Keller S, Denbaars S P, Mishra U K, *IEEE Electron Device Lett.* **33**, 44 (2012).

[33] Lu J, Hu Y L, Brown D F, Wu F, Keller S, Speck J S, DenBaars S P and Mishra U K, *Japan. J. Appl. Phys*. **51**, 115502 (2012).

[34] Wienecke S, Romanczyk B, Guidry M, Li H, Ahmadi E, Hestroffer K, Zheng X, Keller S, and Mishra U K, *IEEE Electron Device Lett.* **38**, 359 (2017).

[35] Romanczyk B, Guidry M, Wienecke S, Li H, Ahmadi E, Zheng X, Keller S, and Mishra U K, *in Electron Devices Meeting (IEDM), 2016 IEEE International,* San Francisco, USA, 3-7 Dec. 2016, pp. 67-70.

[36] Romanczyk B, Wienecke S, Guidry M, Li H, Ahmadi E, Zheng X, Keller S, and Mishra U K, *IEEE Trans. Electron Devices,* **65** 45 (2018).

[37] Palacios T, Rajan S, Chakraborty A, Heikman S, Keller S, DenBaars S P, and Mishra U K, *IEEE Trans. Electron Devices* **52**, 2117 (2005).

[38] Zheng X, Guidry M, Li H, Ahmadi E, Hestroffer K, Romanczyk B, Wienecke S, Keller S and Mishra U K, *IEEE Electron Device Lett.* **37**, 77 (2016).

[39] Zheng X, Li H, Guidry M, Romanczyk B, Ahmadi E, Hestroffer K, Wienecke S, Keller S and Mishra U K, *IEEE Electron Device Lett.* **39**, 409 (2018).

[40] Singisetti U, Wong M H, and Mishra U K, *Appl. Phys. Lett.* **101**, 012101 (2012).

[41] Lu J, Zheng X, Guidry M, Denninghoff D, Ahmadi E, Lal S, Keller S, Denbaars S P, Mishra U K, *Appl. Phys. Lett.* **104**, 092107 (2014).

[42] Ahmadi E, Keller S, Mishra U K, *J. Appl. Phys.* **120**, 115302 (2016).

[43] Elaheh Ahmadi, "Growth Optimization of III-N Electronic Devices by Plasma-Assisted Molecular Beam Epitaxy", Ph.D. dissertation, University of California, Santa Barbara, 2015.

[44] Lu J, Denninghoff D, Yeluri R, Lal S, Gupta G, Laurent M, Keller S, DenBaars S P and Mishra U K, *J. Appl. Phys.* **102**, 232104 (2013).

[45] Keller S, Suh C S, Fichtenbaum N A, Furukawa M, Chu R, Chen Z, Vijayraghavan K, Rajan S, DenBaars S P, Speck J S, and Mishra U K, *J. Appl. Phys.* **104**, 093510 (2008).

Chapter 2

Impact of thin GaN cap layers on the properties of AlGaN/GaN heterostructures

With 3% lattice mismatch between GaN and AlN, the critical thickness, d_{crit}, of the $Al_xGa_{1-x}N$ layers, corresponding to the maximum thickness at which an unrelaxed layer can be deposited, significantly decreases with increasing x_{Al}.[1,2,3] To minimize strain-related degradation, in typical Ga-polar devices $Al_xGa_{1-x}N$ layers with $x \leq 0.3$ are utilized. At thicknesses beyond d_{crit}, relaxation-related defects form, initially in form of platelets and trenches, followed by surface cracks and channel cracks, the latter of which can laterally propagate until terminating at another crack or the wafer edge.[2,4,5,6] This defect formation is accompanied by a degradation of the electrical properties of the HEMT structures. [7,8,9] Therefore, the sheet charge density of the 2DEG is limited by the thickness of the high-Al-composition AlGaN layer that can be grown without detrimental degradation.[10] In particular for scaled transistors, however, high-Al-composition AlGaN or AlN gating layers are very attractive, as they enable the design of device structures with very thin gating layers while maintaining a high channel charge.[11] Previous experiments showed that in-situ deposited Si_3N_4 cap layers could mitigate the defect formation and improve electrical properties in $Al_xGa_{1-x}N$/GaN HEMT structures with $x_{Al} = 0.3 – 0.4$.[12,13,14] An increase in critical thickness was also observed for AlGaN layers embedded in superlattice structures.[15] Following the Matthews-Balkeslee model,[16] the critical thickness of sandwiched lattice-mismatched epitaxial layers was twice of that in single heterostructures.[17] While single GaN

cap layers have been investigated in the past, their impact was studied primarily on $Al_xGa_{1-x}N$/GaN structures with $x \leq 0.3$. The application of thicker GaN cap layers was limited as the sheet charge density in the 2DEG decreases with increasing GaN cap layer thickness.[18] Thinner cap layers were mainly employed to reduce gate and drain leakage currents[19] and current collapse.[20] A thin GaN cap layer was also shown to result in smoother surface step edges compared to uncapped samples.[9] In this study, we presented a comprehensive investigation on the impact of 0.6 to 2.4 nm thick GaN cap layers on the structural and electrical properties of $Al_xGa_{1-x}N$/GaN HEMT structures with $x_{Al} \sim 0.5$ and AlGaN layer thicknesses ranging from 5 to 30 nm. The results show that GaN cap layers as thin as 0.6 nm can result in a significant improvement of the surface morphology and increase in the sheet charge density (n_s) and/or electron mobility (μ) of the 2DEG compared to uncapped samples. In addition, GaN was shown to be a superior capping material than in-situ grown Si_3N_4, which was also investigated for comparison.

2.1 *Experiment*

The Ga-polar AlGaN/GaN HEMT structures were deposited on c-plane sapphire substrates by metalorganic chemical vapor deposition (MOCVD) using the precursors trimethylgallium (TMGa), trimethylaluminum (TMAl) and ammonia (NH_3). The 2 μm S.I. GaN base layers were grown using the standard two-step method.[21] 5 to 30 nm thick $Al_xGa_{1-x}N$ layers with x_{Al} varying from 0.47 to 0.53 were grown using a constant TMGa flow of 4.5 μmol/min and varying the TMAl flow from 5.6 to 8.3 μmol/min. The ammonia flow was kept constant at 0.18 mol/min. The growth temperature and reactor pressure were 1145 °C and 100 Torr. The HEMT structures were then capped with 0, 0.6, 1.2, or 2.4 nm

thick GaN layers grown under the same condition as the AlGaN layers with a TMGa flow of 17 μmol/min. For comparison, selected experiments were performed using an in-situ Si_3N_4 cap, which was grown at 1020 °C and 500 Torr, with 0.27 mol/min ammonia flow and 0.45 mmol/min disilane flow. No AlN interlayer was used in these experiments in order to ease the data analysis.

High-resolution X-ray diffraction (XRD) with a Panalytical MRD PRO Materials Research Diffractometer was used to determine Al composition and AlGaN layer thickness of the samples. In addition, reciprocal space maps were recorded around the asymmetric $(10\bar{1}5)$ reflection to determine the degree of relaxation of the AlGaN layers. Atomic force microscopy (AFM) images were taken with a Veeco Dimension 3000 Scanning Probe Microscope to analyze the surface morphology. The sheet charge density and mobility of the 2DEG were determined by room temperature Van der Pauw - Hall measurements.

2.2 *Impact of 2.4 nm thick GaN cap on AlGaN/GaN heterostructures*

2.2.1 Surface morphology

The AFM images for the samples with different AlGaN thickness in Figure 2.1 represent the typical morphologies for $Al_xGa_{1-x}N$/GaN heterostructures. While uncapped samples with thin and/or low x_{Al} layers exhibited surface steps similar to the GaN layer underneath,[21] thick and/or high x_{Al} layers resulted in a surface morphology characterized by small platelets separated by trenches, as shown in Figure 2.1(b) and (d), in which the $Al_{0.53}Ga_{0.47}N$ layers were 5.7 and 21 nm thick, respectively. Even thicker and/or higher-Al-composition AlGaN layers, as shown in Figure 2.1(f) for 29.5 nm thick $Al_{0.53}Ga_{0.47}N$, exhibited extended channel

cracks, predominantly along the <11$\bar{2}$0> direction. As reported previously, fewer platelets and trenches were seen in areas adjacent to channel cracks[4]. Interestingly, an in-situ grown 2.4 nm GaN cap significantly suppressed the formation of platelets and trenches for the samples with an $Al_{0.53}Ga_{0.47}N$ thickness up to 21 nm [Figure 2.1(c)], which exhibited only short surface cracks starting at the intersections of the threading dislocations (TDs) with the surface. While channel cracks are unstable and propagate laterally until terminating at another crack or the wafer edge, surface cracks are self-limiting in lateral extent.[1,2,3] When AlGaN layers with high x_{Al} exceeded a certain thickness, channel cracks formed for both, uncapped and capped samples. For the capped samples, some of the cracks could be overgrown [Figure 2.1(e)].

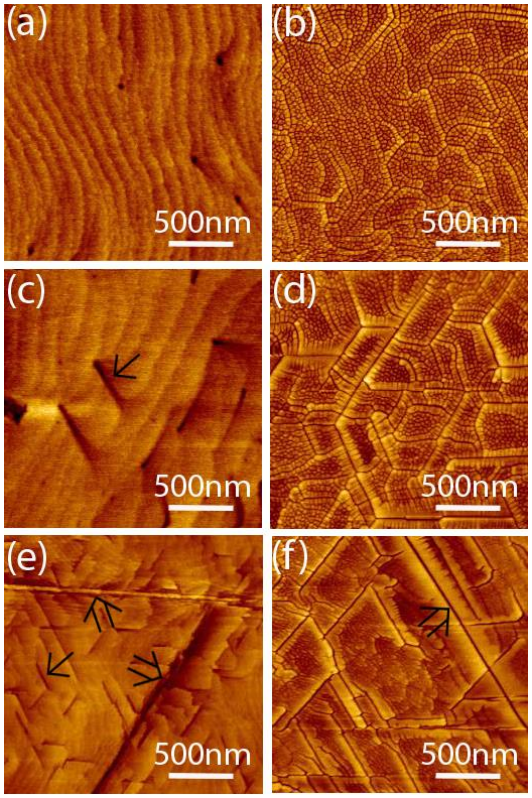

Figure 2.1 AFM images of $Al_{0.53}Ga_{0.47}N$/GaN HEMT samples with 2.4 nm thick GaN cap layers and AlGaN thickness of a) 5.7 nm, c) 21 nm, and e) 29.5 nm; uncapped

complementary samples with AlGaN thickness of b) 5.7 nm, d) 21 nm, and f) 29.5 nm (grey scale: 5 nm for (a)(c), 10 nm for others); Examples of surface and channel cracks are marked by single and double line arrows, respectively.

2.2.2 Electrical properties

The impact of GaN cap layers on the electrical properties of the 2DEG in AlGaN/GaN HEMT structures with different AlGaN layer thickness is illustrated in Figure 2.2, comparing the sheet charge density and electron mobility of the uncapped and 2.4 nm thick GaN capped samples with $Al_{0.53}Ga_{0.47}N$ layers of different thickness. For samples with 5.7 nm thick AlGaN layers, the cap increased the n_s and μ values from 5.5×10^{12} to 1.2×10^{13} cm^{-2} and 30 to 1370 cm^2/Vs, respectively. For those with $Al_{0.53}Ga_{0.47}N$ layers between 11 and 18 nm, the n_s values were largely unaffected by the GaN caps, and also the mobility was only about 100 cm^2/Vs higher for capped samples. For samples with even thicker $Al_{0.53}Ga_{0.47}N$ layer, the capped one exhibited high n_s and μ values while the uncapped sample was highly resistive. Nevertheless, when the AlGaN layer thickness exceeded 30 nm, also the electron mobility of the capped sample dropped to 170 cm^2/Vs. Surprisingly, the n_s value remained high (1.9×10^{13} cm^{-2}).

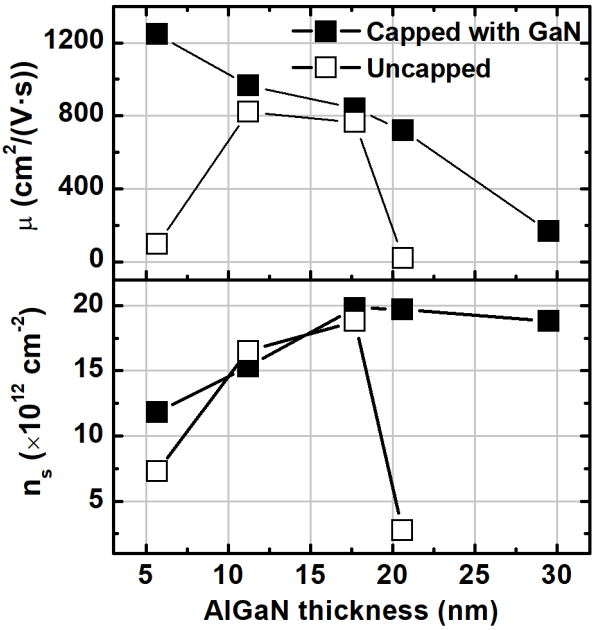

Figure 2.2 Sheet charge density and electron mobility of the 2DEG for either capped or uncapped $Al_{0.53}Ga_{0.47}N$/GaN HEMT structures with different AlGaN layer thickness; solid square: samples capped with 2.4 nm thick GaN layers, hollow square: uncapped samples.

2.2.3 Discussion

The energetically preferred relaxation mechanisms in strained (0001) AlGaN are roughening and cracking rather than misfit dislocation (MD) formation, due to the absence of an effective primary slip system.[1,3,5,6] Cracks can either initiate at threading dislocations,[5] shown as black dots in Figure 2.1(a), or at minima of the surface profile.[22,23] These cracks are initially localized. As the strain in the layer increases, channel cracks also form, which propagate laterally without constraints,[2,3,4,5] as shown in Figure 2.1(e) and (f). In addition to crack formation, the strain in the epitaxial layer can be relieved through roughening,[3,6,23] here seen in the form of the platelets, or mesas as called by Vennéguès *et al.*, and trenches

[Figure 2.1(b) and (d)]. [24] The trenches between the mesas were characterized by well-defined inclined facets, differentiating them from cracks, as shown in the TEM investigations of similar samples by Vennéguès *et al*.[24] The trenches reached or got close to the (Al,Ga)N/GaN interface in thin samples, but not thicker ones.

As the sheet charge of the 2DEG which forms at the AlGaN/GaN interface results from the spontaneous and piezoelectric polarization in the AlGaN layer, the surface morphologies are closely related to the electrical properties of the investigated heterostuctures.[7,8,9] Thereby the electron mobility can be affected even in the absence of trenches or cracks penetrating through the (Al,Ga)N interface, as the local relaxation of the AlGaN layer in the vicinity of shallower trenches still results in lateral fluctuations in the piezoelectric field leading to increased electron scattering.

While all uncapped samples with 5.7 to 18 nm thick $Al_{0.53}Ga_{0.47}N$ layers exhibited platelets and trench networks, only the sample with 5.7 nm thick $Al_{0.53}Ga_{0.47}N$ layer was highly resistive [Figure 2.2]. The observation that the platelets and trenches on the surfaces of the uncapped samples [Figure 2.1(b) and (d)] only affected the electrical properties of the sample with the 5.7 nm thick $Al_{0.53}Ga_{0.47}N$ layer, but not the 18 nm thick one, for example, suggests that the apexes of trenches got close to the AlGaN/GaN interface only for the thinner AlGaN layers, similar to the observations by Vennéguès *et al*.[24] For this reason, the thin GaN cap layers, which suppressed the degradation of the AlGaN layer, led to a strong improvement of the electrical properties of the samples with thin AlGaN layers.

The results further indicate that for samples with thicker $Al_{0.53}Ga_{0.47}N$ layers up to a thickness of 18 nm, the platelets and trenches only formed in the top section of the uncapped AlGaN layers, whereas the bottom of the AlGaN layer was unaffected, as observed

previously by Vennéguès *et al*. as well.[24] For this reason the GaN cap layers did not lead to a significant improvement of the electrical properties for samples with 18 nm thick $Al_{0.53}Ga_{0.47}N$ layers [Figure 2.2]. For the sample with thickest GaN cap layer of 2.4 nm, the n_s value slightly dropped as expected for samples with coherent AlGaN layers.[18] The electron mobility slightly increased with GaN cap thickness, most likely again due to the more efficient mitigation of the relaxation process.

When the thickness of the $Al_{0.53}Ga_{0.47}N$ layer further increased to 21 nm, the properties of the uncapped AlGaN layer degraded and both n_s and μ values drastically declined [Figure 2.2]. The trenches deepened and probably penetrated close to the AlGaN/GaN interface [Figure 2.1(d)]. In contrast, the complimentary sample with 2.4 nm GaN cap exhibited a smooth surface with only short surface cracks [Figure 2.1(c)] and maintained a high n_s value. The electron mobility only slightly declined in comparison to the sample with 18 nm thick AlGaN, indicating onset of relaxation.

At an $Al_{0.53}Ga_{0.47}N$ thickness of 29.5 nm, when channel cracks emerged in addition to trenches, the uncapped sample was highly resistive and also the 2.4 nm thick GaN cap layer could no longer prevent the structural degradation of the AlGaN layer. As observed previously,[5] the channel cracks penetrated through the entire AlGaN layer, leading to a drastic decrease of the μ value to 170 cm^2/Vs even for the capped sample. Surprisingly the sheet carrier density measured for this sample, 1.9×10^{13} cm^{-2}, was only slightly lower compared to the one with 21 nm thick $Al_{0.53}Ga_{0.47}N$ layer. Presumably the channels penetrated to the (Al,Ga)N/GaN interface only locally, affecting predominantly the electron mobility.

2.3 *GaN cap layers with different thicknesses*

2.3.1 Surface morphology

Figure 2.3 presents the AFM images of GaN/AlGaN/GaN heterostructures with GaN cap thickness of 2.4 to 0 nm. With decreasing cap thickness, the surface morphology changed from exhibiting small surface crack segments for the samples with 2.4 and 1.2 nm caps [Figure 2.3(a) and (b)], to the formation of somewhat longer surface cracks for the samples with 0.6 nm caps [Figure 2.3(c)]. The uncapped samples exhibited again platelets and trenches [Figure 2.3(d)]. A detailed transmission electron microscopy (TEM) study of AlGaN/GaN samples with very similar morphologies was reported by Vennéguès *et al*.[24]

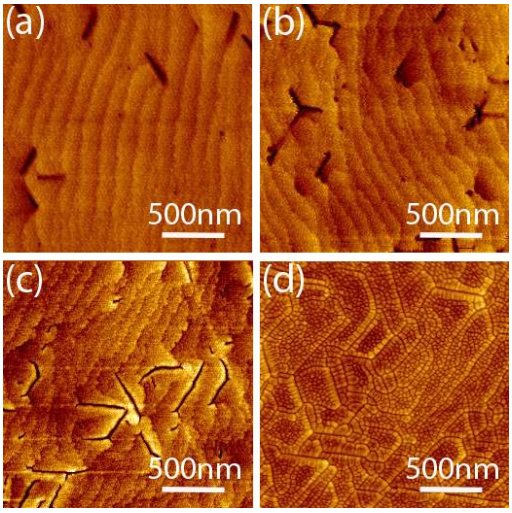

Figure 2.3 AFM images of AlGaN/GaN HEMT structures with 18 nm thick $Al_{0.53}Ga_{0.47}N$ layers capped with a) 2.4 nm, b) 1.2 nm, and c) 0.6 nm thick GaN, and d) no GaN cap layer (grey scale: 5 nm for (a)(b)(c), 10 nm for (d)).

2.3.2 Electrical properties

The influence of the GaN cap layer thickness on the electrical properties of samples with different AlGaN thickness is illustrated in Figure 2.4. For samples with 5.7 nm thick $Al_{0.53}Ga_{0.47}N$ layers, GaN cap layers as thin as 0.6 nm led to an increase of n_s and μ from 5.5×10^{12} to 1.1×10^{13} cm^{-2} and 30 to 1160 cm^2/Vs, respectively. When the cap thickness was increased to 2.4 nm, the n_s value stayed almost the same but μ further increased to 1370 cm^2/Vs. A similar increase of the n_s and μ values was observed when samples with 5.3 nm thick $Al_{0.47}Ga_{0.53}N$ layer were capped with a 2.4 nm thick GaN layer. In contrast, for samples with 18 nm thick $Al_{0.53}Ga_{0.47}N$ layers, the n_s value increased from 1.9×10^{12} cm^{-2} for the uncapped sample to 2.2×10^{13} cm^{-2} for the sample with 0.6 nm thick GaN cap. The electron mobility slightly decreased, most likely caused by the higher n_s value. The n_s value slightly dropped to 2×10^{13} cm^{-2} when the cap thickness was further increased to 2.4 nm, accompanied by an increase in μ from 590 to 840 cm^2/Vs. Due to their higher sheet charge density, the electron mobility measured for the capped 18 nm thick $Al_{0.53}Ga_{0.47}N$ samples was generally lower compared to the thinner samples.[7]

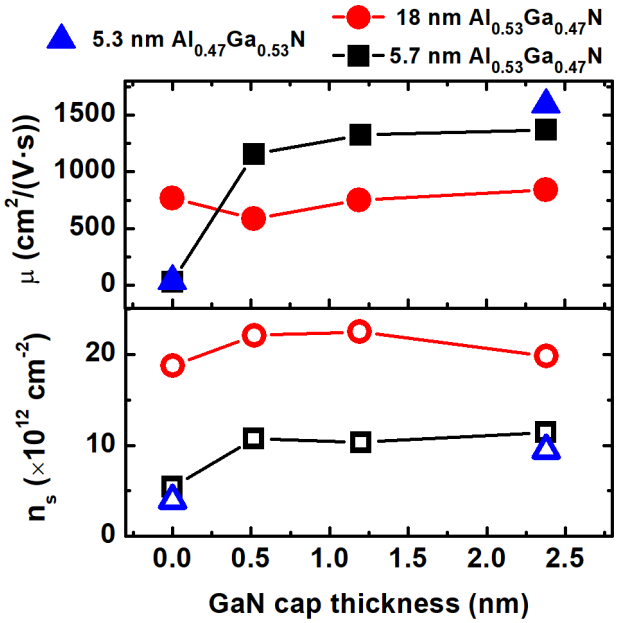

Figure 2.4 Sheet charge density and electron mobility of the 2DEG for AlGaN/GaN HEMT structures with different GaN cap thicknesses; red circle: samples with 18 nm thick $Al_{0.53}Ga_{0.47}N$ layers, black square: samples with 5.7 nm thick $Al_{0.53}Ga_{0.47}N$ layers, blue triangle: samples with 5.3 nm thick $Al_{0.47}Ga_{0.53}N$ layers.

2.3.3 Discussion

Given that the GaN cap layer was ultra-thin, it is reasonable to suggest that the surface morphology observed in Figure 2.3(c) followed the AlGaN layer underneath, indicating that the AlGaN layer with 0.6 nm thin GaN cap exhibited no platelets, unlike the uncapped complementary sample. As the GaN cap layer was deposited immediately after the AlGaN layer at the same temperature, this observation implied that the platelets and trenches observed for the uncapped sample formed during the cool down process from 1145°C to room temperature, as additional stresses evolved due to the different thermal expansion

coefficients of the layers.[5] The reciprocal space maps of the 21 nm thick $Al_{0.53}Ga_{0.47}N$ layers with and without 2.4 nm thick GaN cap layer showed the former to be fully strained and the latter partially relaxed, confirming that GaN cap layers effectively prevented degradation and relaxation of the AlGaN layers [Figure 2.5].

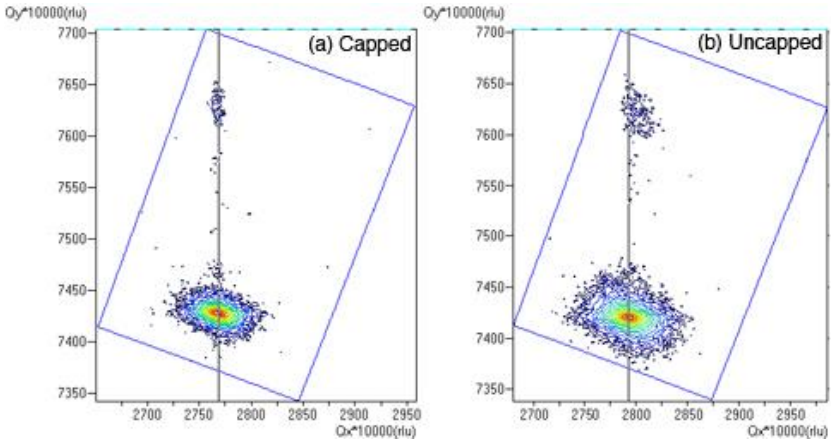

Figure 2.5 Reciprocal space map of (a) capped and (b) uncapped $Al_{0.53}Ga_{0.47}N$ layers with a thickness of 21 nm.

Significant improvements of both morphology and electrical property for the AlGaN/GaN HEMT structures with 5.7 nm thick $Al_{0.53}Ga_{0.47}N$ layers were observed by introducing a GaN cap layer as thin as 0.6 nm. The capped samples featured only short surface cracks, whereas the surfaces of the uncapped samples exhibited platelets and dense trench networks [Figure 0.3(c) and (d)]. While the uncapped sample was highly resistive, the electrical measurements of the capped one revealed n_s and μ values of 1×10^{13} cm^{-2} and 1200 cm^2/Vs, respectively, confirming that the thin GaN cap largely suppressed the relaxation of the AlGaN layer. The n_s and μ values further increased to 1.2×10^{13} cm^{-2} and 1400 cm^2/Vs when the thickness of the GaN cap was increased to 2.4 nm [Figure 2.4]. The surface of this sample exhibited even fewer surface cracks [Figure 2.3(a)], indicating that the

thicker cap layer suppressed the relaxation even more effectively, as a thicker GaN cap layer would normally result in n_s value reduction.

2.4 *Comparison between thin GaN and Si_3N_4 cap layers*

2.4.1 Surface morphology

The AFM images of 5.7 nm thick AlGaN samples capped with 2.4 nm thick in-situ deposited Si_3N_4 layers are depicted in Figure 2.6. While the 2.4 nm thick Si_3N_4 cap layer suppressed platelet formation for the 5.7 nm thick $Al_{0.53}Ga_{0.47}N$ layer [Figure 2.6(b)], trenches still formed and propagated into a network pattern. For comparison, the sample with 2.4 nm thick GaN cap exhibited a smooth surface with no noticeable defects [Figure 2.1(a)], indicating that the Si_3N_4 cap layer was less efficient in preventing structural degradation of the $Al_{0.53}Ga_{0.47}N$ layer. The Si_3N_4 cap layer prevented formation of both platelets and trench networks for the sample with 5.3 nm thick $Al_{0.47}Ga_{0.53}N$ layer though [Figure 2.6(a)].

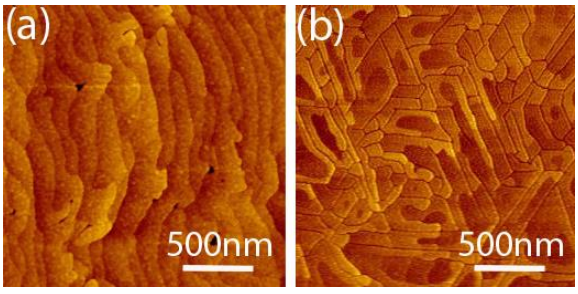

Figure 2.6 AFM images of AlGaN/GaN HEMT structures with 5.7 nm AlGaN layers of different Al composition a) 47%, and b) 53%, which were capped with 2.4 nm thick in-situ Si_3N_4 layers (grey scale: 5 nm for (a), 10 nm for (b)).

2.4.2 Electrical properties

As shown in Table 2.1, 5.3 nm thick $Al_{0.47}Ga_{0.53}N$ or 5.7 nm thick $Al_{0.53}Ga_{0.47}N$ samples with 2.4 nm GaN cap exhibited significantly higher electron mobilities than the also investigated Si_3N_4 capped complementary samples, given the same cap thickness and comparable sheet charge density. Furthermore, the Si_3N_4 cap became even less efficient at higher x_{Al}. The electron mobilities for the Si_3N_4 capped samples with x_{Al} = 47% and x_{Al} = 53% were only half and one-fifth of those capped with GaN, respectively.

Table 2.1 Influence of the capping materials on the sheet charge density (n_s) and electron mobility (μ) of the 2DEG for AlGaN/GaN HEMT structures with 5.3 nm $Al_{0.47}Ga_{0.53}N$ and 5.7 nm $Al_{0.53}Ga_{0.47}N$.

	2.4 nm GaN cap		2.4 nm Si_3N_4 cap	
Al composition	n_s (cm^{-2})	μ (cm^2/Vs)	n_s (cm^{-2})	μ (cm^2/Vs)
47%	9.45×10^{12}	1592	9.43×10^{12}	813.9
53%	1.14×10^{13}	1368	1.2×10^{13}	247.6

2.4.3 Discussion

Considering that the Si_3N_4 was deposited at 1020°C, which was lower than the AlGaN growth temperature of 1145°C, the trench formation could possibly be attributed to the lack of protection during the temperature drop. For this reason, in a later experiment, Si_3N_4 was deposited at the same temperature as the AlGaN layer on a 5.7 nm thick $Al_{0.53}Ga_{0.47}N$ sample. This sample exhibited $n_s = 1.1\times10^{13}$ cm^{-2} and μ = 630 cm^2/Vs, as well as a smooth

surface without noticeable defects. Therefore, we speculate that some of the trenches formed during the temperature drop from 1145 to 1020 °C, resulting in a lower μ value than that for the sample for which the Si_3N_4 was deposited at 1145 °C. Nevertheless, all Si_3N_4 capped samples exhibited poorer properties compared to the GaN capped ones, mostly likely related to the amorphous character and chemical dissimilarity of Si_3N_4. The effectiveness of GaN caps obviously surpassed Si_3N_4 caps in our study, although the latter yielded better values of n_s and μ than uncapped samples.

2.5 *Conclusion*

Thin GaN cap layers as thin as 0.6 nm were shown to effectively suppress platelets and trench formation on the surface of $Al_xGa_{1-x}N$/GaN heterostructures with $x_{Al} \sim 0.5$, also mitigating the degradation of their electrical properties, and widening the design space for AlGaN/GaN transistors. By introducing a 2.4 nm thick GaN cap, fully strained $Al_{0.53}Ga_{0.47}N$ films up to 21 nm thick in GaN/$Al_{0.53}Ga_{0.47}N$/GaN heterostructures were obtained. Furthermore, the GaN cap layers were shown to be more effective in protecting the samples from degradation compared to the also investigated in-situ grown Si_3N_4 cap layers.

2.6 *Reference*

[1] Hearne S J, Han J , Lee S R, Floro J A, and Follstaedt D M, *Appl. Phys. Lett*. **76**, 1534 (2000).

[2] Floro J A, Follstaedt D M, Provencio P, Hearne S J, and Lee S R, *J. Appl. Phys*. **96**, 7087 (2004).

[3] Lee S R, Koleske D D, Cross K C, Floro J A, and Waldrip K E, *Appl. Phys. Lett.* **85**, 6164 (2004).

[4] Parbrook P J, Wang T, Whitehead M A, Harrison C N, Lynch R J, and Murray R T, *Phys. Stat. Sol.* **0**, 2055 (2003).

[5] Einfeldt S, Kirchner V, Heinke H, Diesselberg M, Figge S, Vogelerm K and Hommel D, *J. Appl. Phys*. **88**, 7029 (2000).

[6] Bourret A, Adelmann A, Daudin B, Rouviere J L, Feuillet G, and Mula G, *Phys. Rev. B*, **63**, 245307 (2001).

[7] Shen B, Someya T, and Arakawa Y, *Appl. Phys. Lett*. **76**, 2746 (2000).

[8] Liu B, Lu Y W, Jin G R, Zhao Y, Wang X L, Zhu Q S, and Wang Z G, *Appl. Phys. Lett.* **97**, 262111 (2010).

[9] Liu Z Y, Zhang J C, Duan H T, Xue J S, Lin Z Y, Ma J C, Xue X Y, and Hao Y, *Chin. Phys. B* **20**, 097701 (2011).

[10] Bykhovski A D, Gaska R, Shur M S, *Appl. Phys. Lett*. **73**, 3577 (1998).

[11] Shinohara K, Regan D C, Tang Y, Corrion A L, Brown D F, Wong J C, Robinson J F, Fung H H, Schmitz A, Oh T C, Kim S J, Chen P S, Nagele R G, Margomenos A D, and Micovic M, *IEEE Trans. Electron Devices*, **60** 2982 (2013).

[12] Derluyn J, Boeykens S, Cheng K, Vandersmissen R, Das J, Ruythooren W, Degroote S, Leys M R, Germain M, and Borghs G, *J. Appl. Phys.* **98** 054501 (2005).

[13] Higashiwaki M, Onojima N, Matsui T, and Mimura T, *Phys. Stat. Sol. (a)* **203**, 1851 (2006).

[14] Cheng K, Leys M, Derluyn J, Degroote S, Xiao D P, Lorenz A, Boeykens S, Germain M, and Borghs G, *J. Cryst. Growth*, **298**, 822 (2007).

[15] Bykhovski A D, Gelmont B L, and Shur M S, *J. Appl. Phys*. **81**, 6332 (1997).

[16] Matthews J W, and Blakeslee A E, *J. Cryst. Growth* **27**, 118 (1974).

[17] Liu X W, Hopgood A A, Usher B F, Wang H, and St J Braithwaite N, *Semicond. Sci. Technol.* **14**, 1154 (1999).

[18] Asgari A, Kalafi M, and Faraone L, *Physica E* **25**, 431 (2005).

[19] Waltereit P, Bronner W, Quay R, Dammann M, Müller S, Köhler K, Mikulla M, Ambacher O, Harm L, Lorenzini M, Rödle T, Riepe K, Bellmann K, Buchheim C, and Goldhahn R, *Phys. Status Solidi (c)* **7**, 2398 (2010).

[20] Arulkumaran S, Egawa T, and Ishikawa H, *Jpn. J. Appl. Phys.* **44**, 2953 (2005).

[21] Keller S, Parish G, Fini P T, Heikman S, Chen C H, Zhang N, DenBaars S P, and Mishra U K, *J. Appl. Phys*. **86**, 5850 (1999).

[22] Yang W H and Srolovitz D J, *Phys. Rev. Lett.* **71**, 1593 (1993).

[23] Tersoff J and LeGoues F, *Phys. Rev. Lett*. **72**, 3570 (1994).

[24] Vennégues P, Bougrioua Z, Bethoux J M, Azize M, and Tottereau O, *J. Appl. Phys*. **97**, 024912 (2005).

Chapter 3

Unintentional Ga incorporation into Metal-polar AlN films

In GaN-based high-electron-mobility transistor (HEMT) structures, AlN interlayers are widely used to improve the mobility of the two-dimensional electron gas (2DEG) which forms at the GaN/(Al,Ga)N interface[1], and even more drastic improvements were observed in GaN/(In,Al)N heterostructures[2]. Metal-polar AlN layers grown by metal-organic chemical vapor deposition (MOCVD), however, were recently shown to contain high amounts of Ga caused by carry over reactions in the MOCVD reactor[3]. In this chapter, previous observations of unintentional Ga incorporation into metal-polar (In,Al)N films are first introduced, followed by our study on the impacts of growth conditions on the compositional and electrical properties of the AlN films. GaN/AlN/AlGaN/GaN heterostructures with various nominal AlN interlayers were also discussed.

3.1 Former observation of unintentional Ga incorporation into metal-polar (In,Al)N films

The presence of unintentional Ga was first noticed in InAlN films in InAlN/GaN HEMT structures.[4] A thin unintended GaN layer between the AlN interlayer and the main InAlN layer was later observed in transmission electron microscopy investigations. This unintended GaN layer was attributed to the pre-deposited GaN in the reactor before growing the AlN

film. While the sample was cooled down from the high growth temperature of the GaN and AlN layers to the significantly lower InAlN deposition temperature, the Ga-species desorbed and migrated to be deposited on the sample surface.[5,6] Unintentional Ga was also detected inside the InAlN layers by the same authors. The possible mechanisms of indium-assisted parasitic Ga incorporation into InAlN films grown in close-coupled showerhead reactors by MOCVD was discussed in detail in several papers.[7,8,9] In Hiroki *et al.*'s paper high amount of Ga was also observed in the AlN interlayer.[7] More detailed atom probe tomography investigations of GaN/AlN/(In,Al,Ga)N heterostructures revealed 50% Ga in MOCVD grown AlN interlayers while the AlN interlayers grown by plasma assisted molecular beam epitaxy (PAMBE) were Ga free.[3,10] The authors suggested that the parasitic Ga in AlN layers most probably came from the hot surfaces in the reactor, considering the much higher growth temperature in the MOCVD growth (>1100 °C) compared to that for MBE deposition (~745 °C). This Ga carry-over reaction is similar to the arsenic carry-over reaction observed in InP/InGaAs heterostructures grown by MOCVD.[11,12]

3.2 Experiments

All samples in this study were deposited on c-plane sapphire substrates by MOCVD using the precursors trimethylgallium (TMGa), trimethylaluminum (TMAl), and ammonia (NH_3). The 2 µm thick semi-insulating (S.I.) GaN base layers were grown using the standard two-step method and Fe doping.[13] For selected samples, a 300 nm thick GaN layer underneath the AlN layer was grown at 100 Torr instead of the standard 600 Torr. The AlN layers were deposited at temperatures between 950 and 1145 °C, with TMAl flows, f_{TMAl}, from 1.7 to 2.5 µmol/min, and ammonia flows, $f_{\mathrm{NH_3}}$, from 45 to 180 mmol/min. The growth

conditions of the $Al_{0.24}Ga_{0.76}N$ and $Al_{0.47}Ga_{0.53}N$ layers were held constant, with f_{TMAl} = 5.8 and 6.05 µmol/min, f_{TMGa} = 14.6 and 4.81 µmol/min, respectively, and f_{NH_3} = 180 mmol/min with growth temperature T = 1050 °C. The reactor pressure was 100 Torr. Experiments were conducted using H_2 or N_2 as the major carrier gas. All (Al,Ga)N layers were capped with a 2.5 nm thick GaN layer grown under the same conditions with f_{TMGa} = 17.5 µmol/min. The thin GaN cap layer was added to suppress relaxation of the (Al,Ga)N layers.[14] Note that the deposition temperature for the intermediate $Al_{0.24}Ga_{0.76}N$ and $Al_{0.47}Ga_{0.53}N$ layers were 1050 °C, which was 95 °C lower than that used for standard transistor structures grown in the same reactor, was chosen to minimize the transition time between the AlN and AlGaN growth steps. Previous investigations of AlN/InAlN samples had shown that an approximately 2.5 nm thick unintentional GaN layer formed between the AlN and InAlN layers while the samples were cooled down from the AlN to InAlN growth temperature, from 1135 °C to 885 °C, over 180 s.[3] For the samples with different AlN and AlGaN growth temperature in this study, the transition time between the AlN and AlGaN growth steps was 60 s, limiting the thickness of a potential unintentional GaN layer to 0.8 nm.

High-resolution x-ray diffraction (XRD) with a Panalytical MRD PRO Materials Research Diffractometer was used to determine the Al composition (x_{Al}) and (Al,Ga)N layer thickness of the samples. The coherence of the (Al,Ga)N layers with respect to GaN was confirmed by recording reciprocal space maps as described in reference 14. Atomic force microscopy (AFM) images were taken with a Veeco Dimension 3000 Scanning Probe Microscope to analyze the surface morphology, and the root mean square (rms) surface roughness values were calculated using the AFM software. The sheet charge density (n_s) and

mobility (μ) of the 2DEG, which formed at the AlN/GaN interface were determined by room temperature Van der Pauw Hall measurements. Two-dimensional (2D) Al III-site distribution in (Al,Ga)N films was taken by atom probe tomography (APT) in planes perpendicular to the growth direction with a Cameca 3000X HR Local Electrode Atom Probe.

3.3 Impact of growth conditions on Ga incorporation

Samples with the structure shown in Figure 3.1 were grown and measured to investigate the impact of growth conditions on unintentional Ga incorporation into AlN layers. Nominally 2–4 nm thick AlN layers were deposited at three different temperatures, 950, 1050 and 1145 °C using H_2 and N_2 as carrier gas, respectively. For selected experiments the NH_3 and TMAl flows were modified. While the standard growth chamber pressure for the GaN layers underneath the AlN layers was 600 Torr, a lower pressure of 100 Torr was also inspected for selected samples.

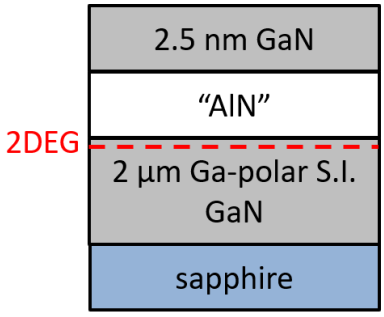

Figure 3.1 Schematic of the sample structures for compositional investigation.

Additionally, AlN layers deposited in regrowth runs were examined. In a regrowth experiment, the growth was interrupted after the deposition of 2 µm thick GaN buffer, which was grown at 600 Torr, and the sample was removed from the growth chamber. After the chamber was cleaned using a H_2 bake process, the sample was reloaded and the growth process continued with the deposition of 300 nm thick GaN layer at 100 Torr, followed by the AlN and GaN cap layers. [Figure 3.2]

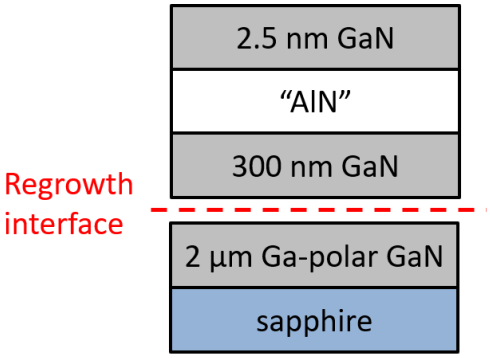

Figure 3.2 Schematic of the sample structure for the regrowth experiment.

3.3.1 Growth temperature and carrier gas

The GaN layers underneath the AlN layers were grown at 600 Torr for all samples discussed in Section Chapter 3 and 3.3.2. While keeping f_{TMAl} = 2.5 µmol/min and $f_{\mathrm{NH_3}}$ = 180 mmol/min constant, the growth temperature varied from 950 to 1145 °C, and H_2 and N_2 were used as major carrier gases respectively. It is shown that the Al composition of the nominal AlN layers decreased with increasing deposition temperature, from 0.62 at 950 °C to 0.52 at 1145 °C for the samples grown in H_2, and from 0.59 to 0.50 for those grown in N_2, respectively [Figure 3.3]. Due to the different transport characteristics, the

overall growth rate was lower in the experiments performed in N_2 carrier gas compared to those conducted in H_2; the trends, however, were the same.

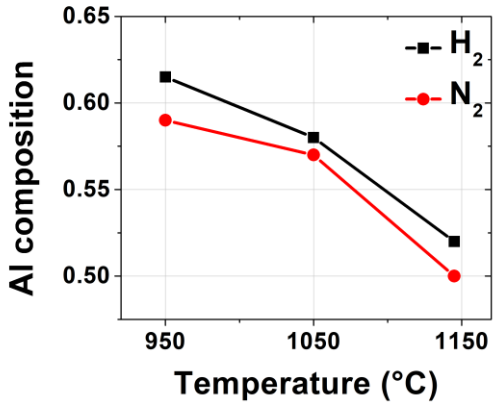

Figure 3.3 Al compositions of the AlN layers grown under different temperatures in H_2 (black square) and N_2 (red circle) carrier gas.

Given the thicknesses and compositions of the nominal AlN layers measured by XRD, the binary AlN and GaN growth rates were calculated, revealing that the binary AlN growth rate was largely independent of the growth temperature. In contrast, the binary GaN growth rate significantly increased with rising temperature [Figure 3.4].

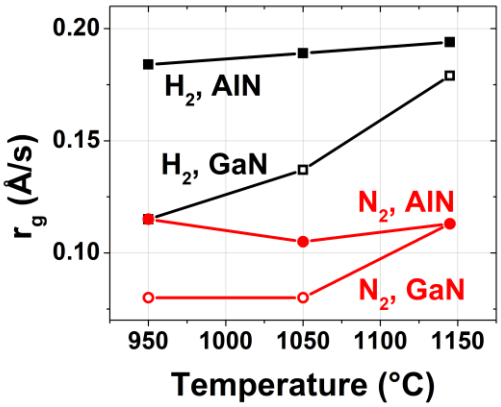

Figure 3.4 Binary AlN (closed symbols) and GaN (open symbols) growth rates for AlN layers grown under different temperatures in H_2 (black square) and N_2 (red circle) carrier gas.

3.3.2 TMAl and NH_3 flows

To further explore the growth at 950 °C in H_2, additional experiments were conducted using (i) a lower TMAl flow of 1.7 µmol/min, and (ii) where the lower TMAl flow was combined with a higher NH_3 flow of 180 mmol/min. Neither of the modifications led to any significant changes in the Al composition of the layers. [Figure 3.5] The measured x_{Al} values of 0.61 and 0.6, respectively, were rather slightly lower compared to the sample grown with higher TMAl flow/growth rate (x_{Al} = 0.62).

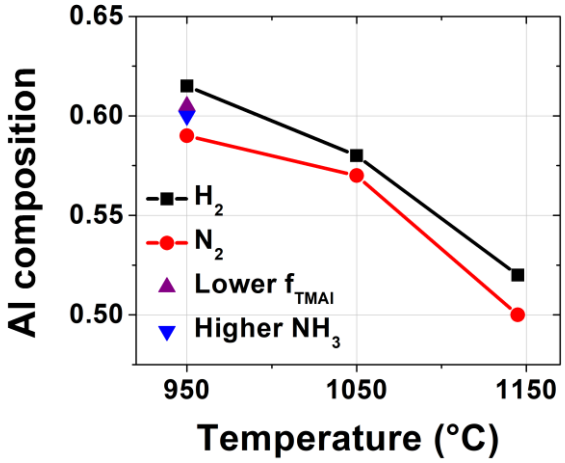

Figure 3.5 Al compositions for AlN layers grown at 950 °C in H_2 using (i) a lower TMAl flow (purple triangle), and (ii) the lower TMAl flow combined with a higher NH_3 flow (blue inverted triangle).

3.3.3 Regrowth

In the regrowth experiments, 300 nm thick GaN layers were first deposited at 100 Torr, followed by the growth of AlN layers at a temperature of 950 °C with standard TMAl and NH_3 flows, f_{TMAl} = 2.5 µmol/min and f_{NH_3} = 180 mmol/min, using H_2 and N_2 as major carrier gases, respectively. Interestingly, the Al content in these layers turned out to be 0.78 and 0.74 for the samples grown in H_2 and N_2, respectively, which are significantly higher than the values of 0.59 and 0.62 obtained in the continuous growth experiment using the same AlN growth parameters.

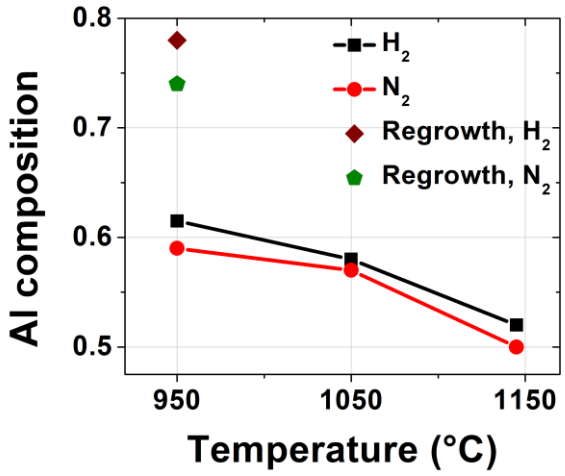

Figure 3.6 Al compositions for the AlN layers grown at 950 °C in regrowth experiments using H_2 (brown diamond) and N_2 (green pentagon) as major carrier gases.

3.3.4 Growth chamber pressure for deposition of GaN underneath AlN

As we noted, for the deposition of GaN layers underneath the AlN layers, the growth chamber pressure was 600 Torr in the continuous growth experiments and 100 Torr in the regrowth. To investigate the impact of the growth chamber pressure for the underlying GaN layers on the unintentional Ga incorporation into AlN layers, two noninterrupted growth experiments with the AlN layers grown at 950 and 1145 °C, respectively, using N_2 as major carrier gas, and with the underlying GaN layer grown at 100 Torr were performed.

By decreasing the growth chamber pressure for the deposition of the 300 nm thick underlying GaN layers from 600 to 100 Torr, the Al compositions in the nominal AlN layers grown at 950 and 1145 °C in N_2 increased from 0.59 to 0.65 and 0.50 to 0.60, respectively [Figure 3.7].

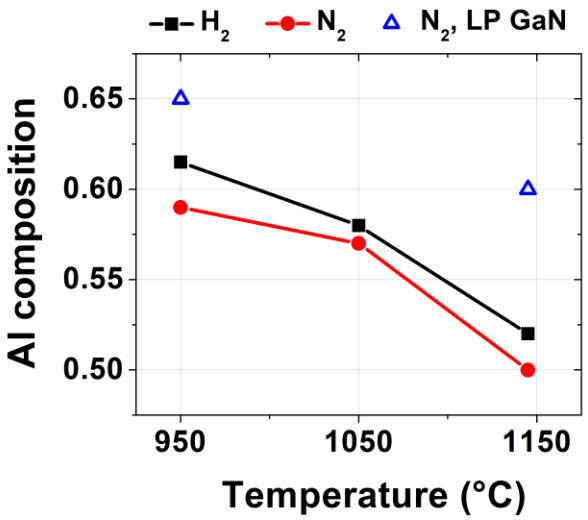

Figure 3.7 Al compositions for the AlN layers grown at various temperatures in N_2 with the underlying GaN layer grown using a low chamber pressure of 100 Torr (blue open triangle) instead of the standard pressure of 600 Torr in other continuous experiments.

3.3.5 Discussion

The significant improvement of Al composition in regrowth experiments compared to the continuous experiments indicated the GaN deposits in the growth chamber formed before AlN growth in the same run, the 2 μm thick GaN buffers in the continuous experiments and the much thinner 300 nm thick GaN layers in the regrowth, to be the major source of the unintentional Ga incorporated in the AlN layers. The evaporation of Ga increased with increasing growth temperature of the AlN layer, leading to a higher Ga incorporation into the nominal AlN films. Thereby gaseous Ga species can form via thermal decomposition,

$$2\ GaN \Leftrightarrow 2\ Ga(g) + N_2 \qquad (3.1)$$

or reaction with H_2,

$$GaN + 3/2\ H_2 \Leftrightarrow Ga(g) + NH_3 \quad (3.2)$$

(instead of $Ga_{(g)}$ Ga hydrides may also form). As hydrogen is a product of the NH_3 decomposition, it is also available when N_2 is used as carrier gas. The desorption of Ga continued until all GaN deposits in hot areas of the reactor chamber were covered by the growing AlN layers. It is plausible that the Ga species majorly came from certain areas in the reactor given a certain gas flow pattern during AlN growth. Thereby, when the growth chamber pressure for the underlying GaN layers changed and the distribution of GaN deposits in the reactor changed accordingly, a different amount of Ga species was available to get incorporated into the AlN layers, resulting in changes of the Al composition. Additionally, we speculated that the Ga incorporation into nominal AlN layers was governed by similar rules as the indium incorporation in InGaN layers. There the indium atoms are captured by the growing GaN layer and the indium incorporation efficiency increases with increasing growth rate, so that at a constant TMIn flow, variations of the TMGa flow/growth rate result in little changes in the In composition.[15] Similarly the Ga content in the nominal AlN layers grown in this study was largely unaffected by the TMAl flow. The results also imply that the parasitic Ga incorporation will depend on the specific reactor design. As mentioned earlier, transmetallation reactions at the reactor inlet were held responsible in another study[7].

3.4 GaN/AlN/GaN heterostructures with AlN grown under different conditions

Following the compositional investigations, the electrical properties and surface morphologies of the nominal S.I. GaN/AlN/2.5 nm GaN samples [Figure 3.1] discussed in

Section Chapter 3and 3.3.2 were also examined by room temperature Van der Pauw Hall measurement and AFM.

3.4.1 Growth temperature and carrier gas

The sheet charge densities and electron mobilities for the samples with AlN layers grown at different temperatures using different carrier gases are illustrated in Figure 3.8. The Al compositions of the nominal AlN layers correspond to the values presented in Figure 3.3. Comparing the samples grown in H_2 and N_2, generally better results were observed for the heterostructures grown in N_2, for which an increase in the sheet charge density, from 9.5×10^{12} to 1.2×10^{13} cm^{-2}, combined with an increase in the electron mobility, from 644 to 852 cm^2/Vs was observed with rising growth temperature. The results for the samples grown in H_2 followed the same trend, however, the electron mobility values were generally lower, with values of 292 and 768 cm^2/Vs at 950 and 1145 °C, respectively. Also the n_s value of 3×10^{12} cm^{-2} measured for the sample grown at 950 °C in H_2, was considerably lower compared to 9.5×10^{12} cm^{-2} obtained for the complementary sample grown in N_2. In contrast, the sheet charge densities were largely unaffected by the carrier gas for the samples grown at 1050 and 1145 °C.

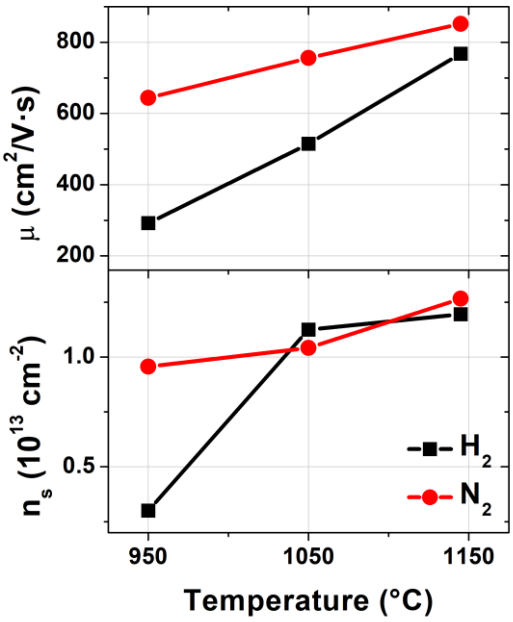

Figure 3.8 Sheet charge density and electron mobility measured at room temperature for the GaN/AlN/2.5 nm GaN samples with nominal AlN layers grown at different temperatures using H_2 (black diamond) and N_2 (red circle) as carrier gas.

The AFM images of the same samples are depicted in Figure 3.9. The surface roughness of the samples grown in N_2 (rms = 210–370 pm) was generally smoother compared to those grown in H_2 (rms = 510–990 pm). Threading dislocation mediated defect formation was observed to a larger extent for samples grown in H_2. In addition, more pronounced defects were observed in the samples grown at 950 °C with the highest Al composition in both series.

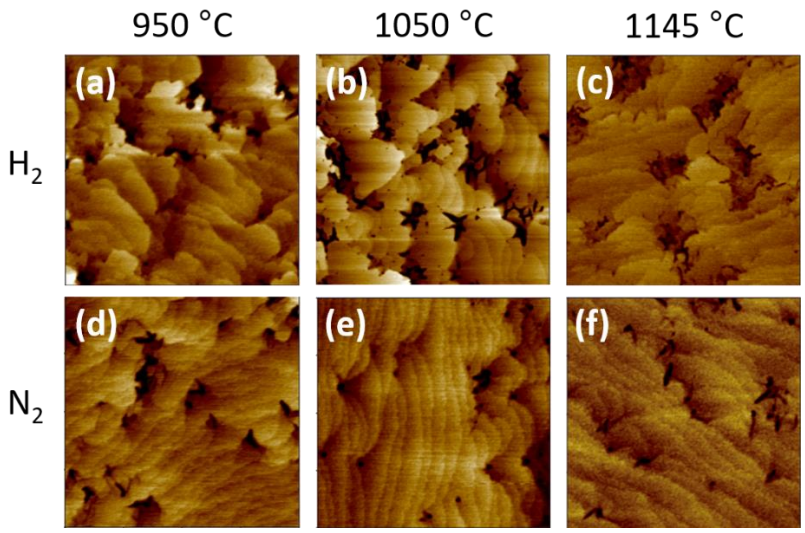

Figure 3.9 2×2 μm^2 AFM images of the nominal GaN/AlN/GaN heterostructures. The growth temperature and major carrier gases for the AlN layers were (a) 950 °C and H_2, (b) 1050 °C and H_2, (c) 1145 °C and H_2, (d) 950 °C and N_2, (e) 1050 °C and N_2, (d) 1145 °C and N_2. The thickness of the nominal AlN layers were (a) 5.3 nm, (b) 5.8 nm, (c) 7.4 nm, (d) 4.9 nm, (e) 6.7 nm, and (f) 7.2 nm. The grey scale for images (a), (b) and (c) is 4 nm, for (d), (e), and (f) is 2.5 nm.

3.4.2 TMAl and NH_3 flows

To investigate the origin of the unusually low n_s and μ values for the samples grown at 950 °C in H_2, the TMAl flow during AlN deposition was lowered to 1.7 μmol/min, resulting in an increase of the sheet carrier density from 3×10^{12} to 7.2×10^{12} cm^{-2}. The electron mobility, however, decreased by ~100 cm^2/Vs. When the lower TMAl flow was combined with a higher NH_3 flow of 180 mmol/min, n_s and μ values of 1.2×10^{13} cm^{-2} and 720 cm^2/Vs, respectively, were obtained, with both n_s and μ values now exceeding those measured for the sample grown in N_2 at the same temperature.

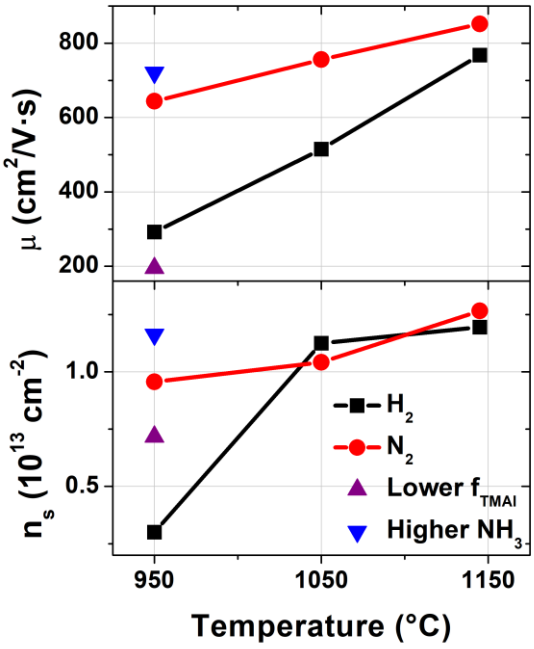

Figure 3.10 Sheet charge density and electron mobility measured at room temperature for the GaN/AlN/2.5 nm GaN samples with nominal AlN layers grown at 950 °C in H_2 with lower f_{TMAl} = 1.7 μmol/min (purple triangle) and the lower f_{TMAl} combined with a higher f_{NH_3} = 180 mmol/min (blue inverted triangle) compared to the standard flows f_{TMAl} = 2.5 μmol/min and f_{NH_3} = 45 mmol/min.

In addition, this sample exhibited a much smoother surface [Figure 3.11(c)] compared to the sample grown with the standard TMAl and NH_3 precursor flows [Figure 3.11(a)], while a higher defect density was observed on the surface of the sample with lower TMAl and standard NH_3 flows [Figure 3.11(b)].

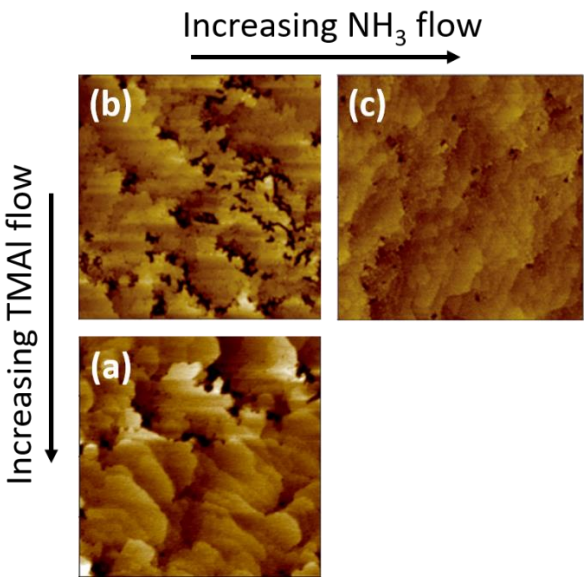

Figure 3.11 2×2 μm^2 AFM images of the nominal GaN/AlN/GaN heterostructures with AlN layers grown at 950 °C in H_2 with (a) f_{TMAl} = 2.5 μmol/min and f_{NH_3} = 45 mmol/min, (b) f_{TMAl} = 1.7 μmol/min and f_{NH_3} = 45 mmol/min and (c) f_{TMAl} = 1.7 μmol/min and f_{NH_3} = 180 mmol/min. The grey scale for images (a) is 4 nm, for (b) is 7 nm and for (c) is 4.5 nm.

3.4.3 Discussion

As discussed before, the composition of the layers grown at 950 °C in H_2 was largely unaffected by the variations of the TMAl and NH_3 flows (x_{Al}~0.6), excluding the impact of Al composition on the electrical results. We suggest that the higher NH_3 flow compensated for the reduced NH_3 decomposition efficiency at lower temperatures, and the lower TMAl flow/growth rate counterbalanced the lower surface mobility of species at lower temperatures. The combined effects partially mitigated defect formation at the low growth

temperature of 950 °C with H_2 as carrier gas, resulting in a smoother surface [Figure 3.11] and higher mobility [Figure 3.10]. However, when only the TMAl flow was reduced, the reduced growth rate of the nominal AlN layer led to a longer exposure of the GaN surface to H species, which reacts with GaN and causes Ga desorption [Equation 3.2], resulting in a rougher GaN/AlN interface and thereby the observed mobility drop [Figure 3.10]. By contrast, when using N_2 as carrier gas, the N_2 stabilized the nitride crystal [Equation 3.1], and less NH_3 was needed to obtain high quality films. Interestingly, the increase in electron mobility with increasing deposition temperature was observed despite the decrease in the Al mole fraction from ~0.6 to ~0.5. The slight variations in the sample thickness also did not significantly influence the trend. It is plausible that the higher AlN film quality obtained at higher growth temperatures had a dominant influence on the 2DEG sheet charge density and mobility, leading to the generally higher electron mobility for samples with AlN layers grown at higher temperatures.

3.5 GaN/(Al,Ga)N/GaN heterostructures with "AlN" and intentionally grown $Al_{0.5}Ga_{0.5}N$ layers

Among the above discussed GaN/AlN/GaN heterostructures, the highest 2DEG mobility of 852 $cm^2/V{\cdot}s$ with $n_s = 1.266\times10^{13}$ cm^{-2} was measured for the sample with the nominal AlN layer grown at 1145 °C in N_2 [Figure 3.10], which turned out to be a 7.2 nm thick $Al_{0.5}Ga_{0.5}N$ layer [Figure 3.12(a)]. A significantly higher 2DEG mobility value of 1247 $cm^2/V{\cdot}s$ with $n_s = 1.182\times10^{13}$ cm^{-2}, however, was observed for a similar structure with an intentionally deposited 5.7 nm thick $Al_{0.53}Ga_{0.47}N$ layer grown using the same temperature and carrier gas [Figure 3.12(b)].

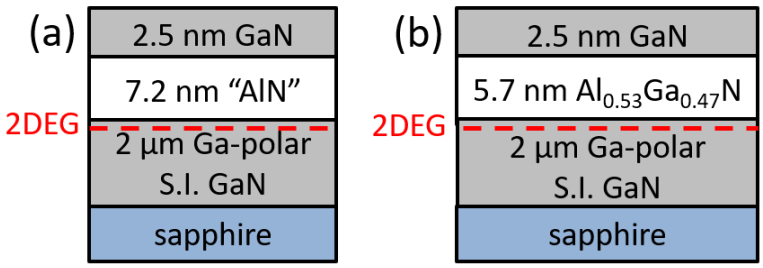

Figure 3.12 Schematic of the (a) nominal GaN/AlN/GaN heterostructures with "AlN" actually being 7.2 nm $Al_{0.5}Ga_{0.5}N$ and (b) GaN/5.7 nm $Al_{0.53}Ga_{0.47}N$/GaN heterostructures.

The surface morphology of both samples was measured by AFM. As shown in Figure 3.13, the GaN/AlN/GaN heterostructure with the nominal AlN layer exhibited more developed defects compared to the sample with intentionally grown AlGaN, which had a similar layer thickness and Al composition.

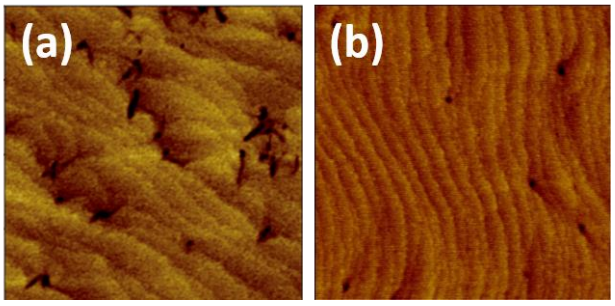

Figure 3.13 2×2 μm^2 AFM images of the (a) nominal GaN/AlN/GaN heterostructures with "AlN" actually being 7.2 nm $Al_{0.5}Ga_{0.5}N$ and (b) GaN/5.7 nm $Al_{0.53}Ga_{0.47}N$/GaN heterostructures. The grey scale for (a) is 2.5 nm and for (b) is 3 nm.

A separate sample with both the nominal AlN layer and the intentionally deposited AlGaN layer was grown and measured by atom probe tomography. The growth conditions used in the above mentioned heterostructures were maintained for both layers. Interestingly,

the intentionally grown AlGaN layer showed more uniform distribution of Al atoms across the plane perpendicular to the growth direction compared to the nominal AlN layer. As mentioned in section 3.3.5, we speculate that the unintentional Ga incorporation was governed by similar rules as the indium incorporation in InGaN layers. InGaN layers are well known for their local fluctuations in the indium composition,[16] which can result from local differences in the surface step density.[17] Thereby, it is understandable to have stronger variations of Al distribution in the nominal AlN layers.

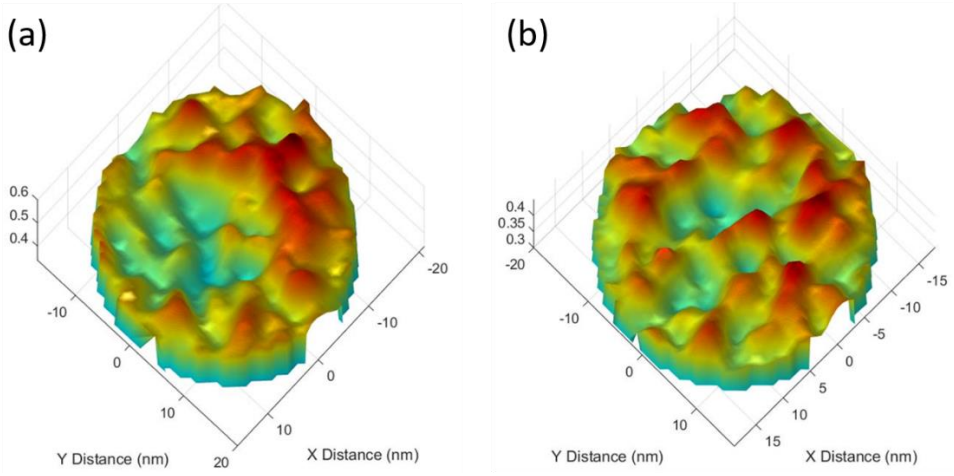

Figure 3.14 Al III-site distribution in (a) nominal AlN layer and (b) intentionally grown $Al_{0.5}Ga_{0.5}N$ layer taken using atom probe tomography in a plane perpendicular to the growth direction.

We believe both the lower material quality and the stronger local fluctuation of Al composition, the latter of which increased alloy cluster scattering[18], in the nominal AlN layers account for the lower mobility compared to the sample with intentionally deposited $Al_{0.53}Ga_{0.47}N$ layer.

3.6 GaN/AlN/AlGaN/GaN heterostructures with different AlN interlayer thicknesses

In the following experiments, the impact of the AlN layer growth conditions on the electrical properties of Ga-polar HEMT structures [Figure 3.15], S.I. GaN buffer/AlN interlayer/AlGaN barrier/GaN cap, was investigated. Two different nominal AlN interlayer thicknesses, 0.7 and 2 nm, were examined in the HEMT structures with 20 nm thick $Al_{0.24}Ga_{0.76}N$ barriers. Six different growth conditions were again examined with growth temperatures of 950, 1050 and 1145 °C and major carrier gases of H_2 and N_2, respectively. Samples with 14 nm thick $Al_{0.47}Ga_{0.53}N$ barriers and 0.7 nm thick nominal AlN interlayers grown under selected conditions were also analyzed. Note that due to the unintentional Ga incorporation in AlN films, the actual interlayer thickness was about twice the nominal one.

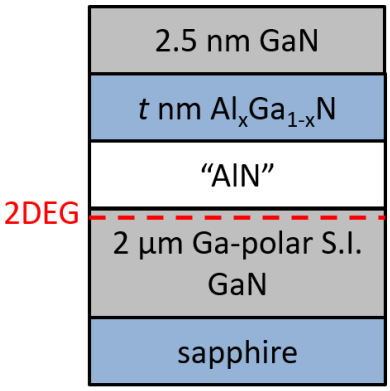

Figure 3.15 Schematic of the sample structures for nominal AlN interlayer investigation with 20 nm thick $Al_{0.24}Ga_{0.76}N$ and 14 nm thick $Al_{0.47}Ga_{0.53}N$ barriers respectively.

3.6.1 0.7 nm AlN interlayers

For the samples with nominally 0.7 nm thick AlN interlayers, 20 nm thick $Al_{0.24}Ga_{0.76}N$ barriers and sheet charge densities around 1×10^{13} cm^{-2}, electron mobility values between 2000 and 2200 cm^2/Vs were obtained, largely independent of the interlayer growth temperature [Figure 3.16]. Two of the samples grown in N_2 exhibited somewhat higher μ values compared to the complementary samples deposited in H_2, but their n_s values were slightly lower, possibly leading to the somewhat higher electron mobility[19].

By contrast, for the heterostructures with nominally 0.7 nm thick AlN interlayers, 14 nm thick $Al_{0.47}Ga_{0.53}N$ barriers and sheet charge densities around 1.8×10^{13} cm^{-2}, lower mobilities around 1200 cm^2/Vs were measured.

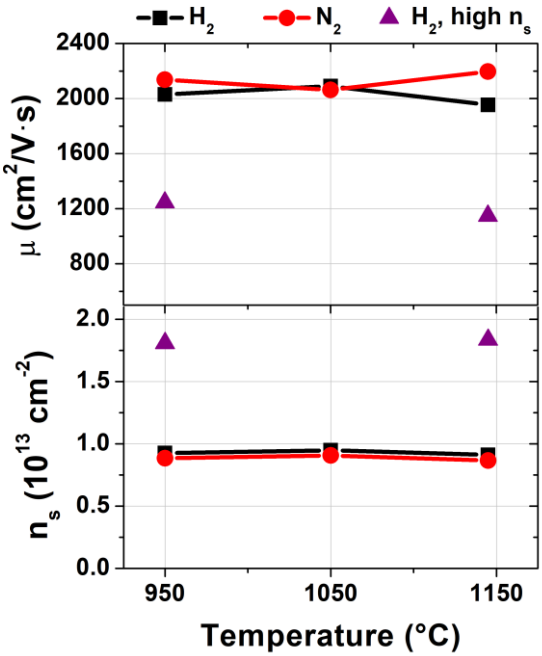

Figure 3.16 Sheet charge density and electron mobility measured at room temperature for (i) 2 μm GaN/0.7 nm AlN/20 nm $Al_{0.24}Ga_{0.76}N$/2.5 nm GaN samples with nominal AlN layers grown at different temperatures using H_2 (black diamond) and N_2 (red circle) as

carrier gas; (ii) 2 µm GaN/0.7 nm AlN/14 nm $Al_{0.47}Ga_{0.53}N$/2.5 nm GaN samples nominal AlN layers grown at different temperatures using H_2 (purple triangle).

3.6.2 2 nm AlN interlayers

Rather low electron mobility values were obtained for the samples with nominally 2 nm thick AlN interlayer [Figure 3.17], which increased from values between 900 and 1000 to ~1200 cm^2/Vs with increasing temperature, at n_s values around 1×10^{13} cm^{-2} for all samples. The results were minimally affected by the carrier gas.

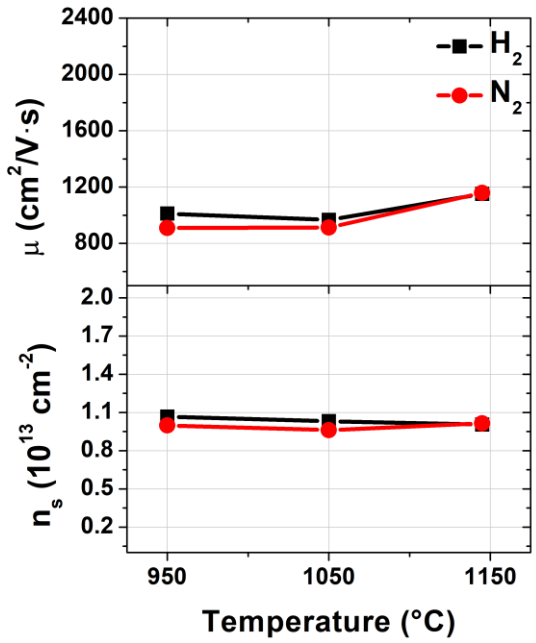

Figure 3.17 Sheet charge density and electron mobility measured at room temperature for 2 µm GaN/2 nm AlN/20 nm $Al_{0.24}Ga_{0.76}N$/2.5 nm GaN samples with nominal AlN layers grown at different temperatures using H_2 (black diamond) and N_2 (red circle) as carrier gas

3.6.3 Discussion

The observation can be understood by evaluating the band structure of samples with 20 nm thick $Al_{0.24}Ga_{0.76}N$ barriers, with and without a 1.4 nm thick $Al_{0.5}Ga_{0.5}N$ interlayer [Figure 3.18].[20] Due to the piezoelectric effects, the 1.4 nm thick $Al_{0.5}Ga_{0.5}N$ interlayer results in a significant shift of the conduction (and valence) band towards higher energies, leading to a higher "effective" band offset between GaN and $Al_{0.24}Ga_{0.76}N$ layers, similar to the findings in reference21. The higher band offset reduces the penetration of the electron wave function into the barrier layer, thereby reducing scattering and resulting in a higher electron mobility[22]. By adding a nominally 0.7 nm thick AlN interlayer, the electron mobility increased from around 1200 cm^2/Vs to above 2000 cm^2/Vs for the heterostructures with $Al_{0.24}Ga_{0.76}N$ barriers.

Nevertheless, when the Al compositions in the AlGaN barriers were close to 0.5, which was the case for the nominal heterostructures GaN/AlN/$Al_{0.47}Ga_{0.53}N$/ GaN with sheet charge density around 1.8×10^{13} cm^{-2}, the 1.4 nm thick $Al_{0.5}Ga_{0.5}N$ interlayer has little impact on the effective conduction band offset, resulting in a limited 2DEG mobility improvement of ~ 200 cm^2/Vs compared to similar structures without the nominal AlN interlayers.

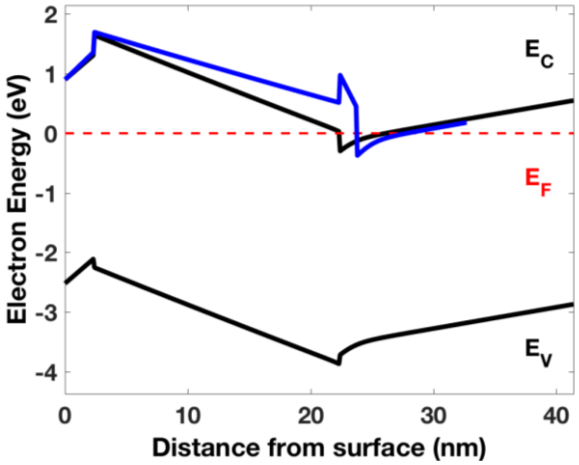

Figure 3.18 Band diagrams of S.I. GaN/20 nm $Al_{0.24}Ga_{0.76}N$/GaN structures with (blue line) and without (black line) a 1.4 nm $Al_{0.5}Ga_{0.5}N$ interlayer between the GaN channel and the AlGaN barrier.

According to simulation, a further reduction in barrier penetration of the of the wave function was expected with increasing $Al_{0.5}Ga_{0.5}N$ interlayer thickness. The experiments, however, showed the opposite trend: for the samples with 20 nm thick $Al_{0.24}Ga_{0.76}N$ barriers, the electron mobilities declined from ~2000 to ~1200 cm^2/Vs when the nominal AlN interlayer thickness was increased from 0.7 to 2 nm, corresponding to 1.4 to 4 nm thick $Al_{0.5}Ga_{0.5}N$ interlayers. This can be understood by taking into account the stronger alloy cluster scattering in the nominal AlN layers compared to the intentionally deposited AlGaN layers as discussed in section 3.5, which became more noticeable with increasing nominal AlN interlayer thickness. This speculation was supported by a high mobility of 1950 cm^2/Vs with $n_s = 8.6\times10^{12}$ cm^{-2} when the nominal 2 nm thick AlN layer was replaced by a 4 nm thick $Al_{0.5}Ga_{0.5}N$ layer. The recovery of mobility indicated the significant scattering introduced by the nominal 2 nm thick AlN interlayer. In samples with 0.7 nm thick nominal

AlN interlayers the Ga alloy fluctuations played only a subordinate role due to their thin nature in combination with the screening effect of the main 20 nm thick $Al_{0.24}Ga_{0.76}N$ barrier layer. Therefore, high electron mobility values above 2000 cm^2/Vs were measured after adding the 0.7 nm thick nominal AlN interlayer, similar to AlN/AlGaN structures with pure AlN layers grown by MBE.[1,10]

3.7 Conclusion

In conclusion, the unintentional Ga incorporation into the metal-polar AlN layers in this study was attributed to evaporation of Ga species from GaN deposits in the MOCVD reactor chamber. The unintentional Ga incorporation could be suppressed at lower AlN growth temperatures, resulting in an increase of the Al composition from 0.5 to 0.6. Decreasing the growth chamber pressure for the deposition of GaN layers underneath the AlN layers from 600 to 100 Torr also led to a x_{Al} increase of 0.06−0.10 at different temperatures. The nominal AlN film with highest x_{Al} of 0.78 were obtained in regrowth experiments. Non-optimal growth conditions for the underlying GaN layers where the 2DEGs locate and interruptions in the epitaxial process are, however, undesirable for transistor fabrication. The increase in x_{Al} from 0.5 to 0.6 at lower deposition temperatures did not result in measurable improvements in the electrical properties of the investigated GaN/(Al,Ga)N heterostructures. The unintentional Ga incorporation had a negligible effect on the electrical properties of GaN/AlN/AlGaN structures with thin nominal AlN interlayers (0.7 nm) and sheet carrier densities in the order of 1×10^{13} cm^{-2}, which exhibited electron mobilities above 2000 cm^2/Vs, comparable to samples with pure AlN interlayers grown by MBE. The thin nominal AlN interlayers in structures with higher sheet carrier densities of 1.8×10^{13} cm^{-2},

however, only improved the mobility by ~200 cm^2/Vs, resulting in μ ~ 1200 cm^2/Vs. In addition, the unintentional Ga incorporation led to a degradation of the electrical properties of heterostructures with thicker nominal AlN layers or interlayers compared to the samples with intentionally deposited $Al_{0.5}Ga_{0.5}N$ layers, probably due to the stronger local nonuniformity of Ga distribution in the nominal AlN films. Further investigations are needed to enable the fabrication of pure metal-polar AlN layers by MOCVD.

3.8 *Reference*

[1] Smorchkova I P, Chen L, Mates T, Shen L, Heikmann S, Moran B, Keller S, DenBaars S P, Speck J S and Mishra U K, *J. Appl. Phys.* **90**, 5196 (2001).

[2] Gonschorek M, Carlin J F, Feltin E, Py M A and Grandjean N, *Appl. Phys. Lett*. **89**, 062106 (2006).

[3] Lu J, Hu Y L, Brown D F, Wu F, Keller S, Speck J S, DenBaars S P and Mishra U K, *Japan. J. Appl. Phys*. **51**, 115502 (2012).

[4] Trejo M, Jessen G H, Crespo A, Gillespie J K, Langley D, Denninghoff D, Via G D, Carlin J, Tomich D, Grant J, and Smith H, *Proc. CS Mantech Conf.*, Chicago, Illinois, USA, 14-17 April 2008, p.129.

[5] Leach J H, Ni X, Li X, Wu X, Özgür Ü, Morkoç H, Zhou L, Cullen D A, Smith D J, Cheng H, Kurdak Ç, Meyer J R, and Vurgaftman I, *J. Appl. Phys*. **107**, 083706 (2010).

[6] Zhou L, Cullan D A, Mc Cartney M R, Leach J H, Fan Q, Morkoç H and Smith D J, *Phys. Status Solidi* C **7**, 2436 (2010).

[7] Hiroki M, Oda Y, Watanabe N, Maeda N, Yokoyama H, Kumakura K, Yamamoto H, *J. Cryst. Growth* **382**, 36 (2013).

[8] Choi S, Kim H J, Lochner Z, Kim J, Dupuis R D, Fischer A M, Juday R, Huang Y, Li T, Huang J Y, Ponce F A and Ryou J, *J. Cryst. Growth* **388**, 137 (2014).

[9] Kim J, Lochner Z, Ji M, Choi S, Kim H J, Kim J S, Dupuis R D, Fischer A M, Juday R, Huang Y, Li T, Huang J Y, Ponce F A and Ryou J, *J. Cryst. Growth* **388**, 143 (2014).

[10] Mazumder B, Kaun S W, Lu J, Keller S, Mishra U K and Speck J S, *Appl. Phys. Lett.* **102**, 111603 (2013).

[11] Keller B P, Brühl H G, Seifert W, *Cryst. Res. Technol*. **27**, 617 (1992).

[12] Wagner J, Peter M, Winkler K, and Bachem K H, *J. Appl. Phys*. **83**, 4299 (1998).

[13] Keller S, Parish G, Fini P T, Heikman S, Chen C H, Zhang N, DenBaars S P and Mishra U K, *J. Appl. Phys*. **86**, 5850 (1999).

[14] Li H, Keller S, DenBaars S P and Mishra U K, *Jpn. J. Appl. Phys.* **53**, 095504 (2014).

[15] Keller S, Keller B P, Kapolnek D, Abare A C, Masui H, Coldren L A, Mishra U K and DenBaars S P, *Appl. Phys. Lett*. **68**, 3147 (1996).

[16] Wu Y R, Shivaraman R, Wang K C and Speck J S, *Appl. Phys. Lett*. **101**, 083505 (2012).

[17] Kryśko M, Franssen G, Suski T, Albrecht M, Łucznik B, Grzegory I, Krukowski S, Czernecki R, Grzanka S, Makarowa I, Leszczyński M, and Perlin P, *Appl. Phys. Lett*. **91**, 211904 (2007).

[18] Ahmadi E, Chalabi H, Kaun S W, Shivaraman R, Speck J S, and Mishra U K, *J. Appl. Phys.* **116**, 133702 (2014).

[19] Zhang Y and Singh J, *J. Appl. Phys*. **85**, 587 (1999).

[20] Grundmann M BANDENG (http://my.ece.ucsb.edu/mgrundmann/bandeng)

[21] Keller S, Heikmann S, Shen L, Smorchkova I P, DenBaars S P and Mishra U K, *Appl. Phys. Lett*. **80**, 4387 (2002).

[22] Lu J, Zheng X, Guidry M, Denninghoff D, Ahmadi E, Lal S, Keller S, DenBaars S P and Mishra U K, *Appl. Phys. Lett*. **104**, 092107 (2014).

Chapter 4

Unintentional Ga incorporation into N-polar AlN films

In the last chapter, the observations of unintentional Ga incorporation into metal-polar AlN layers grown by MOCVD were discussed in detail. Similar experiments were conducted on N-polar AlN layers grown on the -*c* $(000\bar{1})$ plane. In this chapter, the impact of a variety of deposition conditions on the compositional and electrical properties of the nominal N-polar AlN layers is presented. The Al composition (x_{Al}) profiles were evaluated by atom probe tomography (APT) and the properties of 2DEGs in S.I. GaN/AlN/GaN heterostructures were investigated.

4.1 *Al compositions of N-polar thin AlN films (t_{AlN} < 4 nm) measured by atom probe tomography*

4.1.1 Experiments

All samples were grown on c-plane sapphire substrates with 4 ° misorientation towards the a-plane using MOCVD.[1] Trimethylgallium (TMGa), trimethylaluminum (TMAl), ammonia (NH_3), disilane (Si_2H_6), and ferrocene (Cp_2Fe) were used as precursors. On the sapphire substrates, 1.2 µm thick N-polar GaN base layers were firstly grown using the procedure reported previously[2], followed by AlN films deposited at three different temperatures, 960 °C, 1065 °C, and 1155 °C, and using two different carrier gases, H_2 or N_2. All AlN layers were grown at 100 Torr, with a NH_3 flow of 44.6 mmol/min, and a TMAl

flow of 2.48 µmol/min. A series of three samples with AlN layers deposited at different temperatures was grown. Each sample consisted of two AlN layers with a nominal thickness of 2 nm, deposited in H_2 and N_2 as carrier gas respectively [Figure 4.1(a), Table 4.1]. Between the two AlN layers was a 30 nm thick GaN spacer layer grown at 1155 ˚C using N_2 as the carrier gas. Under the same growth condition, a 200 nm thick GaN top layer was deposited, which was required for the sample preparation for the APT measurement. A S.I. GaN/AlGaN/AlN/GaN HEMT structure with an AlN interlayer was also examined [Figure 4.1(b)] to investigate the x_{Al} value of AlN in an actual device structure[3]. The growth temperature was 1155 ˚C and the carrier gas was H_2 for the AlN film. The NH_3 and TMAl flows were 178.4 mmol/min and 11.02 µmol/min, respectively.

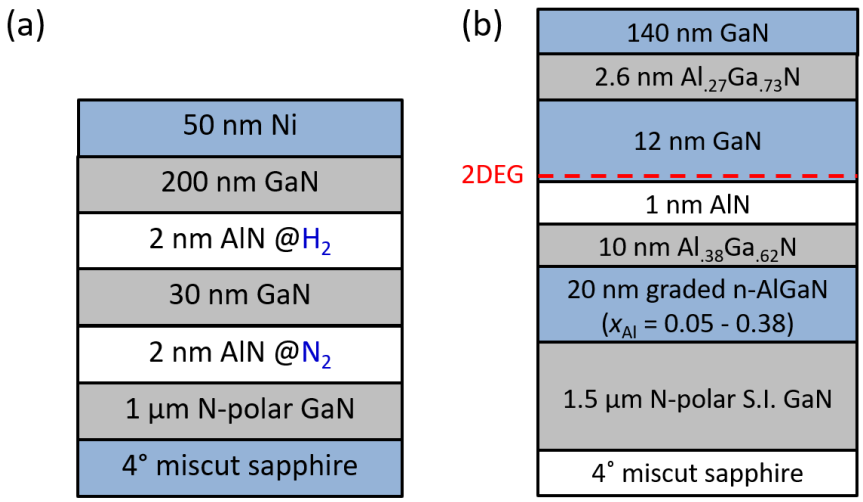

Figure 4.1 (a) Schematic structure of the samples with N-polar AlN layers grown under different conditions and (b) the N-polar S.I. GaN/AlGaN/AlN/GaN HEMT structure for atom probe tomography measurement.

Table 4.1 Growth temperature and carrier gas for each N-polar AlN layer in structure Figure 4.1(a).

Sample number	Top AlN layer	Bottom AlN layer
#1	960 °C, H_2	960 °C, N_2
#2	1065 °C, H_2	1065 °C, N_2
#3	1155 °C, H_2	1155 °C, N_2

All samples were examined by APT, which provided Al composition information for all the thin AlN layers ranging from 1 to 4 nm in thickness. APT sharp tips were prepared with a FEI Helios 600 dual beam focused ion beam (FIB) instrument following standard procedure with final FIB voltage down to 2 kV to minimize Ga induced damages[4]. The milling of the APT specimen was optimized to obtain the apex of the tip in the GaN capping layer. The APT analysis was performed with a °Cameca 3000X HR Local Electrode Atom Probe (LEAP) operated in laser-pulse mode (13 ps pulse, 532 nm green laser, 10 µm laser spot size) with a sample based temperature of 40 K. A detection rate of 0.005 atoms.pulse^{-1} was set during the analysis. The laser pulses intensities and the field applied at the surface of the APT specimen are known to induce variations in the composition measurements in AlGaN based alloy.[5,6] In this study different evaporation conditions were tested on the samples, which did not lead to significant changes in the measured AlN and AlGaN composition. The III site atomic ratio was measured since N detection artifacts are known to induce discrepancies from the theoretical 1:1 stoichiometry and the measured APT III-N ratio.[7] APT 3D reconstruction was carried out using commercial software IVAS^{TM}. The

reconstruction was optimized by using the scanning electron microscope image of the tip as in reference.[8]

In addition, the surface morphology of a 2.7 nm thick AlN film deposited at 960 ˚C in H_2 carrier gas was evaluated by atomic force microscopy (AFM) using a Veeco Dimension 3000 Scanning Probe Microscope.

4.1.2 N-polar AlN films grown under different conditions

Figure 4.2(a) depicts the 25x25x50 nm^3 sampling volume extracted from the APT reconstruction of the sample grown at 1155 °C. (Courtesy of Dr. Bastien Bonef from UCSB) The two AlN layers could be clearly identified. However, a few Ga atoms were also observed in the AlN layers. Since the FIB used in this study to prepare the APT specimen was only equipped with a Ga ions source, some Ga ions could be implanted in the AlN layers during the sample preparation.[9] The trimethylgallium used for GaN growth in this study was expected to exhibit Gallium's natural isotopic ratio (60.1% for ^{69}Ga and 39.9% for ^{71}Ga). However, the ion source in the FIB instrument contains monoisotopic ^{69}Ga. Figure 4.2(b) shows the ^{69}Ga and ^{71}Ga peaks in the mass spectrum extracted from the top AlN layer. Here, the natural isotopic ratio between the two peaks was respected and the Ga observed in the AlN layers was therefore inherent to the sample and not to the sample preparation. This assumption was verified for each AlN layers.

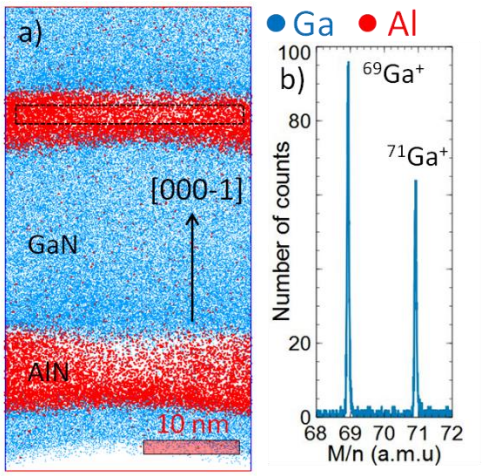

Figure 4.2 (a) 3D reconstruction of two N-polar AlN layers grown at 1155 °C in H_2 and N_2 carrier gas respectively for the top and the bottom layer. Ga atoms (blue) and Al atoms (red) were shown. (b) ^{69}Ga and ^{71}Ga peaks in the mass spectrum extracted from the top AlN layer in (a). (Courtesy of Dr. Bastien Bonef from UCSB)

Figure 4.3 shows the Al III site fraction measured by APT across the six AlN layers. The sampling volumes to draw the profiles were 25x25x15 nm^3. (Courtesy of Dr. Baishakhi Mazumder from Oak Ridge National Laboratory) The thickness of the AlN film was measured as the full width at half maximum of the Al profile. The obtained values varied between 2.7 nm and 3.7 nm. Despite of the different growth temperatures and carrier gases used for the AlN film deposition, all layers exhibited Al fractions equal to or above 0.95. While in metal-polar AlN layers the Al mole fraction in nominal AlN films increased from 0.5 to 0.6 when the growth temperature was reduced from 1145 to 950 °C, in this study the highest Al fraction of 0.99 was obtained for the AlN film grown at the highest growth temperature of 1155 °C and using H_2 as carrier gas [Figure 4.3(e)]. Similar to the

observations for metal-polar AlN layers, the Al composition of the layers grown in H_2 as carrier gas was slightly higher compared to the ones deposited in N_2.

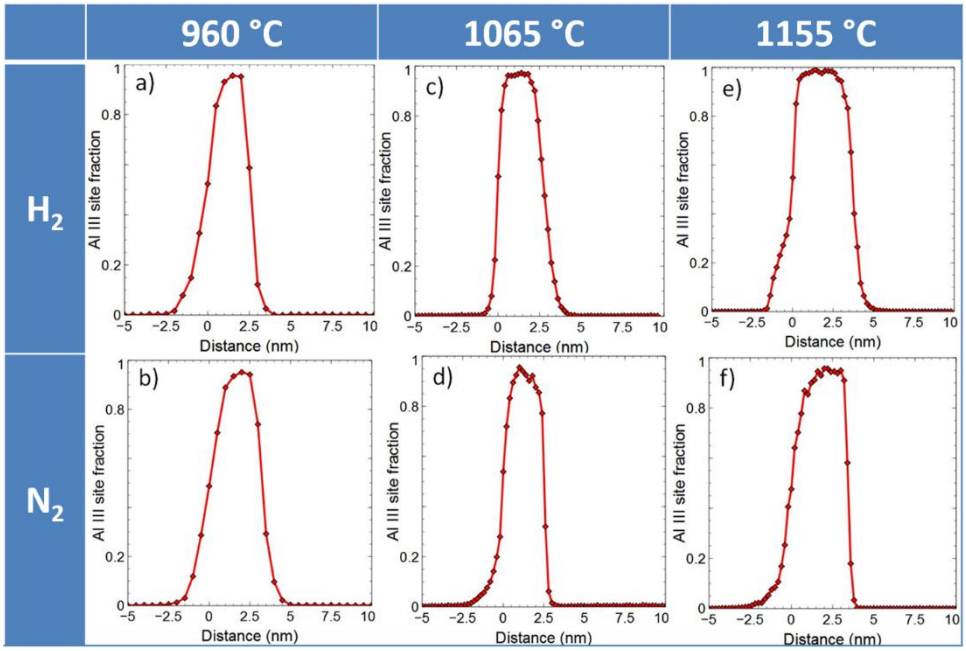

Figure 4.3 APT 1D composition profiles of Al in the N-polar AlN layers grown at (a) 960 °C, H_2, (b) 960 °C, N_2, (c) 1065 °C, H_2, (d) 1065 °C, N_2, (e) 1155 °C, H_2, (f) 1155 °C, N_2. (Courtesy of Dr. Baishakhi Mazumder from Oak Ridge National Laboratory)

There was no clear trend of the GaN/AlN interface sharpness, possibly related to the circumstance that the APT sampling area was small compared to the theoretical terrace length of 7.4 nm, corresponding to the typical step height of 0.52 nm of the 4° misoriented N-polar GaN layer[10]. Additional step bunching in the AlN layer may have resulted from the 3% lattice mismatch to GaN.[11] The AlN surface steps could be clearly seen in the AFM image of the 2.7 nm thick AlN layer deposited at 960 °C in H_2 carrier gas [Figure 4.4]. Since the AlN layers were only 2.7 ~ 3.7 nm thick, their composition profiles can be markedly

influenced by the step formation in the sampling area, especially in the case of step bunching.

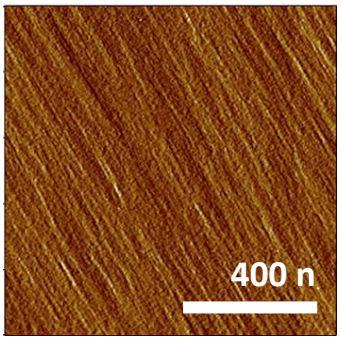

Figure 4.4 The AFM amplitude image of the surface of a 2.7 nm thick AlN film deposited on N-polar GaN layer with 4° misorientation under a growth temperature of 960 ˚C and in H_2 carrier gas. The grey scale was 1.2 nm.

4.1.3 AlN interlayer in a typical N-polar AlGaN/GaN HEMT structure

Figure 4.5(a) depicts a 25x25x70 nm^3 APT volume extracted from the reconstruction of the N-polar S.I. GaN/AlGaN/AlN/GaN HEMT structure. (Courtesy of Dr. Bastien Bonef from UCSB) The associated Al and Ga profiles are shown in Figure 4.5(b). The Al fraction in the AlN layer grown on top of the AlGaN barrier layer was shown to have an Al fraction around 0.9, confirming that the AlN interlayer in an actual device contained little Ga as well. The average Al fraction in the top AlGaN layer was 0.28, in good agreement with the expected value of 0.27. A similar good agreement was observed between the nominal and measured AlGaN barrier composition. The lower Al fraction measured in the AlN interlayer compared to those in the AlN films in the GaN/AlN/GaN structures could be due to the fact that the nominal thickness of the AlN interlayer in the HEMT structure was only 1 nm,

increasing the possibility that steps at the interfaces introduced additional uncertainty in the composition profile. The interface steps may have also contributed to the broadening of the AlN layer thickness from the nominal 1 nm to the measured 2.6 nm. In addition, reconstruction artifacts in APT could also lead to thickness inaccuracy. While the z-direction reconstruction of APT volumes assumes a perfectly hemispherical tip shape, the fact that AlN is more difficult to evaporate than GaN led to a higher GaN evaporation rate during the evaporation of the top GaN/AlN interface[5,12], resulting in a modification of the tip shape[13]. The tip flattened at the interface and local variations of the projection law of the ions led to local magnification effects. These artifacts were responsible for the Al under-density observed at the GaN/AlN interfaces in Figure 4.2(a) and prevented accurate depth reconstruction. On the other hand, it is worth mentioning that for transistor fabrication the devices are always positioned in such a way that the current flows parallel to the surface/interface steps[1], mitigating the impact of uncertainties in the composition profile introduced by the steps on the device performance.

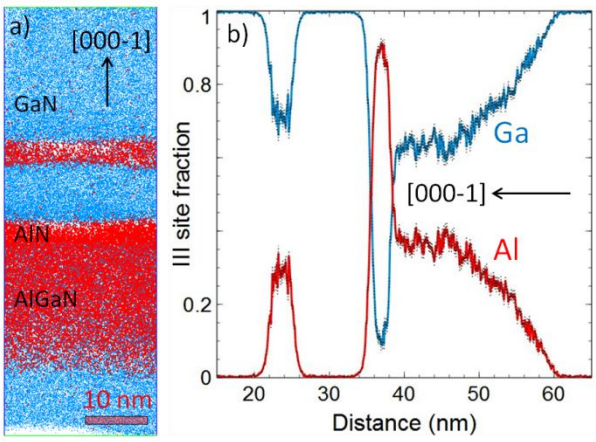

Figure 4.5 (a) 3D reconstruction of the N-polar S.I. GaN/AlGaN/AlN/GaN HEMT structure and (b) associated 1D Ga and Al concentration profiles. (Courtesy of Dr. Bastien Bonef from UCSB)

4.2 *Characterization of N-polar GaN/AlN/GaN heterostructures*

In order to examine the electrical properties of the AlN layers grown under various conditions, GaN/AlN/GaN heterostructures as shown in Figure 4.6 were grown and characterized. Three series of samples with varying growth temperatures and carrier gases for the AlN layers were investigated. Other growth parameters for the structure were the same as those described in Section 4.1.1. The AlN layers for series-1 was grown at 960 °C in H_2, series-2 was grown at 1155 °C in H_2 and series-3 was grown at 1155 °C in N_2 [Table 4.2]. Each series included three to four samples with varying AlN thicknesses around 1−11 nm. The corresponding AlN growth rate was obtained according to the measured thickness, which was the full width at half max (FWHM) of the Al composition profiles obtained by APT, of the AlN layers presented in Section 4.1.2 grown under the same conditions.

The sheet charge density (n_s) and electron mobility (μ) of the 2DEG were measured by room temperature Van der Pauw Hall measurements. Sheet resistance parallel ($R_{sh,//}$) and perpendicular ($R_{sh,\perp}$) to the steps were obtained by transfer-length measurement (TLM), and the parallel and perpendicular electron mobilities ($\mu_{//}$ and $\mu_{\perp}$) were calculated accordingly using n_s measured by hall. The strain status of selected samples were analyzed using reciprocal space map taken by high-resolution x-ray diffraction (XRD) with a Panalytical MRD PRO Materials Research Diffractometer. Atomic force microscopy (AFM) images were taken with a Veeco Dimension 3000 Scanning Probe Microscope to analyze the surface morphology. The layer structures of the samples were identified by atomic STEM-

high angle annular dark field (HAADF) images obtained in a JEOL ARM200F microscope. (? Is it?)

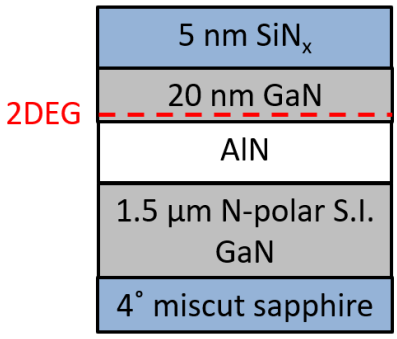

Figure 4.6 Schematic structure of the N-polar GaN/AlN/GaN heterostructures with AlN layers grown under various conditions for electrical property investigation.

Table 4.2 Growth temperatures and major carrier gases for each series of the N-polar GaN/AlN/GaN heterostructures.

Sample series	Growth temperature	Major carrier gas
#1	960 °C	H_2
#2	1155 °C	H_2
#3	1155 °C	N_2

4.2.1 Strain status and the surface morphology

The surface morphologies of the samples with the thickest AlN layer in each series were presented in Figure 4.7. Only the structure with 11.3 nm thick AlN in series-2 showed surface crack segments.

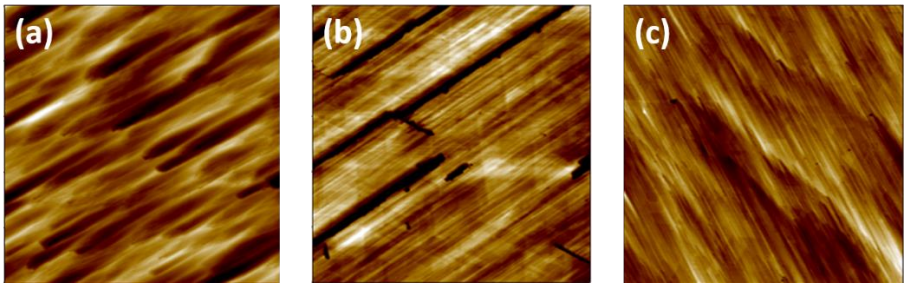

Figure 4.7 AFM images of the surface morphologies of GaN/AlN/GaN heterostructures with (a) 7.6 nm thick AlN grown at 960 °C in H_2, (b) 11.3 nm thick AlN grown at 1155 °C in H_2 and (c) 10.9 nm thick AlN grown at 1155 °C in N_2. Each AlN thickness was the largest in the corresponding series of samples.

The reciprocal space map confirms that the 8.1 nm thick AlN layer grown at 1155 °C in H_2 is fully strained [Figure 4.8]. The noise level in XRD measurement of N-polar samples is generally higher due to the interface steps originating from the crystal misorientation. Moreover, the small thickness of the AlN layer resulted in low intensity of the AlN peak. Therefore, a separate scan with a longer step-time and smaller range was conducted to better present the AlN peak as shown in the red square in Figure 4.8.

According to the images of surface morphologies and the reciprocal space map, we know that in the GaN/AlN/GaN heterostructures under investigation, the 8.1 nm thick AlN layer is fully strained and the 11.3 nm thick one is partially relaxed. Above a certain thickness between these two values, the AlN layer started to relax.

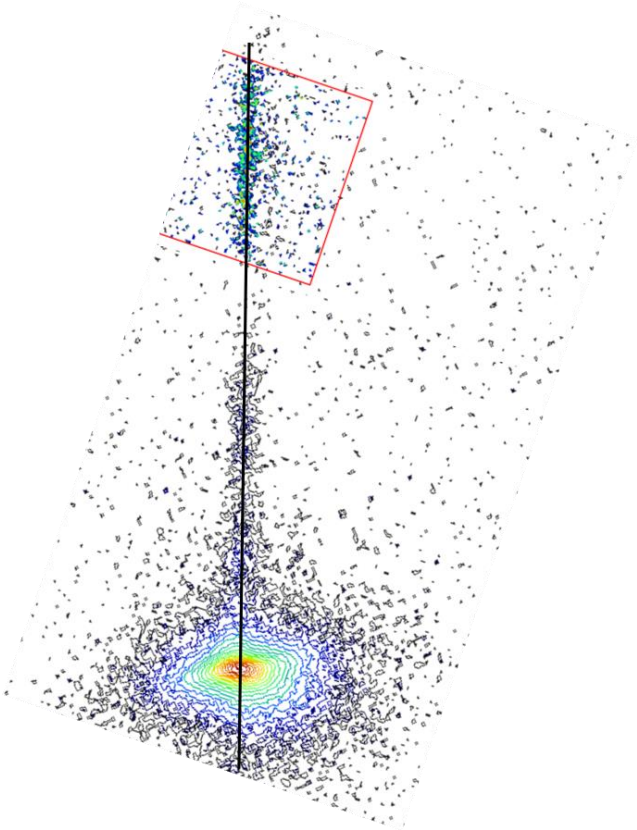

Figure 4.8 Reciprocal space map of the GaN/AlN/GaN heterostructure with 8.1 nm thick AlN layer grown at 1155 °C in H_2. Due to the low intensity of the AlN peak, the image within the red square was obtained separately using a longer step time.

4.2.2 Electrical properties

As mentioned before, since 4˚ misoriented substrates were used to ensure the growth of high quality N-polar films, the associated crystal misorientation resulted in the formation of surface steps, which in turn lead to a higher electron mobility parallel to the steps compared to the perpendicular direction. The μ values determined in Hall measurements are typically 20% lower than the values parallel to the surface steps extracted from TLM measurements.[14,15] In devices, the higher μ parallel to the steps is taken advantage of by

aligning the devices in such a way that the electron transport occurs parallel to the steps.[1] Therefore, both hall and TLM measurement were conducted on the series with the AlN layers grown at 950 °C in H_2 to obtain the parallel μ, which is a better indication of the electrical property of N-polar heterostructures grown on miscut substrates.

For the samples in series-1 with AlN layers grown at 950 °C in H_2, as the AlN thickness increased from 1.2 to 7.6 nm, the sheet charge density of the 2DEG increased from 7.9×10^{12} to 3.5×10^{13} cm^{-2}, with the best observed Hall mobility of 820 cm^2/Vs at t_{AlN} = 5.1 nm and n_s = 2.5×10^{13} cm^{-2} [Figure 4.9]. We speculate that for thinner AlN layers, the charged interface states at the AlN/GaN back interface, a kind of remote coulombic scattering center, got close to the 2DEG and affected the mobility significantly [Figure 4.10].[16] This effect subsided sharply as the scattering centers moved away from the 2DEG, that is, as the AlN layer thickness increased. The μ dropped from 820 to 637 cm^2/Vs when n_s increased from 2.5×10^{13} to 3.5×10^{13} cm^{-2}, probably because the 2DEG moved towards the AlN/GaN top interface with increasing n_s, and the μ was strongly influenced by the interface related scattering. Although the penetration of the 2DEG wavefunction into the AlN layer also increased, alloy scattering was unlikely to be a major reason for the μ drop because the AlN layer contained only around 5% Ga. Despite the mobility drop for the sample with highest n_s, the sheet resistance maintained very close to the sample with the best μ.

Given the parallel sheet resistance measured by TLM and the n_s value measured by hall, the parallel mobility was calculated for each sample, exhibiting a highest parallel mobility of 1100 cm^2/Vs [Figure 4.9]. This value is higher than the mobility of 800 cm^2/Vs for a Ga-polar GaN/AlN heterostructure grown by MBE with a pure AlN layer and similar sheet charge density[17], indicating high material quality.

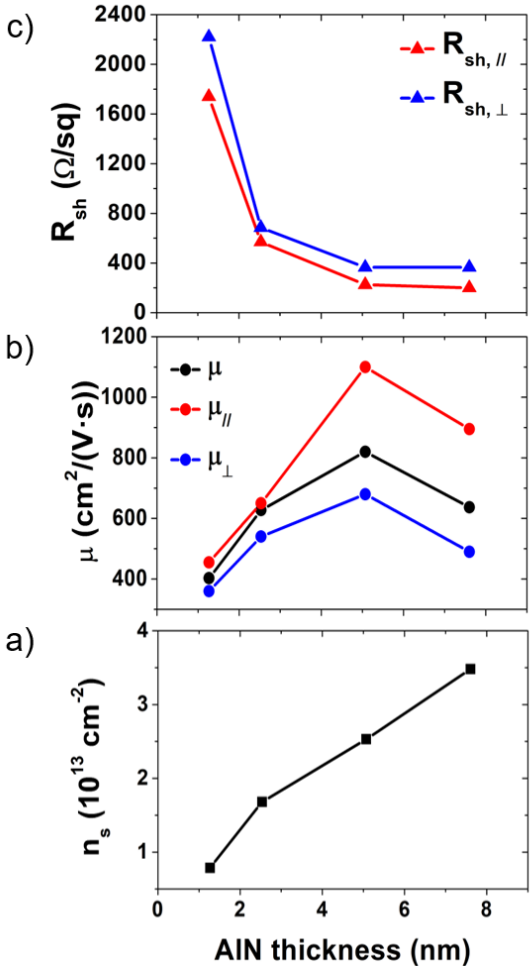

Figure 4.9 (a) Sheet charge density, (b) electron mobility from Hall measurements and derived from TLM measurements parallel and perpendicular to the surface steps (black, red and blue dots, respectively) and (c) parallel and perpendicular sheet resistance (red and blue triangles, respectively) of the N-polar GaN/AlN/GaN heterostructures with AlN layers of different thicknesses grown at 960 °C in H_2.

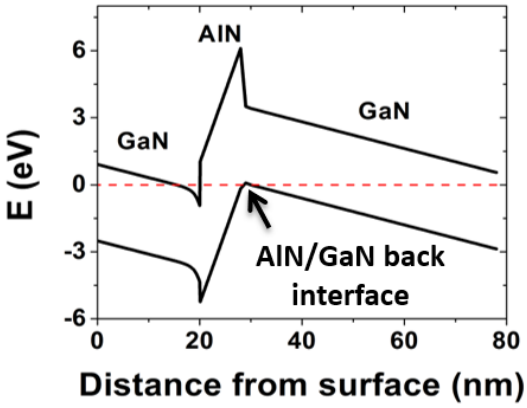

Figure 4.10 Band diagram of a N-polar GaN/AlN/GaN heterostructure with a thin AlN layer. The valance band at the back GaN/AlN interface reaches fermi level.

In series-2, AlN layers with a thickness varying from 6.5 to 11.3 nm were deposited at 1155 °C in H_2. The best mobility in Hall measurements of 1086 cm^2/Vs was obtained for t_{AlN} = 6.5 nm and $n_s = 9.6\times10^{12}$ cm^{-2}, and μ decreased monotonically to 628 cm^2/Vs as t_{AlN} increased to 11.3 nm [Figure 4.11]. The n_s increased monotonically to 2.2×10^{13} cm^{-2}. Different from the samples in series-1, the smallest AlN thickness in series-2 is 6.5 nm and the AlN/GaN back interface had minimal impact on the 2DEG mobility. On the other hand, we believe the AlN/GaN top interface related scattering was still one of the major reasons for the mobility drop with increasing t_{AlN} when the 2DEG moved towards the AlN barrier and got more strongly affected. The possible partial relaxation in the AlN layers of a thickness above 8.1 nm could also contribute to the mobility drop.

In series-3 the AlN layers were deposited at 1155 °C using N_2 as carrier gas. The n_s increased from 3×10^{12} to 1.7×10^{13} cm^{-2} when t_{AlN} was increased from 4.7 to 10.9 nm [Figure 4.11]. Insufficient screening of scattering centers due to the low n_s of 3×10^{12} cm^{-2} was likely to account for the low μ of 474 cm^2/Vs for the sample with t_{AlN} = 4.7 nm. The best Hall

mobility of 1270 cm^2/Vs was observed for t_{AlN} = 7.8 nm with $n_s = 9.8\times10^{12}$ cm^{-2}. Note that $\mu_{//}$ is usually 20 % higher than μ_{hall} as mentioned before.[14,15]

Despite the differences in n_s and μ for samples with three different AlN deposition conditions, the sheet resistance reached around 280-380 ohm/sq for each series as the AlN layer grew thicker [Figure 4.11(c)].

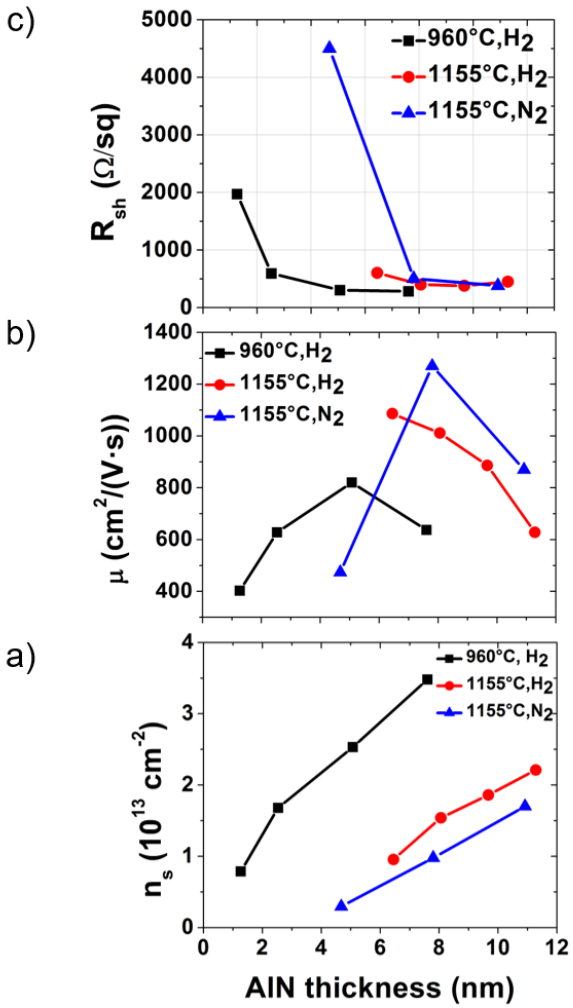

Figure 4.11 (a) sheet charge density, (b) Hall electron mobility and (c) sheet resistance of the N-polar GaN/AlN/GaN heterostructures with the AlN layer of different thicknesses grown at 960 °C in H_2 (black square), at 1155 °C in H_2 (red dot) and at 1155 °C in N_2 (blue triangle).

In Figure 4.12, the Hall mobility was plotted against sheet charge density. The highest μ was observed for the sample with 7.8 nm thick AlN grown at 1155 °C in N_2 and n_s = 9.8×10^{12} cm^{-2}. The μ was slightly lower for the sample with a similar n_s = 9.6×10^{12} cm^{-2} and 6.5 nm thick AlN grown at the same temperature in H_2, implying a better material quality of the AlN layer grown in N_2. With a similar n_s, the significantly lower μ when the AlN layer was grown at 960 °C in H_2 most probably resulted from the ultra-thin AlN of 1.2 nm as discussed before.

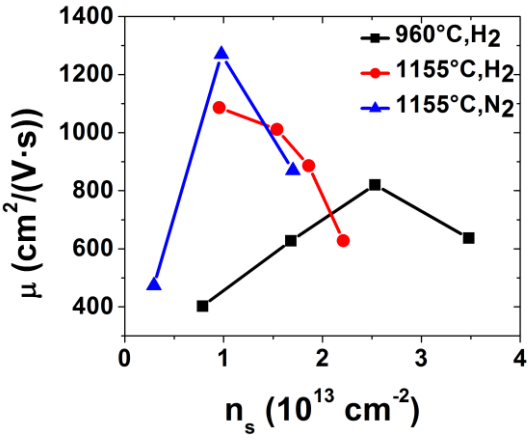

Figure 4.12 2DEG mobilities of the N-polar GaN/AlN/GaN heterostructures measured by Hall with the AlN layers grown at 960 °C in H_2 (black square), at 1155 °C in H_2 (red dot) and at 1155 °C in N_2 (blue triangle).

For samples with similar AlN thicknesses, it is observed that those in series-1 had around 2×10^{13} cm^{-2} higher sheet charge densities than the ones in the other two series. Several aspects of the structures were analyzed to identify the possible reasons for the discrepancy. First, CV measurements proved the accuracy of channel thicknesses for all structures. The second possibility is a higher oxygen impurity concentration in the low

temperature (LT) AlN layers. However, in order to introduce an extra n_s of 2×10^{13} cm^{-2}, the oxygen concentration in the low temperature AlN layer need to be 4×10^{19} cm^{-3} higher than those grown at high temperature (HT) assuming a full ionization, given the AlN thicknesses of couple nanometers. According to our impurity test of the growth reactor, such a high impurity concentration is unlikely. Therefore, although the higher oxygen concentration in low temperature AlN might contribute to the higher n_s in the structures, we believe it is not the major reason. The third aspect, the error in AlN thickness, was evaluated by the scanning transmission electron microscopy (STEM) and identified to be the dominate effect, which is presented in the following subsection.

4.2.3 Layer structure identified by scanning transmission electron microscopy (STEM)

The darker contrast in the STEM images [Figure 4.13] (courtesy of Dr. Feng Wu and Dr. Bastien Bonef from UCSB) indicates the AlN layers grown in the GaN/AlN/GaN heterostructures. The AlN layer in Figure 4.13(a) was grown at 960 °C while the one in Figure 4.13(b) was grown at 1155 °C. Both layers were deposited in H_2. More severe step bunching was observed in the HT AlN layer, which was supported by the AFM images of surface morphologies for AlN layers of different thicknesses grown at 960 °C [Figure 4.14(a)(b)(c)] and 1155 °C [Figure 4.14 (d)(e)(f)], respectively, using H_2 as the major carrier gas.

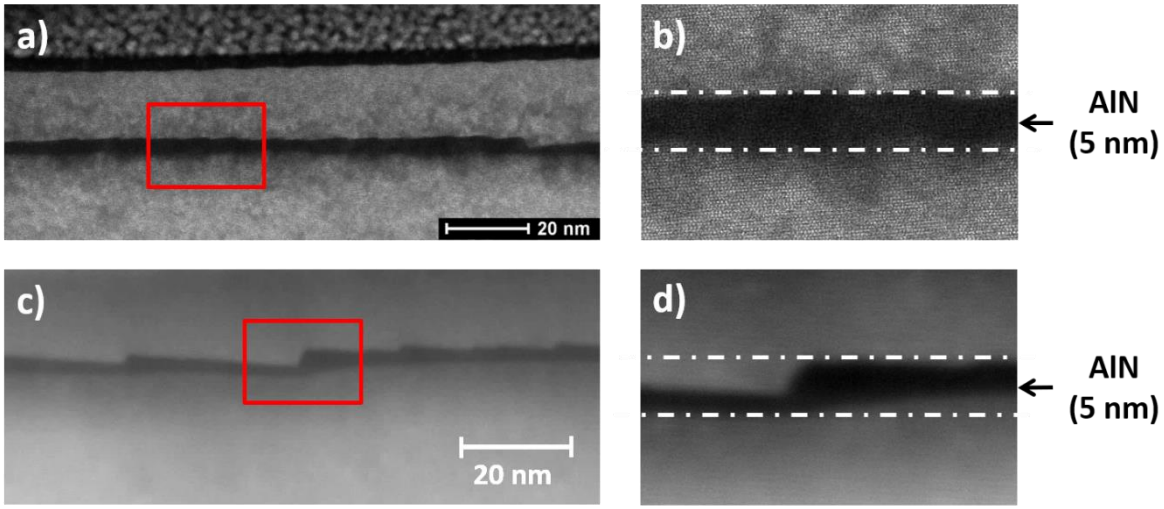

Figure 4.13 Scanning transmission electron microscopy (STEM) images of GaN/AlN/GaN heterostructures with AlN layers grown (a), (b) at 950 °C and (c), (d) at 1155 °C using H_2 as major carrier gas. (b) and (d) are the magnified images of the areas marked by the red square in (a) and (c), respectively. (Courtesy of Dr. Feng Wu and Dr. Bastien Bonef from UCSB)

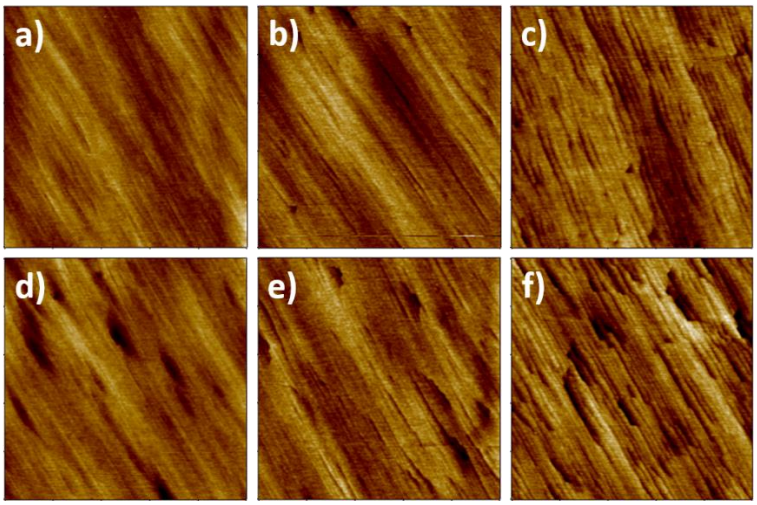

Figure 4.14 AFM images of the surface morphology of AlN layers grown (a), (b), (c) at 950 °C, (d), (e), (f) at 1155 °C using H_2 as major carrier gas. The AlN thickness for (a) and

(d) was 2.7 nm, for (b) and (e) was 5 nm and for (c) and (f) was 9.7 nm. The grey scale is 4 nm.

As mentioned before, the AlN thicknesses in each GaN/AlN/GaN heterostructures was determined by the growth time in the recipe and the growth rate calculated according to the APT results presented in Session 4.1.2. The expected thickness of the LT AlN layer shown in Figure 4.13(a) and (c) was 5.1 nm while that of the HT AlN layer presented in Figure 4.13(b) and (d) was 9.7 nm. However, according to the STEM results, that while the layer thickness of the sample grown at 950 °C was close to the projected one, for the sample grown at 1155 °C significant deviations were observed. The nominally 9.7 nm thick HT AlN layer exhibited a maximum thickness of ~ 5 nm and a minimum thickness of ~ 2 nm due to severe step bunching [Figure 4.13(d)]. The discrepancy between the expected and measured thicknesses of the HT AlN layer explained the large difference of n_s between the samples with LT and HT AlN layers of similar expected thicknesses. The observations suggest that the HT AlN thickness deviations were at least in part associated with the strong step bunching at higher growth temperatures, which was predicted by Tersoff *et al.* for vicinal surfaces under stress[18]. Note that similar bunching effects were observed for thin N-polar InN layers grow on misoriented GaN.[19]

4.2.4 Al composition profile

Selected GaN/AlN/GaN heterostructures grown at 960 or 1155 °C in H_2 were further investigated by APT. (Courtesy of Dr. Bastien Bonef from UCSB) Interestingly, except for

the nominally 2.5 nm thick AlN layer grown at 960 °C, all other nominal AlN layers were actually comprised of a graded AlGaN layer from the GaN buffer and an $Al_xGa_{1-x}N$ layer with x_{Al} = 0.85−0.95 [Figure 4.15]. As we discussed in Session Chapter 2, for the very thin AlN layers of couple nanometers, both the small APT sampling area and the step structures for N-polar samples might lead to inaccuracy of the composition profile. Thinner AlN layers were affected more significantly. Therefore, we consider all the measured $Al_xGa_{1-x}N$ (x_{Al} = 0.85−0.95) layers as AlN layers with very little Ga incorporation in this chapter. Again we considered the full width at half max (FWHM) the thickness of the AlN layer. While the measured thickness of 3.2 and 5.3 nm were very close to the nominal values of 2.5 and 5.1 nm for the LT AlN layers [Figure 4.15(a) and (b)], the nominally 6.5 nm thick HT AlN layer turned out to be a 5.5 nm AlN plus 7 nm graded $Al_xGa_{1-x}N$ (x_{Al} = 0-0.5) [Figure 4.15(c)] and the nominally 9.7 nm thick HT AlN turned out to be 4.5 nm AlN plus 7 nm graded $Al_xGa_{1-x}N$ (x_{Al} = 0-0.5) [Figure 4.15(d)]. Note that we consider the measured thickness of 3.2 nm very close to the nominal thickness of 2.5 nm considering the inaccuracy of the APT composition profile. Also, there was a less pronounced 5.2 nm thick graded $Al_xGa_{1-x}N$ (x_{Al} = 0-0.5) layer below the measured 5.3 nm thick LT AlN.

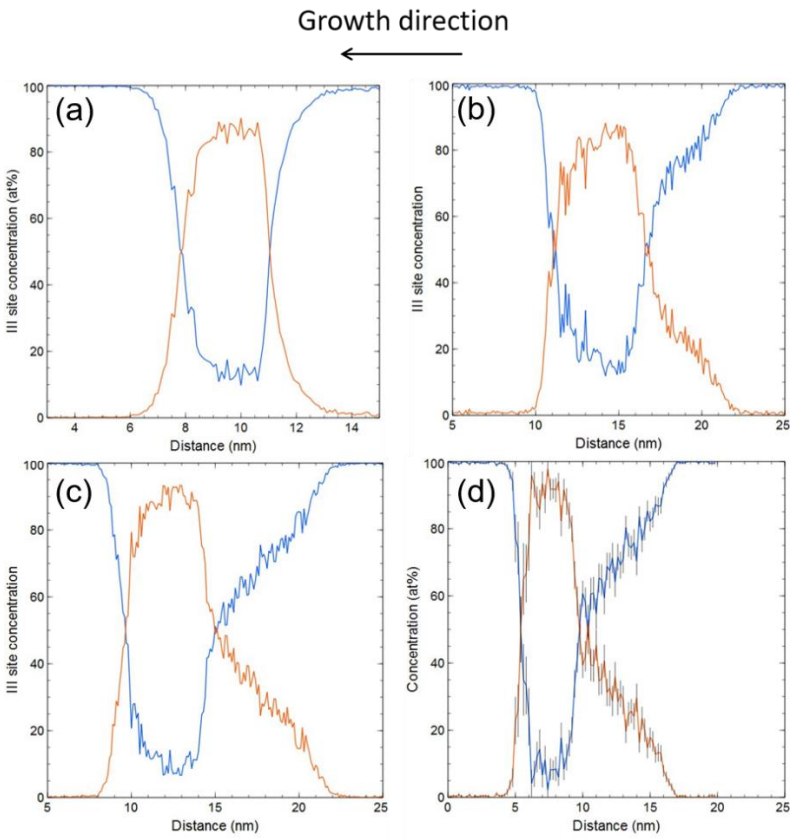

Figure 4.15 Al composition profiles measured by APT for GaN/AlN/GaN heterostructures with (a) nominally 2.5 nm thick AlN layer grown at 960 °C, (b) nominally 5.1 nm thick AlN layer grown at 960 °C, (a) nominally 6.5 nm thick AlN layer grown at 1155 °C, (a) nominally 9.7 nm thick AlN layer grown at 1155 °C. All AlN layers were grown in H_2. (Courtesy of Dr. Bastien Bonef from UCSB)

Figure 4.15(c) and (d) confirmed that the thicknesses of HT AlN layers were thinner than expected, as revealed by the STEM images [Figure 4.13], however, the reasons for the formation of the graded AlGaN layers in this series of samples were unclear. One possible explanation is the composition pulling effect due to the different misfit strains in GaN and AlN layers. Tsai *et al.*[20] and Lin *et al.*[21] reported lower Al incorporation in the initial stage

growth of $Al_xGa_{1-x}N$ layers on sapphire substrates, attributing the phenomenon to Al atoms being expelled to reduce the strain energy from the thermodynamics aspect. Lower x_{Al} in $Al_xGa_{1-x}N$ films deposited on GaN than on $Al_{0.04}Ga_{0.96}N$ was also observed by Chen *et al*.[22]. Higher binary GaN growth rate was measured for the $Al_xGa_{1-x}N$ films on GaN layers, while the binary AlN growth rate remained similar, indicating a stronger effect of the strain on Ga rather than Al incorporation. Similar observations were reported on InGaN/GaN heterostructures.[23,24] Thereby the compositional pulling effect could have played a stronger role compared to the first AlN/GaN heterostructures discussed in paragraph 4.1.2., figure 4.3.due to the nominally thicker AlN layers. While the compositional pulling effect could be part of the reason for the unexpected graded AlGaN layers underneath the AlN layers, the impact of growth temperature remained unclear

Very similar layer thicknesses were observed for the two samples shown in Figure 4.15(c) and (d) while one of the layer growth time was 50% longer than the other one. The discrepancy could be explained by the large local variation of AlN layer thicknesses due to severe step bunching [Figure 4.13(c)], given the relatively small sampling area of atom probe tomography (20 nm in diameter) and the large step width which could be > 30 nm.

4.3 *Comparison between Metal-polar and N-polar AlN*

In previous studies of metal-polar AlN and InAlN films, the parasitic Ga incorporation was associated with different causes, for example transmetallation reactions at the reactant inlet nozzle[25] or carry-over processes in the MOCVD reactor[26]. In the latter case GaN can desorb from GaN deposits in the hot zones of reactor chamber once the TMGa injection was stopped and the GaN deposits had not been coated with AlN or InAlN yet.[26,27] In addition,

In-Ga eutectic formation was discussed as the source of Ga incorporation into InAlN layers.[28] These causes, however, are all tool and/or process dependent but unrelated to the polarity of the grown layers.

The main difference between N- and metal-polar AlN films is that in the N-polar case the surface is terminated with N-atoms compared to Al-atoms for metal-polar layers [Figure 4.16]. We speculate that the nitrogen surface layer may decrease the probability of Al – Ga - exchange reactions compared to the metal-polar case where the metal atoms are positioned directly on the surface. Further investigations are necessary to understand how the polarity influences the unintentional Ga incorporation into AlN layers.

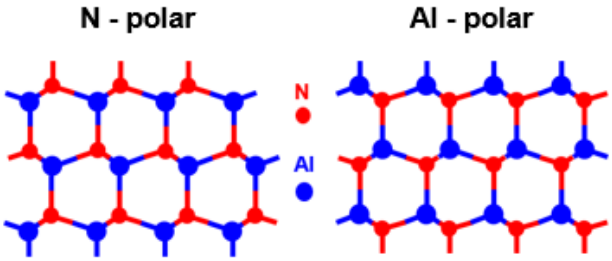

Figure 4.16 Schematic atomic structure of Al- and N-polar AlN.

4.4 *Conclusion*

In conclusion, thin N-polar AlN layers with Al compositions equal or above 0.95 embedded into GaN were demonstrated by MOCVD under a wide range of growth conditions. The highest Al fraction of 0.99 was obtained for the AlN film grown at the highest growth temperature of 1155 °C and using H_2 as carrier gas. The nominally 1 nm thick AlN interlayer in the N-polar GaN/AlN/AlGaN HEMT structure exhibited an Al

fraction of 0.92, confirming little unintentional Ga incorporation into the AlN interlayers in actual N-polar HEMT devices. The reason for the much less unintentional Ga incorporation into N-polar AlN layers compared to Ga-polar, however, is unclear and needs further investigation.

The surface morphology, strain status, electrical properties, layer structures and composition profiles of GaN/AlN/GaN heterostructures with varying AlN thicknesses and growth conditions were investigated. The 8.1 nm thick AlN layer grown at 1155 °C in H_2 was proved to be fully strained by reciprocal space map and smooth surfaces were observed for all samples except for the one with 11.3 nm thick AlN grown in 1155 °C in H_2, which exhibited segments of surface cracks. High electron mobilities were observed in the structures with different AlN growth conditions and optimal AlN thicknesses under investigation, indicating good electrical properties of the AlN films grown under various conditions. The high temperature AlN layers, however, exhibited severe step bunching and noticeably thinner than expected layer thicknesses. Graded AlGaN layers were also observed underneath the HT AlN layers. While the compositional pulling effect could be one of the reasons for the graded AlGaN layers, it didn't explain the thickness discrepancy and the impact of growth temperature needs further investigation.

4.5 *Reference*

[1] Keller S, Fichtenbaum N A, Wu F, Brown D, Rosales A, Denbaars S P, Spect J S and Mishra U K, *J. Appl. Phys.* **102**, 083546 (2007).

[2] Keller S, Suh C S, Chen Z, Chu R, Rajan S, Fichtenbaum N A, Furukawa M, DenBaars S P, Speck J S, and Mishra U K, *J. Appl. Phys.* **103**, 033708 (2008).

[3] Wienecke S, Romanczyk B, Guidry M, Li H, Ahmadi E, Hestroffer K, Zheng X, Keller S, and Mishra U K, *IEEE Electron Device Lett.* **38** 359 (2017).

[4] Thompson K, Lawrence D, Larson D J, Olson J D, Kelly T F, and Gorman B, *Ultramicroscopy* **107**, 131 (2007).

[5] Bonef B, Lopez-Haro M, Amichi L, Beeler M, Grenier A, Robin E, Jouneau P-H, Mollard N, Mouton I, Haas B, Monroy E and Bougerol C, *Nanoscale Research Letters* **11**, 461 (2016).

[6] Rigutti L, Mancini L, Hernández-Maldonado D, Lefebvre W, Giraud E, Butté R, Carlin J F, Grandjean N, Blavette D, Vurpillot F, *J. Appl. Phys.* **119**, 105704 (2016).

[7] Rigutti L, Bonef B, Speck J, Tang F and Oliver R A, Scripta Materialia (2016), http://dx.doi.org/10.1016/j.scriptamat.2016.12.034.

[8] Vurpillot F, Gault B, Geiser B P, and Larson D J, *Ultramicroscopy* **132**, 19 (2013).

[9] Tang F, Moody M P, Martin T L, Bagot P A J, Kappers M J and Oliver R A, *Microsc. Microanal.* **21**, 544 (2015).

[10] Keller S, Li H, Laurent M, Hu Y, Pfaff N, Lu J, Brown D F, Fichtenbaum N A, Speck J S, DenBaars S P and Mishra U K, *Semicond. Sci. Technol.* **29**, 113001 (2014).

[11] Phang Y H, Zhang Z and Lagally M G, *Phys. Rev. Lett.* **75**, 2730 (1995).

[12] Mazumder B, Wong M H, Hurni C A, Zhang J Y, Mishra U K and Speck J S, *Appl. Phys. Lett.* **101**, 091601 (2012).

[13] Vurpillot F, Larson D J and Cerezo A, *Surface and Interface Analysis* **36**, 552 (2004).

[14] Lu J, Denninghoff D, Yeluri R, Lal S, Gupta G, Laurent M, Keller S, DenBaars S P and Mishra U K, *J. Appl. Phys.* **102**, 232104 (2013).

[15] Keller S, Suh C S, Fichtenbaum N A, Furukawa M, Chu R, Chen Z, Vijayraghavan K, Rajan S, DenBaars S P, Speck J S, and Mishra U K, *J. Appl. Phys.* **104**, 093510 (2008).

[16] Ahmadi E, Keller S, Mishra U K, *J. Appl. Phys.* **120**, 115302 (2016).

[17] Smorchkova I P, Chen L, Mates T, Shen L, Heikman S, Moran B, Keller S, DenBaars S P, Speck J S and Mishra U K, *J. Appl. Phys*. **90**, 5196 (2001).

[18] Tersoff J, Phang Y H, Zhang Z and Lagally M G, *Phys. Rev. Lett.* **75**, 2730 (1995).

[19] Lund C, Catalano M, Wang L, Wurm C, Mates T, Kim M, Nakamura S, DenBaars S P, Mishra U K, Keller S, *J. Appl. Phys.* **123**, 055702 (2018).

[20] Tsai Y L, Wang C L, Lin P H, Liao W T, and Gong J R, *Appl. Phys. Lett.* **82**, 31 (2003).

[21] Lin H Y, Chen Y F, Lin T Y, Shih C F, Liu K S, Chen N C, *J. Cryst. Growth* **290**, 225 (2006).

[22] Chen Z, Pei Y, Newman S, Brown D, Chung R, Keller S, DenBaars S P, Nakamura S, and Mishra U K, *Appl. Phys. Lett.* **94**, 171117 (2009).

[23] Pereira S, Correia M R, Pereira E, O'Donnell K P, Trager-Cowan C, Sweeney F, and Alves E, *Phys. Rev. B* **64**, 205311 (2001).

[24] Hao M, Ishikawa H, Egawa T, Shao C L, and Jimbo T, *Appl. Phys. Lett*. **82**, 4702 (2003).

[25] Hiroki M, Oda Y, Watanabe N, Maeda N, Yokoyama H, Kumakura K and Yamamoto H, *J. Cryst. Growth* **382**, 36 (2013).

[26] Lu J, Hu Y L, Brown D F, Wu F, Keller S, Speck J S, DenBaars S P and Mishra U K, *Jpn. J. Appl. Phys.* **51**, 115502 (2012).

[27] Li H, Keller S, Chan S H, Lu J, Denbaars S P and Mishra U K, *Semicond. Sci. Technol.* **30**, 055015 (2015).

[28] Choi S, Kim H J, Lochner Z, Kim J, Dupuis R D, Fischer A M, Juday R, Huang Y, Li T, Huang J Y, Ponce F A and Ryou J, *J. Cryst. Growth* **388**, 137 (2014).

Chapter 5

Channel scaling for N-polar GaN/AlGaN/GaN HEMTs

As discussed in the introduction chapter, for N-polar HEMTs, as the channel thickness (t_{ch}) decreases, the electric field in the channel increases, the sheet charge density (n_s) in the channel decreases and the centroid of the 2DEG moves closer to the back-barrier/channel interface, resulting in a sharp decrease of the electron mobility (μ) in HEMT structures with ultra-scaled channels.[1] Considering that the alloy scattering is suppressed by the AlN interlayer between the AlGaN back-barrier and GaN channel, we suggest that the scattering at the AlN/GaN interface is the major reason for the mobility drop with decreasing t_{ch}. In a recent report, Ahmadi *et al*. attributed this mobility drop to an increase in charged interface states (CIS) scattering, which worsens as the 2DEG wavefunction moves closer to the AlN/GaN interface and as the n_s of the 2DEG reduces due to less screening.[2]

Three different methods to maintain low sheet resistance (R_{sh}) for N-polar HEMTs are discussed in this work: (i) increasing the intentional Si doping in the back-barrier to increase ns; (ii) decreasing the Al composition (x_{Al}) of the AlGaN cap to increase n_s and display the 2DEG away from the AlN/GaN interface; (iii) adding an InGaN layer between the GaN channel and the AlGaN cap to increase n_s and display the 2DEG away from the AlN/GaN interface. The third solution is called a GaN/InGaN composite channel design to be distinguished from the conventional epi structures with a pure GaN channel.

5.1 Conventional N-polar HEMT structures with pure GaN channel

The conventional N-polar HEMT structures studied in this subsection consisted of a 1.5 µm thick semi-insulating (S.I.) GaN buffer, a 10 nm thick Si-doped GaN layer, a 20 nm thick Si-doped graded $Al_xGa_{1-x}N$ (x_{Al} = 0.05 - 0.38) back-barrier, a 10 nm thick unintentionally doped (UID) $Al_{0.38}Ga_{0.62}N$ back-barrier, a 0.7 nm thick AlN interlayer, a GaN channel of different thicknesses, a 2.6 nm thick $Al_xGa_{1-x}N$ cap with x_{Al} = 0.27 or 0.46 and a 5 nm thick in-situ SiN_x layer for surface protection [Figure 5.1]. Three series of samples were grown. For series-1, the Si doping level was 4×10^{18} cm^{-3} and x_{Al} for the AlGaN caps was equal to 0.46; for series-2, the Si doping level was 7×10^{18} cm^{-3} and x_{Al} for the AlGaN caps was equal to 0.46; and for series-3, the Si doping level was 9×10^{18} cm^{-3} and x_{Al} for the AlGaN caps was equal to 0.27. [Table 5.1]

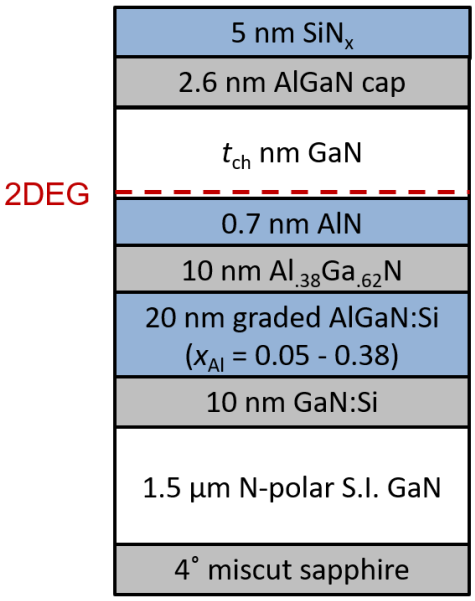

Figure 5.1 Schematic of N-polar HEMT structures with varying GaN channel thicknesses.

Table 5.1 The Si doping level and Al composition for the AlGaN cap in the samples of each series.

Series #	Si doping level (cm^{-3})	x_{Al} for AlGaN cap
1	4×10^{18}	0.46
2	7×10^{18}	0.46
3	9×10^{18}	0.27

5.1.1 Experiment

All HEMT structures were deposited on c-plane sapphire substrates with 4˚ misorientation towards a-plane using metal-organic chemical vapor deposition (MOCVD).[3] Trimethylgallium (TMGa), trimethylaluminum (TMAl), trimethylindium (TMIn), ammonia (NH_3), disilane (Si_2H_6) and ferrocene (Cp_2Fe) were used as precursors. A 1.5 µm thick N-polar S.I. GaN base layer was first deposited on the sapphire substrate as reported previously.[4] Ferrocene was introduced to compensate the unintentionally incorporated oxygen impurities and obtain a semi-insulating layer. On top of the base layer, a 10 nm thick n+ GaN layer was deposited at 1200 °C and 100 Torr with an NH_3 flow of 11.7 µmol/min and a growth rate of ~ 3 Å/s. A disilane flow in the order of 10^{-0} nmol/min was introduced to achieve a doping level between 4×10^{18} and 9×10^{18} cm^{-3}. Then the growth temperature was decreased to 1155 °C and the major carrier gas was switched to N_2. The 20 nm thick graded $Al_xGa_{1-x}N$ (x_{Al} = 0.05 - 0.38) layer, the 10 nm thick $Al_{0.38}Ga_{0.62}N$ layer, the GaN channel of different thickness and the 2.6 nm thick $Al_xGa_{1-x}N$ (x_{Al} = 0.27 or 0.46) cap were then deposited with an NH_3 flow of 11.7 µmol/min and a growth rate of ~ 1 Å/s. A disilane flow

in the order of 10^{-1} nmol/min was introduced into the graded AlGaN layer to achieve a doping level between 4×10^{18} and 9×10^{18} cm^{-3}. The 0.7 nm thick AlN interlayer was deposited under the same conditions except using H_2 as the major carrier gas and with a growth rate ~ 0.5 Å/s. The structure was finished with a 5 nm thick in-situ SiN_x film grown at 1030 ˚C and 500 Torr with an NH_3 flow of 268 mmol/min and a growth rate of ~ 1 A/s. Because the exact flows of the metal-organic sources and disilane changed with time (from 2011 to 2015), only the approximate growth rates were provided.

The Al compositions of the AlGaN layers were calibrated by high-resolution x-ray diffraction (XRD) with a Panalytical MRD PRO Materials Research Diffractometer. The sheet charge density and electron mobility were measured by room temperature Van der Pauw Hall measurements.

5.1.2 Increasing Si doping in the back-barrier

For the first series of the samples with a Si doping level of 4×10^{18} cm^{-3} in both the 10 nm thick GaN and 20 nm thick graded AlGaN layers and 2.6 nm thick $Al_{0.46}Ga_{0.54}N$ caps, the 2DEG mobility dropped from 1569 to 628 cm^2/Vs with an also decreasing n_s from 9.8×10^{12} to 6.4×10^{12} cm^{-2} when the channel thickness decreased from 20 nm to 10 nm. The corresponding sheet resistance values increase from 404 to 1540 ohm/sq. [Figure 5.2] The most significant n_s and μ drop occurred for the samples with the thinnest channels. When t_{ch} decreased from 12 to 10 nm, n_s and μ dropped from 9.8×10^{12} to 6.4×10^{12} cm^{-2} and 1080 to 628 cm^2/Vs, respectively, manifesting the challenges to fabricate N-polar HEMT structures with ultra-scaled channels.

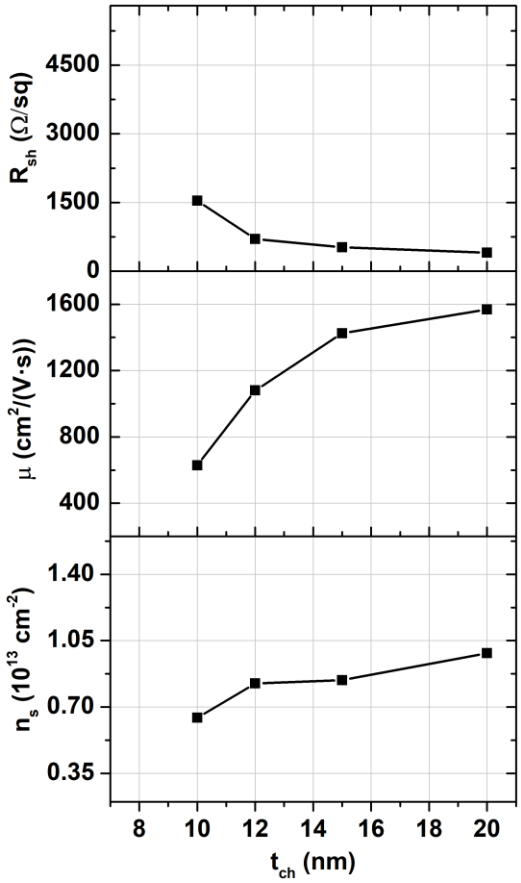

Figure 5.2 The sheet resistance, Hall electron mobility and sheet charge density for the N-polar HEMT structures with 2.6 nm thick $Al_{0.46}Ga_{0.54}N$ caps and 4×10^{18} cm^{-3} Si doping in the 10 nm thick GaN and graded AlGaN layers with varying channel thicknesses.

In order to compensate the n_s drop with decreasing t_{ch}, the Si doping in the 10 nm thick GaN and the 20 nm thick graded AlGaN layers was increased from 4×10^{18} to 7×10^{18} cm^{-3} (Series-2). Around 20% of increase in n_s was observed. [Figure 5.3] For the samples with 12 and 10 nm thick channels the μ increased from 1080 to 1343 cm^2/Vs and 628 to 798 cm^2/Vs, respectively, possibly because the higher sheet charge density provided better screening of scattering centers. The sheet resistance for the 10 nm channel sample dropped by ~ 40% to 925 ohm/sq.

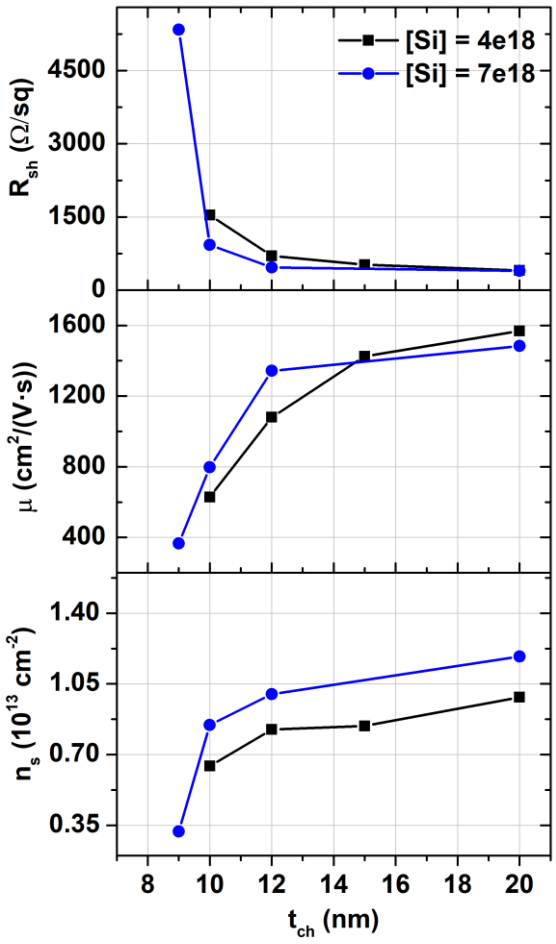

Figure 5.3 The sheet resistance, Hall electron mobility and sheet charge density of the 2DEGs in N-polar HEMT structures with 2.6 nm thick $Al_{0.46}Ga_{0.54}N$ caps and varying channel thicknesses. The Si doping in the graded AlGaN and 10 nm GaN layers was 4×10^{18} cm^{-3} (black square) and 7×10^{18} cm^{-3} (blue dot) respectively.

However, as the channel thickness further decreased to 9 nm, both n_s and μ dropped sharply to 3.12×10^{12} cm^{-2} and 367 cm^2/Vs, with a corresponding R_{sh} = 5430 ohm/sq. [Figure 5.3] Since the possible parasitic 2DEG formation in highly doped layers limits the highest Si doping level in the graded AlGaN and 10 nm thick GaN layers, alternative solutions for further scaled channels are necessary.

5.1.3 Decreasing the Al composition of the AlGaN cap

The Si doping level was increased to 9×10^{18} cm^{-3} and the Al composition of the AlGaN cap was decreased to 0.27 for the samples in Series-3. As shown in Figure 5.4, the sheet charge density for the 12 and 10 nm channel samples increased by around 7×10^{12} cm^{-2} because of the higher Si doping as well as the lower x_{Al} for the AlGaN cap which led to reduced electric field in the channel. Additionally, a significant improvement of the electron mobility was observed for the 10 and 8 nm channel sample, exhibiting $n_s = 1.373\times10^{13}$ cm^{-2}, $\mu = 1073$ cm^2/Vs, $R_{sh} = 424$ ohm/sq and $n_s = 1.217\times10^{13}$ cm^{-2}, $\mu = 738$ cm^2/Vs, $R_{sh} = 695$ ohm/sq, respectively. The mobility of the sample with 12 nm channel was slightly lower most probably due to the high n_s of 1.485×10^{13} cm^{-2}.

It is worth mentioning that the 8 nm channel sample with a Si doping of 9×10^{18} cm^{-3} and $x_{Al} = 0.27$ for the AlGaN cap exhibited a R_{sh} of 695 ohm/sq, which is similar to the R_{sh} of 702 ohm/sq for the 12 nm channel sample with a Si doping of 4×10^{18} cm^{-3} and $x_{Al} = 0.46$ for the AlGaN. By modifying the Si doping level in the graded AlGaN and 10 nm thick GaN layers and the x_{Al} for the AlGaN cap, the channel thickness was scaled down to 8 nm for the conventional N-polar AlGaN/GaN HEMT structures while maintaining reasonable sheet charge density and electron mobility. However, in order to achieve high breakdown voltages, we need to keep a reasonable thickness and Al composition of the AlGaN cap layers.

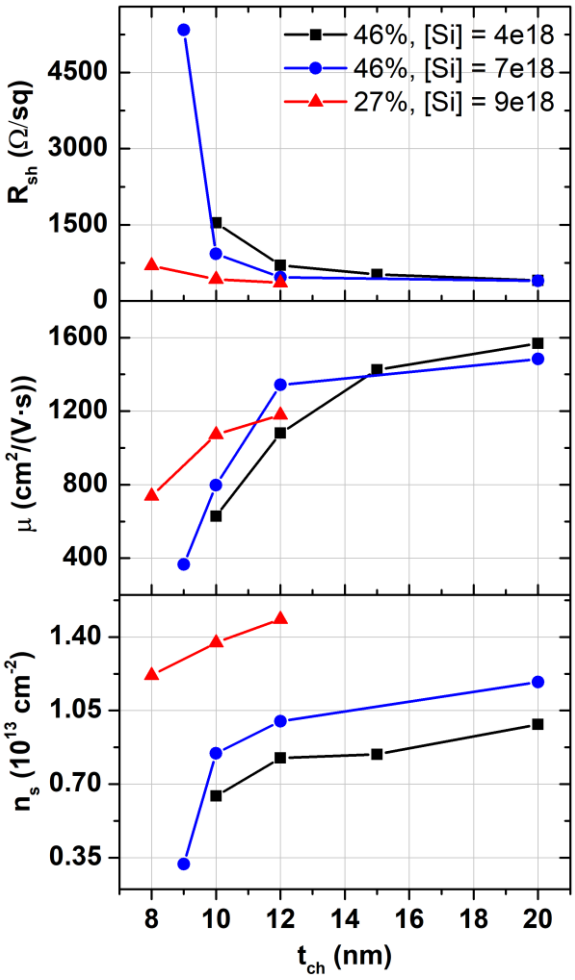

Figure 5.4 The sheet resistance, electron mobility and sheet charge density of the 2DEGs in N-polar HEMT structures with varying channel thicknesses. The Al compositions for the AlGaN cap and the Si doping in the graded AlGaN and 10 nm GaN layers are (i) 46%, 4×10^{18} cm^{-3} (black square), (ii) 46%, 7×10^{18} cm^{-3} (blue dot), (iii) 27%, 9×10^{18} cm^{-3} (red triangle).

5.1.4 Discussion

In a conventional N-polar AlGaN/GaN HEMT structure, as the GaN channel thickness decreases, the electric field in the channel increases, the sheet charge density decreases and

the 2DEG moves towards the AlN/GaN interface, leading to stronger interface related scattering and lower electron mobility. Low sheet charge density could result in insufficient screening of scattering centers as well. As presented above, both increasing the Si doping level and decreasing x_{Al} for the AlGaN cap led to an increase of ns. By reducing x_{Al} for the AlGaN cap, the electric field in the channel decreased and the 2DEG moved away from the AlN/GaN interface, reducing the impact of interface related scattering.

The highest 2DEG mobility obtained for each channel thickness of conventional HEMT structures was plotted in Figure 5.5. Different Si doping levels in the graded AlGaN and 10 nm thick GaN layers and different x_{Al} for the AlGaN caps were chosen to achieve the optimal mobility for each channel thickness. While a relatively gradual decrease was observed when t_{ch} decreased from 20 to 11 nm, the mobility dropped sharply from 1327 to 738 cm^2/Vs when t_{ch} decreased from 11 nm to 8 nm, although the Si doping level and x_{Al} for the AlGaN cap were both optimized. A mobility drop from 1105 to 738 cm^2/Vs was observed when the channel thickness decreased from 9 to 8 nm. The steeper drop of mobility for thinner channels manifested the strong impact of the interface related scatterings, majorly the interface roughness scattering[1] and charged interface states scattering[42], on the 2DEG mobility as we scale down the channel thickness to couple nanometers. Besides an increase of Si doping level and decrease of x_{Al} for the AlGaN cap, both of which had their own limitations, alternative solutions are necessary to further scale down the channel thicknesses.

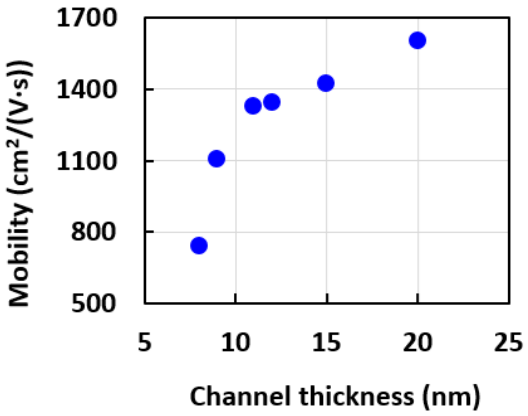

Figure 5.5 Electron mobility of conventional HEMT structures with different channel thicknesses measured at room temperature using Van der Pauw Hall measurement. The Si doping level in the graded AlGaN and 10 nm thick GaN layers and the x_{Al} for the AlGaN cap were modified to optimize the electron mobility.

5.2 A novel design: GaN/InGaN composite channel N-polar HEMT structures

A design of N-polar HEMT structure with InGaN/GaN composite channel was proposed to achieve ultra-scaled channel thicknesses for the N-polar HEMT structures. By replacing the upper portion of the GaN channel with a thin $In_xGa_{1-x}N$ (x_{In} = 0.05 - 0.15) layer, a net positive polarization charge is introduced at the GaN/InGaN interface, which increases n_s, decreases the electric field in the GaN channel and thereby increases d_{2DEG}, mitigating the scattering at the interface [Figure 5.6]. Moreover, the $In_xGa_{1-x}N$ layer led to an increased reverse electric field in the $Al_{0.27}Ga_{0.73}N$ cap under the gate, which we expect to increase the breakdown voltage.

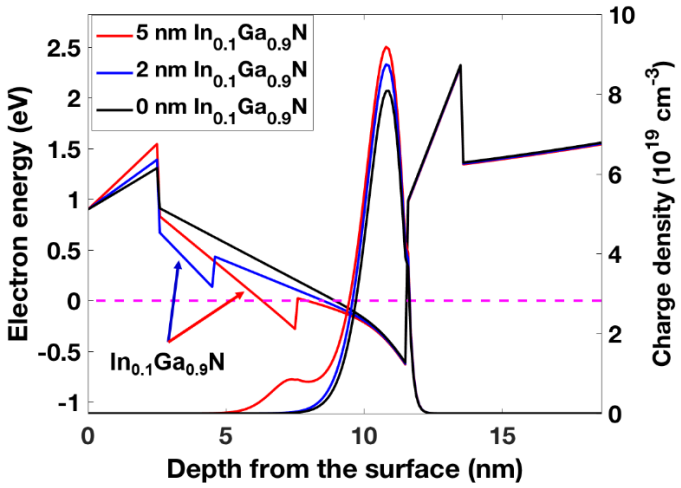

Figure 5.6 Electron band diagrams showing the conduction band profiles for N-polar HEMT structures with 0, 2 and 5 nm thick $In_{0.1}Ga_{0.9}N$ layers in 9 nm thick channels and the corresponding charge distributions of the 2DEGs.

5.3 N-polar GaN/InGaN composite channel HEMTs demonstrated by MOCVD

The N-polar HEMT structures studied in this subsection consisted of a 1.5 µm thick semi-insulating (S.I.) GaN buffer, a 20 nm thick Si-doped graded $Al_xGa_{1-x}N$ (x_{Al} = 0.05 - 0.38) back-barrier, a 10 nm thick unintentionally doped (UID) $Al_{0.38}Ga_{0.62}N$ back-barrier, a 0.7 nm thick AlN interlayer, a conventional GaN channel or a composite GaN/InGaN channel, a 2.6 nm thick $Al_{0.27}Ga_{0.73}N$ cap and a 5 nm thick in-situ SiN_x layer for surface protection [Figure 5.7]. To understand the impact of InGaN thickness (t_{InGaN}) and indium composition (x_{In}) on the HEMT structures, five series of samples with different channel structures were investigated [Table 5.2]. For series-1, 2, 3, the structure parameters were x_{In} = 0.1 and t_{ch} = 9 nm, 6 nm and 4 nm, respectively, with varying $t_{InGaN} < t_{ch}$ and GaN

thickness $t_{GaN} = t_{ch} - t_{InGaN}$. For series-4, the channel consisted of a 6 nm thick GaN layer and a 3 nm thick $In_xGa_{1-x}N$ layer with x_{In} = 0.08, 0.11 and 0.15. For series-5, the channel consisted of a 4 nm thick GaN layer and a 2 nm thick $In_xGa_{1-x}N$ layer with x_{In} = 0.05, 0.10 and 0.15.

Additionally, three different growth conditions were examined on the structures with 4 nm GaN / 5 nm $In_{0.1}Ga_{0.9}N$ channels.

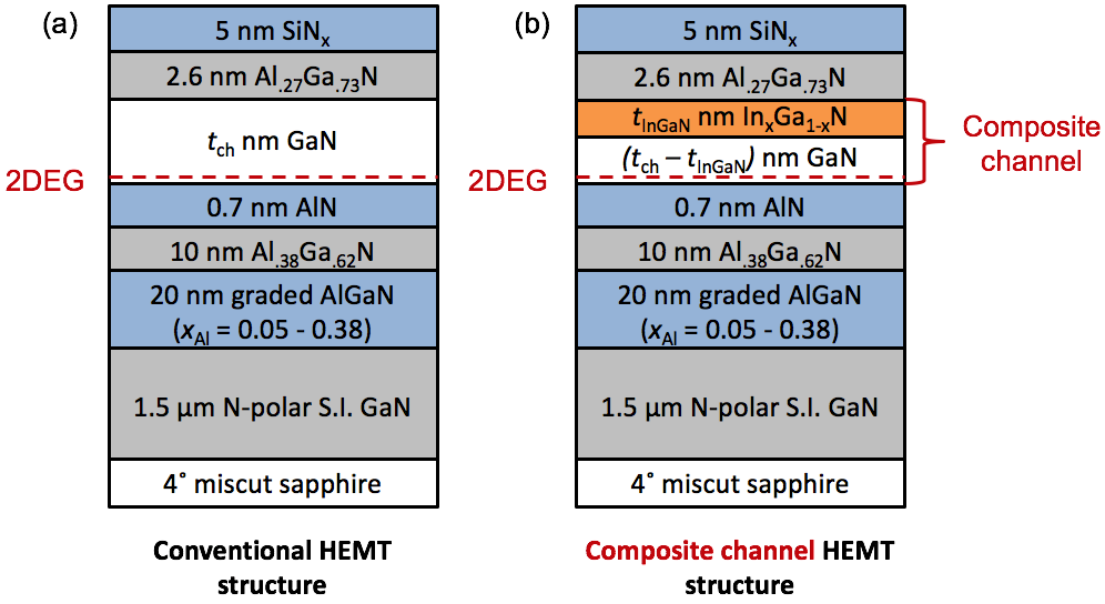

Figure 5.7 N-polar (a) conventional and (b) GaN/InGaN composite channel HEMT structures with same total channel thicknesses. The indium composition varied from 0.05 to 0.15. The total channel thickness was 9, 6 and 4 nm, while the $In_xGa_{1-x}N$ thickness varied from 0 to 9 nm with the GaN thickness $t_{GaN} = t_{ch} - t_{InGaN}$.

Table 5.2 Indium compositions, channel thicknesses, GaN thicknesses and $In_xGa_{1-x}N$ thicknesses for the investigated five series of N-polar HEMT structures.

Series #	x_{In}	t_{ch} (nm)	t_{InGaN} (nm)	t_{GaN} (nm)
1	0.1	9	0 - 9	9 - 0
2	0.1	6	0 - 3	6 - 3
3	0.1	4	0 - 2	4 - 2
4	0.08 - 0.15	9	3	6
5	0.05 - 0.15	6	2	4

5.3.1 Experiments

All HEMT structures were deposited on c-plane sapphire substrates with 4˚ misorientation towards a-plane using metal-organic chemical vapor deposition (MOCVD).[3] Trimethylgallium (TMGa), trimethylaluminum (TMAl), trimethylindium (TMIn), ammonia (NH_3), disilane (Si_2H_6) and ferrocene (Cp_2Fe) were used as precursors. A 1.5 µm thick N-polar S.I. GaN base layer was first deposited on the sapphire substrate as reported previously.[4] Ferrocene was introduced to compensate the unintentionally incorporated oxygen impurities and obtain a semi-insulating layer. On top of the base layer, a 20 nm thick graded $Al_xGa_{1-x}N$ (x_{Al} = 0.05 - 0.38) layer, followed by a 10 nm thick $Al_{0.38}Ga_{0.62}N$ layer, was deposited. The TMGa and NH_3 flows (f_{TMGa} and f_{NH_3}) for the AlGaN layers were 11.7 µmol/min and 178 mmol/min, respectively. The TMAl flow (f_{TMAl}) varied from 0.8 to 9.2 µmol/min for the graded layer and was 9.2 µmol/min for the $Al_{0.38}Ga_{0.62}N$ layer. A disilane flow ($f_{Si_2H_6}$) between 0.53 and 0.18 nmol/min was introduced into the graded AlGaN layer to achieve a doping level between 4×10^{18} and 9×10^{18} cm^{-3}, maintaining n_s in

HEMT structures with different t_{ch}. The AlGaN layers were grown at 1155 ˚C and 100 Torr. Following the AlGaN layers, a 0.7 nm thick AlN interlayer was deposited with $f_{TMAl} = 11.0$ μmol/min and a 0 to 9 nm thick GaN layer was grown with $f_{TMGa} = 9.6$ μmol/min using the same f_{NH_3} as that for the AlGaN layers. Afterwards, the growth temperature was decreased to 915 – 955 ˚C and the reactor pressure increased to 500 Torr. A thin $In_xGa_{1-x}N$ (x_{In} = 0.05 - 0.15) film with layer thickness varying from 0 to 9 nm was grown using $f_{TMIn} = 34.3$ μmol/min, $f_{TMGa} = 9.6$ μmol/min and $f_{NH_3} = 178$ mmol/min. On top of the $In_xGa_{1-x}N$ layer, a 2.6 nm thick $Al_{0.27}Ga_{0.73}N$ cap was deposited under the same growth condition with $f_{TMAl} = 2.5$ μmol/min and $f_{TMGa} = 4.4$ μmol/min. The structure was finished with a 5 nm thick in-situ SiN_x film grown at 1030 ˚C and 500 Torr, with $f_{Si_2H_6} = 4.5$ μmol/min and $f_{NH_3} = 268$ mmol/min.

Besides the typical growth conditions described above, two variations were tested out on structures with 4 nm GaN / 5 nm $In_{0.1}Ga_{0.9}N$ channels: (i) the growth temperature dropped from 1155 to 940 °C after the AlN interlayer deposition, and the 4 nm thick GaN channel was grown under the InGaN growth condition with $f_{TMGa} = 9.6$ μmol/min. (ii) the growth temperature dropped from 1155 to 940 °C after the graded AlGaN deposition, and the 10 nm thick UID $Al_{0.38}Ga_{0.62}N$ layer, the AlN interlayer and the 4 nm thick GaN channel were grown under the InGaN growth condition. For the $Al_{0.38}Ga_{0.62}N$ layer, $f_{TMAl} = 5.28$ μmol/min and $f_{TMGa} = 4.4$ μmol/min were used. For the AlN interlayer and the GaN channel, $f_{TMAl} = 2.5$ μmol/min and $f_{TMGa} = 9.6$ μmol/min were used respectively.

The Al and In compositions of the AlGaN and InGaN films were determined by high-resolution x-ray diffraction with a Panalytical MRD PRO Materials Research Diffractometer. Atomic force microscopy images were taken with a Veeco Dimension 3000

Scanning Probe Microscope to analyze the surface morphology. The sheet charge density and electron mobility of the 2DEG were measured by room temperature Van der Pauw Hall measurements. Note that the electron mobility determined in Hall effect measurements is lower than the electron mobility in an actual device where the gate is oriented such that the current flow occurs parallel to the surface steps originating from the crystal misorientation.[5,6] A one-dimensional self-consistent Poisson-Schrödinger solver was used to simulate the band diagrams and electron distributions.[7]

5.3.2 Impact of different growth conditions for the critical layers

Low growth temperatures (LT) for the InGaN layers, which were 915 – 955 ˚C in our experiments, were necessary to obtain the targeted In content of 0.05 – 0.15. On the other hand, a high growth temperature (HT), which was 1155 °C in our experiments, was preferable to grow smooth films and suppress carbon incorporation. After the HT layers, the samples were cooled down with purging flows of N_2 and NH_3 ($f_{NH_3} = 178$ mmol/min). The interface exposed to the gas flows during cool down, the cool-down interface, might degrade during the temperature change, adversely affecting the electron mobility if the 2DEG is close to the interface. To investigate the trade-off between the better layer quality due to HT growth and the possible degradation of the interlayer quality, three different cool-down interfaces were examined: (a) the 4 nm GaN/ 5 nm $In_{0.1}Ga_{0.9}N$ interface; (b) the AlN interlayer / 4 nm GaN interface and (c) the graded AlGaN / 10 nm AlGaN interface. [Figure 5.8]

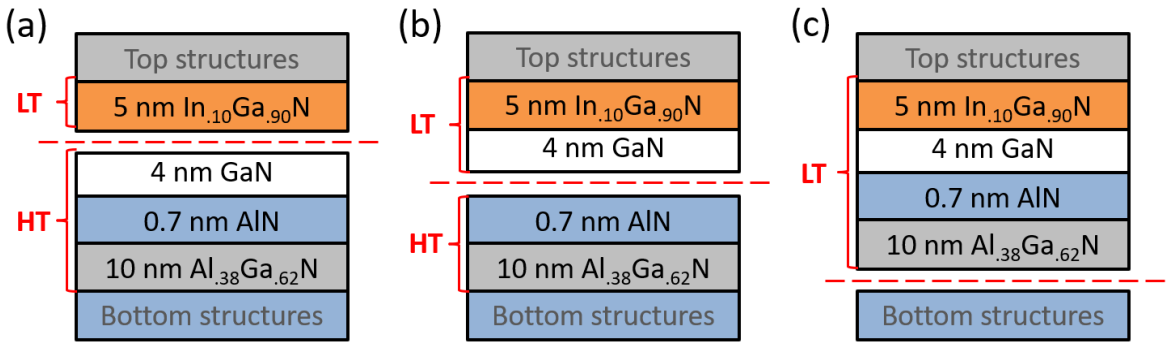

Figure 5.8 Diagrams of the N-polar HEMT structures with different cool-down interfaces: (a) the 4 nm GaN/ 5 nm $In_{0.1}Ga_{0.9}N$ interface; (b) the AlN interlayer / 4 nm GaN interface and (c) the graded AlGaN / 10 nm AlGaN interface.

The relatively low mobility for sample (b) of 547 cm^2/Vs was anticipated since the 2DEG formed at the cool-down interface AlN interlayer / 4 nm GaN and the GaN channel was grown at LT.[Table 5.3] Interestingly, when the cool-down interface was moved away from the 2DEG to the graded AlGaN / 10 nm AlGaN interface (Sample (c)) with the upper part of the structure, 10 nm AlGaN/AlN/GaN/InGaN, grown at LT , a similar mobility of 521 cm^2/Vs was obtained with a corresponding $n_s = 1.515\times10^{13}$ cm^{-2} and R_{sh} = 791 ohm/sq, while for the Sample (b), $n_s = 1.229\times10^{13}$ cm^{-2} and R_{sh} = 929 ohm/sq. A slightly lower R_{sh} was measured when the cool-down interface was moved backward and far away from the 2DEG, but no improvement in mobility was observed, indicating that the growth temperature had a stronger impact on the 2DEG mobility than the cool-down interface selection.

The Sample (a) was cooled down at the 4 nm GaN / 5 nm $In_{0.1}Ga_{0.9}N$ interface with the 4 nm thick GaN layer grown at HT, showing $n_s = 1.165\times10^{13}$ cm^{-2}, μ = 989 cm^2/Vs and R_{sh}

= 542 ohm/sq, confirming that a high growth temperature was preferable for the layer where the 2DEG locates.

Table 5.3 Sheet charge density, electron mobility and sheet resistance of the N-polar HEMT structures with 4 nm GaN / 5 nm $In_{0.1}Ga_{0.9}N$ composite channel with various cool-down interfaces: (a) the 4 nm GaN/ 5 nm $In_{0.1}Ga_{0.9}N$ interface; (b) the AlN interlayer / 4 nm GaN interface and (c) the graded AlGaN / 10 nm AlGaN interface.

Variation	n_s ($\times 10^{13}$ cm^{-2})	μ (cm^2/Vs)	R_{sh} (ohm/sq)
(a)	1.165	989	542
(b)	1.229	547	929
(c)	1.515	521	791

N-polar AlGaN/GaN HEMT structures terminated with the 4 nm thick GaN layer were grown and measured by AFM. Figure 5.9(a) and (b) present the surface of the GaN layer grown at 1155 and 940 C, respectively. The HT GaN showed a noticeably smoother surface, which could be one of the reasons for the higher 2DEG mobility when the GaN channel was grown at high temperature.

Given the better electron mobility of sample (a) and smoother surface of the HT GaN layer,

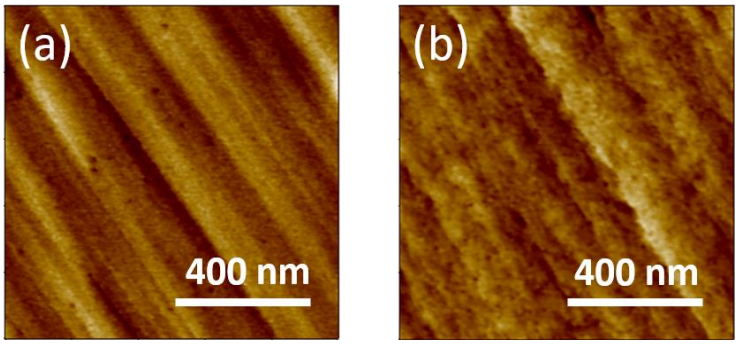

Figure 5.9 Surface morphology of the N-polar AlGaN/GaN HEMT structure with 4 nm thick GaN layer grown at (a) high temperature (1155 C) and (b) low temperature (940 C) as the top layer. The grey scale is 4 nm.

5.3.3 9, 6 and 4 nm thick channel samples with varying InGaN thicknesses

Figure 5.10(a) presents the Hall data and the simulated d_{2DEG} for samples in series-1 with t_{ch} = 9 nm and x_{In} = 0.1. The n_s increased with increasing t_{InGaN} as expected due to the net positive polarization charge at the GaN/$In_{0.1}Ga_{0.9}N$ interface. As t_{InGaN} increased, μ initially increased above the reference value for the sample with a pure GaN channel. This is in agreement with the premise that CIS scattering limits μ and the addition of the $In_{0.1}Ga_{0.9}N$ layer increases d_{2DEG}, thereby improving μ. As a coulombic scattering mechanism, CIS scattering exponentially decreases with increasing d_{2DEG}. Further increases in t_{InGaN} above 2 nm resulted in a mobility drop. This is attributed to the population of a 2DEG in the $In_{0.1}Ga_{0.9}N$ layer [Figure 5.6] which has a lower mobility due to alloy scattering. This effect of alloy scattering was clearly evident from the very low mobility of 98 $cm^2/(V \cdot s)$ for the pure $In_{0.1}Ga_{0.9}N$ channel sample. Therefore, as a tradeoff between scattering mechanisms, for a channel thickness of 9 nm, an optimal t_{InGaN} of 2 nm was found. The observed mobility

of 1446 $cm^2/(V \cdot s)$ and sheet resistance (R_{sh}) of 404.6 Ω/sq offered improvements over the pure GaN channel which showed μ = 1105 $cm^2/(V \cdot s)$ and R_{sh} = 598 Ω/sq.

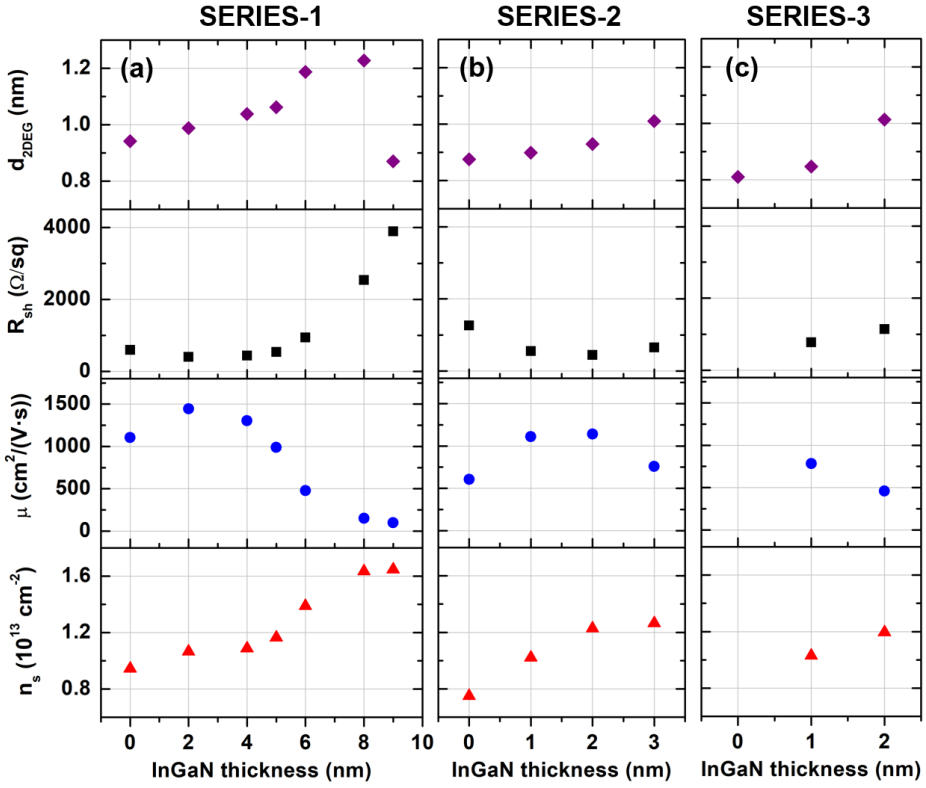

Figure 5.10 Simulated distance between the centroid of the 2DEG and the AlN/(In,Ga)N interface (d_{2DEG}), sheet resistance (R_{sh}), electron mobility (μ) and sheet charge density (n_s) for (a) 9 nm (b) 6 nm (c) 4 nm channel HEMT structures with varying $In_{0.1}Ga_{0.9}N$ thickness. Only d_{2DEG} was presented for the 4 nm pure GaN channel sample which was too resistive to obtain accurate n_s, μ and R_{sh}.

Similar to the samples with 9 nm thick channels, the HEMT structures in series-2 with t_{ch} = 6 nm and x_{In} = 0.1 also exhibited increasing n_s with increasing t_{InGaN}. The highest μ of 1141 $cm^2/(V \cdot s)$ and lowest R_{sh} of 445 Ω/sq were obtained for the sample with a 4 nm GaN / 2 nm $In_{0.1}Ga_{0.9}N$ composite channel, while a low mobility of 606 $cm^2/(V \cdot s)$ was measured

for the one with a 6 nm thick pure GaN channel [Figure 5.10(b)]. Thus, introduction of a 2 nm thick $In_{0.1}Ga_{0.9}N$ layer increased μ by 73%.

HEMT structures with channel thickness as thin as 4 nm were also investigated (series-3). While the sample with a 4 nm thick pure GaN channel was too resistive to obtain accurate n_s, μ and R_{sh}, the 2DEG in a channel composed of 3 nm GaN and 1 nm $In_{0.1}Ga_{0.9}N$ exhibited $n_s = 1.03\times10^{13}$ cm^{-2}, $\mu = 784$ cm^2/(V·s) and $R_{sh} = 773$ Ω/sq, showing a better μ than the sample with an 8 nm thick pure GaN channel [Figure 5.10(c) and Figure 5.12].

5.3.4 9 and 6 nm thick channel samples with varying In composition

To investigate the impact of x_{In} on the HEMT structures, the 4th and 5th series of samples were grown and measured. Samples in the 4th series had composite channels consisting of 6 nm GaN and 3 nm $In_xGa_{1-x}N$ with $x_{In} = 0.08$, 0.11 and 0.15. The samples with $x_{In} = 0.08$ and 0.11 exhibited very similar properties with $n_s \approx 1.18\times10^{13}$ cm^{-2}, $\mu \approx 1360$ cm^2/(V·s) and $R_{sh} \approx 390$ Ω/sq [Figure 5.11(a)]. The dropping mobility to 1228 cm^2/(V·s) when x_{In} was increased to 0.15 implied the formation of a 2DEG in the $In_{0.15}Ga_{0.85}N$ layer. The results show that $x_{In} \leq 0.1$ is preferred for the application in the HEMT structures with 9 nm thick channels.

Samples in the 5th series with 4 nm GaN / 2 nm $In_xGa_{1-x}N$ ($x_{In} = 0.05$, 0.10, 0.15) composite channels showed a different trend from the samples in series-4. A clear optimal composition was found and the best Hall data were obtained for $x_{In} = 0.10$ [Figure 5.11(b)], indicating that for thinner channel samples, a higher x_{In} was required to obtain enough 2DEG displacement away from the AlN/GaN interface. To reach the optimum electron mobility, both t_{InGaN} and x_{In} need to be carefully selected to effectively suppress the

scattering at the AlN/GaN interface while maintaining minimal alloy scattering in the InGaN and CIS scattering at the GaN/InGaN interface.

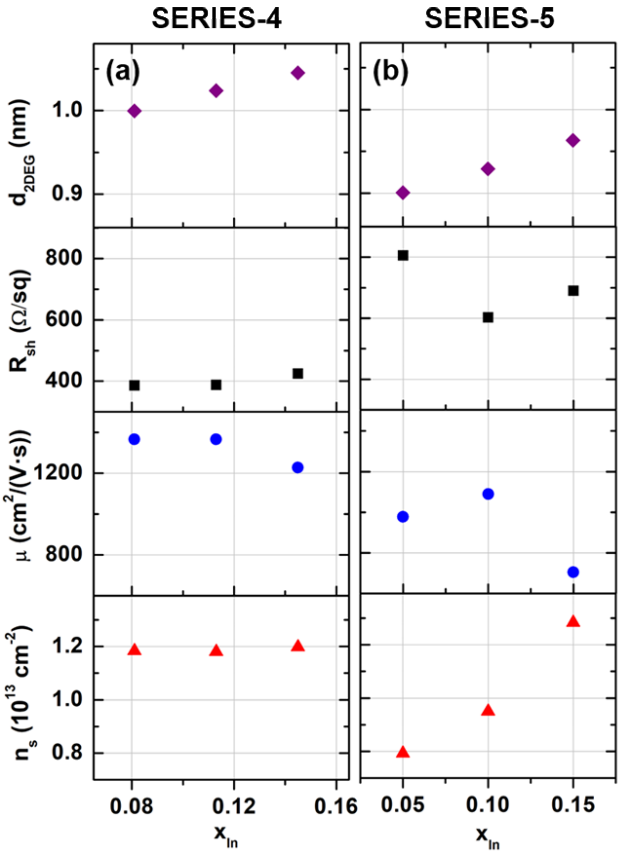

Figure 5.11 Simulated distance between the centroid of the 2DEG and the AlN/(In,Ga)N interface, sheet resistance, electron mobility and sheet charge density for (a) 9 nm channel HEMT structures with 3 nm $In_xGa_{1-x}N$ (x_{In} = 0.08, 0.11, 0.15) and 6 nm GaN and (b) 6 nm channel HEMT structures with 2 nm $In_xGa_{1-x}N$ (x_{In} = 0.05, 0.10, 0.15) and 4 nm GaN.

5.3.5 Discussion

It is worth mentioning that since 4˚ misoriented substrates were used to ensure the growth of high quality N-polar films, the associated crystal misorientation resulted in the

formation of surface steps, which in turn lead to a higher electron mobility parallel to the steps compared to the perpendicular direction. The μ values determined in Hall measurements are typically 20% lower than the values parallel to the surface steps extracted from TLM measurements.[5,8] In devices, the higher μ parallel to the steps is taken advantage of by aligning the devices in such a way that the electron transport occurs parallel to the steps.[3]

As shown in Figure 5.12, the 6 and 4 nm composite channel samples showed slightly higher 2DEG mobility than the 9 and 8 nm conventional channel samples, respectively. The composite channel design significantly expanded the applicable channel thickness and therefore the scalability and design window of N-polar HEMT devices. However, as t_{ch} keeps reducing, the impact of the scattering introduced by the InGaN layer, such as the CIS scattering at the GaN/InGaN interface, alloy scattering and alloy cluster scattering in the InGaN layer, on the 2DEG becomes significant. On this account, further improvements can be expected by improving growth techniques to minimize the interface states at the GaN/InGaN interface and improve the uniformity of indium distribution in the InGaN film.[42,9] Also, by including GaN/InGaN interface and InGaN layer related scattering in Ahmadi's mobility model for N-polar HEMT structures[42], it is possible to establish a model for the GaN/InGaN composite channel HEMTs to predict the optimum t_{InGaN} and x_{In} for different epi structures.

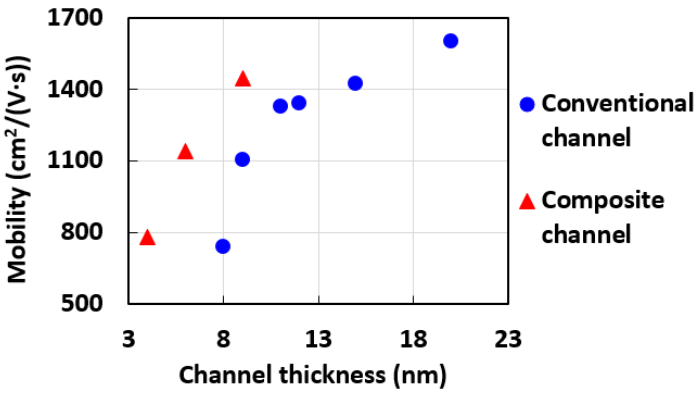

Figure 5.12 Electron mobility of HEMT structures with conventional GaN channels (blue dot) and optimized GaN/InGaN composite channels (red triangle) of different channel thicknesses.

5.4 Conclusion

In this chapter, we first demonstrated the conventional N-polar AlGaN/GaN HEMT structures with channel thicknesses shrinking from 20 to 8 nm while maintaining reasonably low sheet resistances by (i) increasing the Si doping level in the graded AlGaN and 10 nm thick GaN layers to compensate the n_s drop with decreasing t_{ch}; (ii) decreasing the Al composition of the AlGaN cap to reduce the electric field in the channel and displace the 2DEG away from the AlN interlayer / GaN channel interface, suppressing the interface related scattering and improving mobility. However, the formation of parasitic 2DEG in the highly Si-doped regions and the reduction of breakdown voltage with decreasing x_{Al} for the AlGaN cap limited the potential for the conventional AlGaN/GaN HEMT structures with ultra-scaled channels to achieve low sheet resistance.

Thereby, we proposed a N-polar HEMT structure with GaN/InGaN composite channel to maintain high 2DEG mobility when scaling down the channel thickness. By placing a thin InGaN layer between the channel and the AlGaN cap, the electric field in the channel decreased and the distance between the centroid of the 2DEG and the AlN/GaN interface increased, suppressing the scattering at the interface and significantly improving the electron mobility. The sheet charge density also increased due to the net positive polarization charge at the GaN/InGaN interface. Increase of 73% in μ was observed when the 6 nm thick pure GaN channel was replaced by a 4 nm GaN / 2 nm $In_{0.1}Ga_{0.9}N$ composite channel in the HEMT structure. Moreover, the sample with 3 nm GaN / 1 nm $In_{0.1}Ga_{0.9}N$ composite channel exhibited higher μ compared to the sample with 8 nm thick pure GaN channel, reducing the smallest applicable channel thickness by half. This design was proven to significantly improve the channel scalability as measured by Hall, and thus has the potential to improve the lateral scalability of N-polar III-N HEMT devices.

5.5 *Reference*

[1] Singisetti U, Wong M H, and Mishra U K, *Appl. Phys. Lett.* **101**, 012101 (2012).

[2] Ahmadi E, Keller S, Mishra U K, *J. Appl. Phys.* **120**, 115302 (2016).

[3] Keller S, Fichtenbaum N A, Wu F, Brown D, Rosales A, Denbaars S P, Spect J S and Mishra U K, *J. Appl. Phys.* **102**, 083546 (2007).

[4] Keller S, Suh C S, Chen Z, Chu R, Rajan S, Fichtenbaum N A, Furukawa M, DenBaars S P, Speck J S, and Mishra U K, *J. Appl. Phys.* **103**, 033708 (2008).

[5] Lu J, Denninghoff D, Yeluri R, Lal S, Gupta G, Laurent M, Keller S, DenBaars S P and Mishra U K, *J. Appl. Phys.* **102**, 232104 (2013).

[6] Brown D F, Chu R, Keller S, DenBaars S P and Mishra U K, *Appl. Phys. Lett.* **94**, 153506 (2009).

[7] Grundmann M, BANDENG (http://my.ece.ucsb.edu/mgrundmann/bandeng)

[8] Keller S, Suh C S, Fichtenbaum N A, Furukawa M, Chu R, Chen Z, Vijayraghavan K, Rajan S, DenBaars S P, Speck J S, and Mishra U K, *J. Appl. Phys.* **104**, 093510 (2008).

[9] Ahmadi E, Chalabi H, Kaun S W, Shivaraman R, Speck J S, and Mishra U K, *J. Appl. Phys.* **116**, 133702 (2014).

Chapter 6

Summary and future work

6.1 Summary

This dissertation presents an in-depth study on both metal- and N-polar AlN films grown by MOCVD, as well as the effort and achievements of channel scaling in N-polar HEMT structures.

In Chapter 2, the relaxation mechanisms of AlGaN on GaN were discussed and thin GaN cap layers were shown to be highly effective to prevent AlGaN layers from relaxation. With a 2.4 nm thick GaN cap, the $Al_{0.53}Ga_{0.47}N$ film remained strained with a thickness up to 21 nm. This result widened the design window of the structures in the following investigations into AlN films and AlGaN/GaN HEMT structures.

AlN interlayers in the HEMT structures were critical to obtain high electron mobilities in 2DEG structures. However, a high concentration of unintentional Ga was observed in the metal-polar AlN films grown under typical conditions. In this work, the impact of growth temperatures, carrier gases, TMAl and NH_3 flows, reactor pressures and other variations in the growth process on the properties of AlN films were investigated. Three major aspects, the Al compositions, surface morphologies and electrical properties of the GaN/AlN/GaN heterostructures, were examined. The major source of the unintentional Ga was identified to be the hot areas in the reactor, e.g. the susceptor. Since in the growth of AlGaN/GaN HEMT structures deposition of GaN layers before the AlN growth is inevitable, we are not able to

suppress the Ga incorporation by removing the source of the Ga species. Lower growth temperatures were expected to lessen the Ga content in AlN films given the lower partial vapor pressure and desorption rate of the Ga species. The experimental results manifested this speculation, showing 10% less Ga in the metal-polar AlN film grown at 960 °C compared to 1155 °C. However, even grown at 960 °C, the AlN film contained 40% of Ga. Despite of the high Ga concentration in the AlN interlayers, a significant improvement of electron mobility was observed by adding the nominal AlN interlayers, which were actually $Al_xGa_{1-x}N$ with $x_{Al} \sim 0.5 – 0.6$, to the GaN/$Al_{0.24}Ga_{0.76}$N/GaN heterostructures. The nominal AlN interlayers increased the effective barrier heights for the 2DEG, which lessened the wavefunction penetration into the alloy and displaced the 2DEG away from the GaN/Al(Ga)N interface.

N-polar AlN films grown on GaN layers, by contrast, exhibited only 5% or less Ga content regardless of growth temperatures and carrier gases under investigation, which is desirable for HEMT devices. The reason for the difference between metal- and N-polar AlN films is still unclear.

The second part of the dissertation focused on channel thickness scaling for the N-polar AlGaN/GaN HEMTs. Small channel thickness is critical to prevent short channel effects when scaling down the lateral size of N-polar devices. By modifying the Si doping level in the back-barrier and the x_{Al} of the AlGaN cap, the channel thickness of the conventional N-polar HEMT structure was scaled down to 8 nm while maintaining a reasonably low sheet resistance. In order to further reduce the channel thickness, we proposed a N-polar HEMT structure with GaN/InGaN composite channel to maintain high 2DEG mobility as the channel thickness decreased. By placing a thin InGaN layer between the channel and the

AlGaN cap, the electric field in the channel decreases and the distance between the centroid of the 2DEG and the AlN/GaN interface increases, suppressing the scattering at the interface and significantly improving the electron mobility. The sheet charge density also increases due to the net positive polarization charge at the GaN/InGaN interface. An increase of 73% in μ was observed when the 6 nm thick pure GaN channel was replaced by a 4 nm GaN / 2 nm $In_{0.1}Ga_{0.9}N$ composite channel. Moreover, the sample with 3 nm GaN / 1 nm $In_{0.1}Ga_{0.9}N$ composite channel exhibited higher μ compared to the sample with 8 nm thick pure GaN channel, reducing the smallest applicable channel thickness by half. This design was proven to significantly improve the channel scalability, and thus has the potential to improve the lateral scalability of N-polar III-N HEMT devices.

6.2 Future work

6.2.1 Investigations into metal-polar AlN growth conditions to achieve pure AlN

Although it was demonstrated that for metal-polar AlGaN/GaN HEMT structures with $x_{Al} < 0.5$ in the $Al_xGa_{1-x}N$ barrier, adding a thin (0.7 nm) nominal AlN interlayer, which actually contained 40 ~ 50% Ga, significantly improved the 2DEG mobility, pure AlN is necessary for structures with higher x_{Al} in the barrier and 2DEG sheet charge density to improve the electron mobility.

Under the AlN growth conditions discussed in this work, a minimum of 40% Ga was observed in the AlN films in the GaN/AlN/GaN heterostructures grown without interruption. In order to achieve high purity of AlN films, a wider range of growth conditions, especially the growth temperature and TMAl flows, should be investigated.

Yamada et al. reported a reduction of the Ga content in the metal-polar AlN films to 5% by depositing the film at 805 °C in a horizontal reactor, while 50% of Ga incorporation was observed in the layers grown under 960 °C.[1] It will be informative to investigate AlN layers grown at 800 ~ 960 °C in our vertical reactor. For such low growth temperatures, other growth parameters need to be carefully designed to obtain high quality films.

Only two TMAl flow rates, both being relatively low, were examined in this work. Higher TMAl flow is a possible factor to improve the AlN purity and should be examined.

It is likely that a low growth temperature is necessary to deposit pure metal-polar AlN films. In this case, the interfaces exposed to the purge flows during temperature change in the growth of GaN/AlN/GaN heterostructures require extra attention. It is important to study the impact of these interfaces on the electrical property of the heterostructures and methods to improve the interface quality.

It is worth mentioning that the accuracy of x_{Al} in the GaN/AlN/GaN heterostructures obtained by XRD measurement reduces when the AlGaN layer is thin (< 6 nm) and the GaN cap thickness is undefined and comparable to the AlGaN thickness. The AlGaN peaks for thin AlGaN layers are broad and sensitive to the thickness of both the AlGaN and GaN cap. Therefore, measuring the layer thicknesses using alternative methods, like TEM, could significantly improve the accuracy of x_{Al} measured by XRD. Alternative measurements designed for thin layer analysis, like atom probe tomography, could also be used.

6.2.2 Theory for significantly less Ga incorporation into N-polar than metal-polar

The observation of much less Ga content in N-polar AlN films than the metal-polar ones grown under the same conditions requires further inspection. We speculated that the

nitrogen surface layer may decrease the probability of Al – Ga - exchange reactions compared to the metal-polar case where the metal atoms are positioned directly on the surface, leading to less Ga incorporation into the layer. However, this speculation implies that most of the Ga species get incorporated into the films by replacing the Al atoms on the surface, which contradicts with the fact that Al – N bonds are much stronger than the Ga – N bonds. Further study is needed to understand the phenomenon, which will provide more insights into the thermodynamics of surface reactions during growth for samples with different polarities.

6.2.3 Explanation for the graded AlGaN underneath AlN and the AlN thickness discrepancy in N-polar GaN/AlN/GaN heterostructures

As presented in Chapter 4, while the thin N-polar AlN layer with a thickness less than 4 nm showed sharp interfaces, the thicker AlN film in selected GaN/AlN/GaN heterostructure consisted of a graded AlGaN layer with x_{Al} from 0 to 0.5 and an AlN layer on top. [Figure 6.1] The top AlN/GaN interfaces were sharp. The graded AlGaN layers had comparable thicknesses to the AlN layers. Moreover, the two AlN films grown at the higher temperature [Figure 6.1(c) and (d)] showed more pronounced graded AlGaN layers.

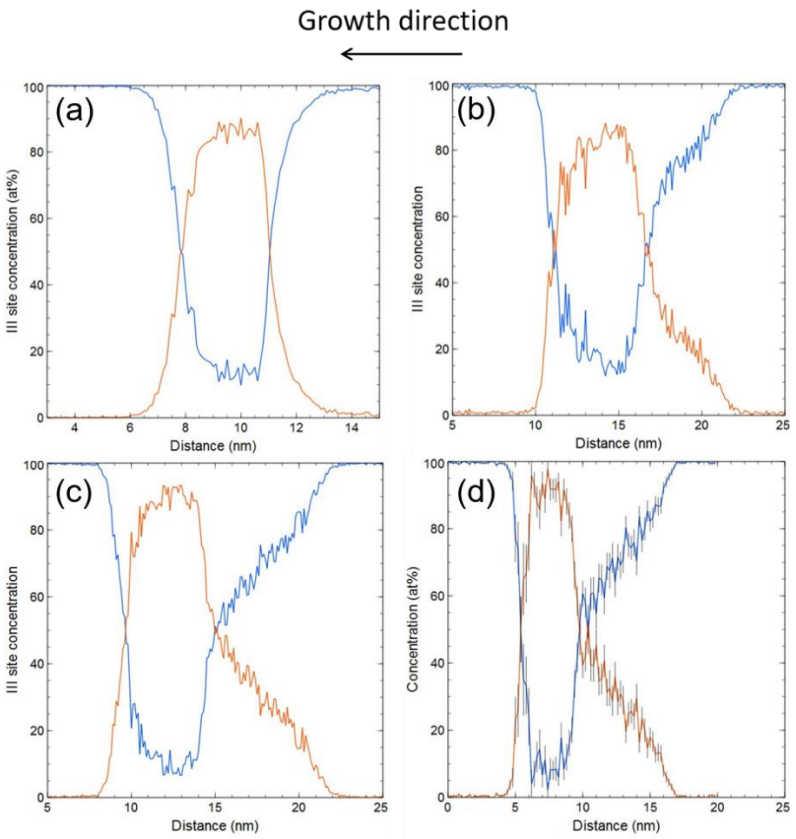

Figure 6.1 Al composition profiles measured by APT for GaN/AlN/GaN heterostructures with (a) nominally 2.5 nm thick AlN layer grown at 960 °C, (b) nominally 5.1 nm thick AlN layer grown at 960 °C, (a) nominally 6.5 nm thick AlN layer grown at 1155 °C, (a) nominally 9.7 nm thick AlN layer grown at 1155 °C. All AlN layers were grown in H_2.

One possible explanation is the composition pulling effect due to the different misfit strains in GaN and AlN layers.[2,3,4] However, there are still questions to be resolved. Why the thin AlN films < 4 nm showed no graded AlGaN layers? Does it mean that the AlN growth started with sharp interface and deposition of pure AlN layer, and as the layer grew thicker the sharp interface turned into a graded AlGaN layer? What's the mechanism of the graded

AlGaN layer formation? What's the impact of growth temperatures? How to prevent the graded AlGaN layer from forming? Further investigations are needed to understand the phenomena and improve the situation.

6.2.4 Establishing a 2DEG mobility model for the N-polar HEMTs with GaN/InGaN composition channels

In a previous report, Ahmadi et al. established a mobility model for the conventional N-polar HEMT structures.[5] By introducing the scattering mechanisms related to the InGaN and GaN/InGaN interface, e.g. alloy scattering and alloy cluster scattering[6] in the InGaN, interface roughness scattering and interface charged states scattering at the GaN/InGaN interface, it is possible to establish a model for the N-polar GaN/InGaN composite channel HEMTs to predict the optimum InGaN thickness and In composition for different channel thicknesses, AlGaN cap thicknesses and compositions, sheet charge densities, etc. The model will significantly simply the structure design process and provide insights into the electron transportation in the N-polar composite channel HEMTs.

6.2.5 Research into the InGaN deposition conditions to minimize InGaN related scattering in the composite channel HEMTs

For the N-polar HEMT structures with GaN/InGaN composite channels, as the channel thickness keeps reducing, the impact of the scattering introduced by the InGaN layer, such as the charged interface states scattering at the GaN/InGaN interface, alloy scattering and alloy cluster scattering in the InGaN layer, on the 2DEG becomes significant. On this

account, further improvements can be expected by improving growth techniques to minimize the interface states at the GaN/InGaN interface and improve the uniformity of indium distribution in the InGaN film.[5,6]

6.2.6 Investigating the impact of the LT AlGaN cap on the composite channel HEMTs and addressing possible drawbacks

In order to prevent desorption of In atoms, a low growth temperature for the AlGaN cap on top of the InGaN layer is required. However, low temperature growth leads to an increase of carbon incorporation due to incomplete pyrolysis, surface roughness and defect formation because of low surface mobility during growth. It's very important to analyze the impact of the LT AlGaN caps on device performance, identify related problems and improve the growth techniques accordingly.

6.2.7 N-polar HEMTs on on-axis substrates for further channel scaling

In order to grow smooth N-polar GaN films free from hexagonal hillocks, substrates with 4° miscut were used. While the vicinal substrates realized the growth of smooth and high-quality N-polar films by MOCVD, the surface steps introduce extra roughness of the interfaces and surfaces, the impact of which on the 2DEG becomes significant for ultra-thin channels. Development of high-quality N-polar material growth on on-axis substrates will be beneficial to the production of N-polar HEMTs with ultra-thin channels.

6.3 *Reference*

[1] Yamada A, Ishiguro T, Kotani J, Tomabechi S, and Nakamura N, *Phys. Status Solidi* B **254**, 1600496 (2017).

[2] Tsai Y L, Wang C L, Lin P H, Liao W T, and Gong J R, *Appl. Phys. Lett.* **82**, 31 (2003).

[3] Lin H Y, Chen Y F, Lin T Y, Shih C F, Liu K S, Chen N C, *J. Cryst. Growth* **290**, 225 (2006).

[4] Chen Z, Pei Y, Newman S, Brown D, Chung R, Keller S, DenBaars S P, Nakamura S, and Mishra U K, *Appl. Phys. Lett.* **94**, 171117 (2009).

[5] Ahmadi E, Keller S, Mishra U K, *J. Appl. Phys.* **120**, 115302 (2016).

[6] Ahmadi E, Chalabi H, Kaun S W, Shivaraman R, Speck J S, and Mishra U K, *J. Appl. Phys.* **116**, 133702 (2014).